이학박사학위논문

Self-Assembly Behavior of Molecularly Designed Block Copolymers with Distinct Characteristics in the Solution and their Applications

뚜렷한 특징을 지니는 분자로 설계된 블록 공중합체의 용액상에서의 자기조립거동과 그 응용

2022 년 8 월

서울대학교 대학원

화학부 고분자화학전공

김 준 영

Ph. D. Dissertation

Self-Assembly Behavior of Molecularly Designed Block Copolymers with Distinct Characteristics in the Solution and their Applications

Junyoung Kim

Research Advisor: Prof. Kyoung Taek Kim

Department of Chemistry

Seoul National University

Self-Assembly Behavior of Molecularly Designed Block Copolymers with Distinct Characteristics in the Solution and their Applications

뚜렷한 특징을 지니는 분자로 설계된 블록 공중합체의 용액상에서의 자기조립거동과 그 응용

지도교수 김 경 택

이 논문을 이학박사 학위논문으로 제출함.
2022년 8월

서울대학교 대학원
화학부 고분자화학 전공
김 준 영

이 정 민의 이학박사 학위논문을 인준함
2022년 8월

위 원 장 최 태 림 (인)

부 위 원 장 김 경 택 (인)

위 원 손 병 혁 (인)

위 원 이 연 (인)

위 원 박 치 영 (인)

ABSTRACT

Self-Assembly Behavior of Molecularly Designed Block Copolymers with Distinct Characteristics in the Solution and their Applications

Junyoung Kim

Polymer Chemistry in Department of Chemistry

The Graduate School

Seoul National University

Constructing well-defined nanostructures with self-assembly becomes significant topic in modern research. Because sorts of morphologies made from self-assembly were so diverse, precise prediction of the nanostructure from molecular level was considered as important subject. Polymers with functional groups or distinct characteristics largely affects their self-assembly behavior in the solution. Their nanostructures can be vary according to the environment of the solution.

This dissertation describes the various preparation methods for the well-defined self-assembly structure of the block copolymers in the solution. For the well-defined self-assembled nanostructurs, molecular engineering of the block copolymers with distinct characteristics were preceded. Various nanostructures were demonstrated using block copolymers composed of different building blocks.

In Chapter 2, we prepared oxidation sensitive poly(ethylene glycol)-b-poly(acrylbenzylborate) (PEG-*b*-PABB). Binary mixture of PEG-b-PABB and PEG-*b*-PS made the oxidation-responsive polymersomes. The presence of H_2O_2 in the medium triggers the oxidation of benzyl borate pendants of PABB to form poly(acrylic acid) (PAA). This transformation results in the perforation of the compartmentalizing membrane of polymersomes by the dissolution of PEG-b-PAA domains embedded in the inert PEG-b-PS matrix. By controlling the composition of the stimuli-responsive block copolymer, the polymersomes of the binary blend exhibit size-selective permeability without losing the structural integrity.

Chapter 3 demonstrated the preparation method for the poly(3-hexylthiophene) (P3HT) based nanofiber networks. Using pseudo-living nature of KCTP, ABA type P(3HT-*b*-3EHT-*b*-3HT) and P(3HT-*b*-3EHT) were synthesized with good manner. The block copolymer could be self-assembled to form 1D nanofibers and their lengths can be controlled in anisole with self-seeding method. ABA type triBCPs form linkage between nanofibers and generate networks. Furthermore, at higher concentration, nanonetwork beame organogel with increased viscosity. In TEM image, interwined network of the nanofibers were observed. After the freeze-drying the organic solvent, we demonstrated the fabrication of porous foam of nanofiber organogels.

In Chapter 4, Discrete polymers with charged ionic blocks were synthesized and self-assembled in the solution. We used the convergent method to synthesize monodisperse and precisely defined block co-oligomers (BCOs) having pendant carboxylic acid or amine as a hydrophilic functional block and oligo(lactic acid) as a hydrophobic block. These oppositely charged BCOs, with an absolutely defined number of cations or anions were mixed for the co-assembly in water. Indeed, ionic interaction between assembled block co-oligomers opposes the membrane's natural curvature and leads to the faceting of the membranes.

Keywords : block copolymer, stimuli-responsive polymersome, solution self-assembly, crystallization-driven self-assembly, discrete polymer

Student Number : 2016-29404

Table of Contents

List of Schemes

List of Tables

List of Figures

Abbreviations

BCP	Block copolymers
DMT	Dimethoxytrityl
ASCII	American standard code for information interchange
MALDI-TOF	Matrix-assisted laser desorption/ionization time-of-flight
TEMPO	(2,2,6,6-Tetramethylpiperidin-1-yl)oxyl
QR code	Quick response code
ESI-MS	Electrospray ionization-mass spectrometry
MS/MS	Tandem mass spectrometry
LC-MS	Liquid chromatography-mass spectrometry
PcL	Poly(phenyllactic-*co*-lactic acid)
P	*rac*-Phenyllactic acid
L	*rac*-Lactic acid
PAH	Poly(α-hydroxy acid)
TBDMS	*tert*-Butyldimethylsilyl
$BF_3{\cdot}Et_2O$	Boron trifluoride etherate
Da	Dalton

NMR	Nuclear magnetic resonance
Prep-SEC	Preparative size-exclusion chromatography
GPC	Gel permeation chromatography
Bz	Benzyl
GOX	Glucoseoxidase
HRP	Horseradish peroxidase
CALB	Candida antarctica lipase B
ABTS	2,2'-azino-bis(3-ethylbenzothiazoline-6-sulphonic acid)
IEG	Iterative exponential growth
PEG-b-PS	Poly(ethylene glycol)-b-polystyrene
PEG-b-PABB	poly(ethylene glycol)-*b*-poly(acrylbenzylborate)
PBS	phosphate buffered saline
PAA	poly(acrylic acid)
GPC	gep permeation chromatography
SEC	size exclusion chromatography
CLSM	confocal laser scanning microscopy
PK	protein kinase

ATRP	atom transfer radical polymerization
RAFT	reversible addition-fragmentation chain transfer
PET-RAFT	photo induced electron transfer-RAFT
AUNP	gold nanoparticle
4-NPA	4-aminophol
AIBN	2,2′-Azobis(2-methylpropionitrile)
CTA	Chain transfer agent
AFM	Atomic force microscopy
FRET	Förster resonance energy transfer
P3HT	Poly(3-hexylthiophene)
P3EHT	Poly(3-ethylhexylthiophene)
CDSA	Crystallization-driven self-assembly
KCTP	Kumada catalyst transfer polymerization
SEM	Scanning electron microscope
TEM	Transmission electron microscope
DLS	Dynamic light scattering

AHBA	s)-4-amino-2-hydroxybutyric acid
MA	L-malic acid
TBAF	tetra-n-butylammonium fluoride
THF	Tetrahydrofuran
EDC	1-Ethyl-3-(3-dimethylaminopropyl)carbodiimide
$Pd(PPh_3)_4$	Tetrakis(triphenylphosphine)palladium(0)
HA	Hydroxyalkanoate
PHA	Polyhydroxyalkanoate
oHA	Oligo(hydroxyalkanoate)
T_m	Melting temperature
$Đ$	Polydispersity index
M_n	Number-average molecular weight
T_g	Glass transition temperature

Chapter 1. Introduction

1.1 Self-assembly of polymersomes as nanoreactors

Nowadays, highly elaborate control of the polymer nanostructures became possible due to the development of precise manipulation of the chemical structures and synthetic chemistry, including polymerization techniques and coupling chemistries.[1-3] The chemical structures and environment of the self-assembly affect both its motion in solution and interactions between polymer and surroundings, resulting in distinct nanostructures with different kinetic and behaviors.[4-10] In solution, block copolymers (BCPs) self-assemble to form micellar, vesicular, and periodic nanostructures. The morphology control of the structures is dictated by the properties of the BCPs such as dispersities, molecular weights, and block ratios.[11,12]

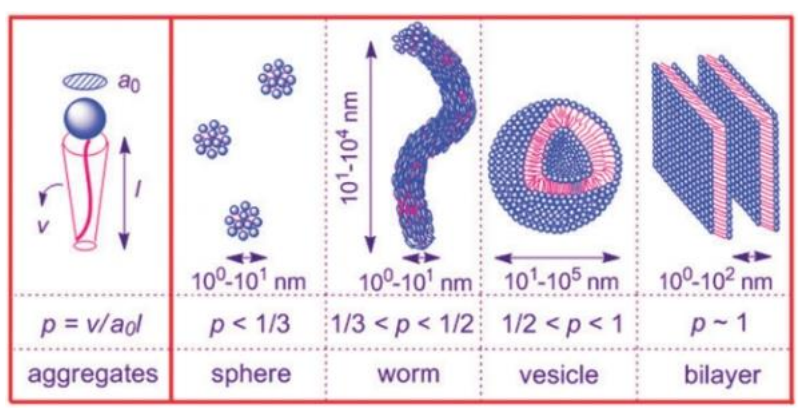

Figure 1-1. Relationship between the packing parameter (p) and the morphology of self-assembled surfactant aggregates.[13]

Among them, Polymersomes (or vesicles) are spherical hollow structures that are surrounded by a polymer bilayer membrane. The polymer must be amphiphilic to induce self-assembly in an aqueous solution. The formation of polymersomes requires the packing parameter of a BCP from 0.5 to 1. (Figure 1-1)[13] And diversity and versatility of the polymer lead to the numerous chemical and mechanical properties of the polymersomes and functional membrane. These properties directly dictated to the membrane permeability. Encapsulating chemical or biological substances within the polymersomes, cell mimetics, drug delivery systems or catalytic nanoreactors can be generated. But, when polymersome serves as nanoreactors, it often suffers from poor bilayer permeability coming from high molecular weight constituents of the polymers.[14] With this challenge in mind, there have been various approaches to employing tunable permeability for membranes. Only a few polymersomes are known to be intrinsically permeable to transport substances. For example, polymersomes made up of polystyrene-b-poly(isocyanoalanine(2-thiophen-3-yl-ethyl)amide) (PS-b-PIAT) are found to be semipermeable.[15,16] By introducing the channel proteins in the polymersome membranes, transportation of small substances across the membrane provides a new avenue for the development of permeable polymersomes.[17,18] Furthermore, recently, polymersomes that can adjust their membrane properties dependent on the environment have been reported.[19,20]

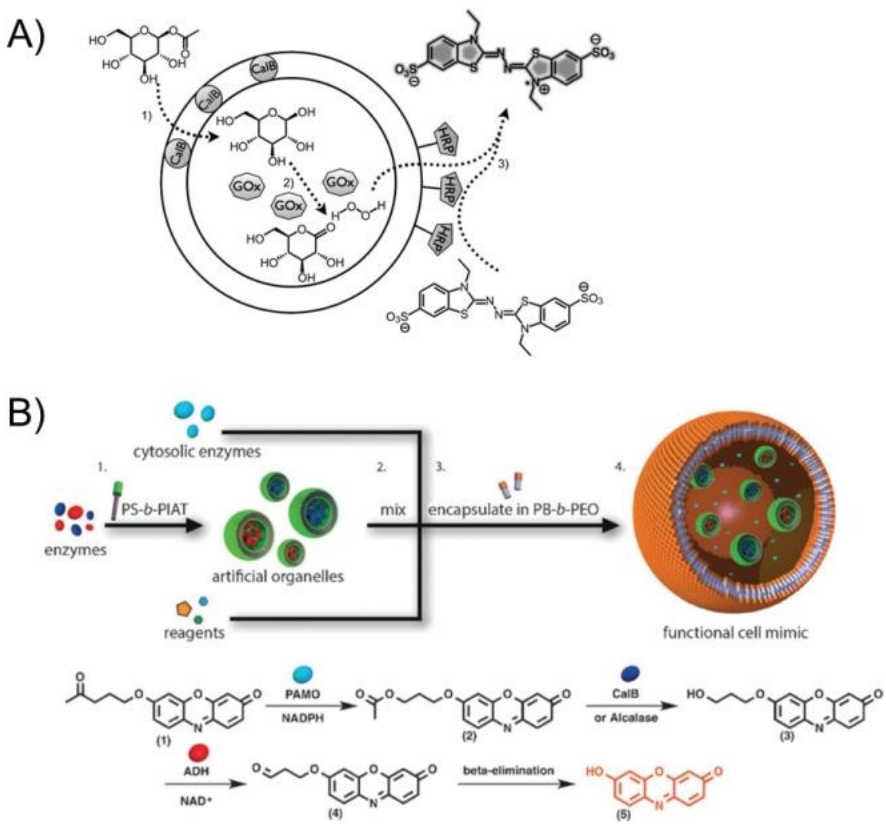

Figure 1-2. (A) Schematic representation of the multi-step reaction taking place in the three-enzyme-polymersome system. (B) Illustration of the functional cell mimic, which demonstrates the initial encapsulation of different enzymes in PS-b-PIAT polymersomes (1), followed by mixing of the nanoreactors, cytosolic enzymes and substrates (2), and encapsulation of the reaction mixture in PB-b-PEA vesicles (3) to create artifical cells (4), inside which enzymatic multicompartment catalysis takes place.

1.1.1.Intrinsically permeable polymersome nanoreactors As already mentioned, Van Hest group have shown that the PS-b-PIAT has a semipermeable membrane owing to the frustrating packing of the polymers. When small substrates such as enzymes or small molecules were encapsulated inside the vesicles, substrates could diffuse across the polymer membranes. For example, a multi-enzyme containing PS-b-PIAT nanoreactor was constructed by positioning different types of enzymes in the lumen and the polymersome membrane. Compartmentalization of enzymes was performed with three different enzymes at different places. In the inner pocket of the polymersomes, glucose oxidase (GOX) was positioned. And horseradish peroxidase (HRP) in the hydrophobic domain of the bilayer of the polymersomes, and Candida Antarctica lipase B (CALB), 1,2,3,4-tetra-O-acetyl-bglucopyranose (GAc4) and 2,2'-azino-bis(3-ethylbenzothiazoline-6-sulphonic acid) (ABTS) in the outside of the polymersomes. The conversion of GAc4 to glucolactone and release of H2O2 indicates the successful cascade reaction of the enzymes. The final product H2O2 was detected by the UV-vis spectrophotometer through the generation of $ABTS^{*+}$ from ABTS.[15] Furthermore, the development of cell mimetic systems having multi-compartmentalization was scarcely reported. To mimic the eukaryotic cell, polymersome-in-polymersome systems were developed and the encapsulated nanoreactors operated as artificial organelles. For the construction of this system, PS-b-PIAT polymersomes were adopted. Generated PS-b-PIAT nanoreactors and cytosolic enzymes and reagents were quantitatively encapsulated in polybutadiene-b-poly(ethylene oxide) (PB-b-PEO) polymersomes emulsion-centrifugation method. With this strategy, PS-b-PIAT polymersomes were captured inside the micron-sized PB-b-PEO polymersomes. Diffusion of the substrates and subsequent enzymatic reactions

inside the artificial organelles were confirmed with activity analysis (Figure 1-2). This polymersome-in-polymersome multi-compartmentalized system can serve as a functional or structural cell mimic.[21] Another polymersome nanoreactor composed of poly(2-methyl-2-oxazoline)-block-polydimethylsiloxane-block-poly(2-methyl-2-oxazoline) (PMOXA-b-PDMS-b-PMOXA) have developed by Meier and coworkers. These polymers were intrinsically permeable for O2, and $O2^{\bullet-}$.[17,18] This property makes MOXA-b-PDMS-b-PMOXA polymersomes a good candidate for the antioxidant nanoreactors via the encapsulation of Cu,Zn superoxide dismutase. Channel proteins, such as aquaporin Z, also can be introduced to the polymersomes and makes them permeable for a wider variety of substrates. The bacterial porin outer membrane protein F (OmpF) was also inserted into the polymersome membranes led to the efficient transportation of small molecules up to 600 Da.[18] To overcome the intrinsic permeability issues of polymersomes, stimuli-responsive polymers were utilized to endow polymersomes with adaptivity. The diverse set of external stimuli and biological signals can be introduced by the use of block copolymers with certain functionalities that can respond to tiny differences in the local environment. Under specific changes, these polymersomes can undergo phase or morphology changes that led to the destruction of permeability change of the membrane and release of the substrate inside the cargo. The unique tools for the engineering polymers have been developed and various stimuli-responsive polymersome nanoreactors have been reported.

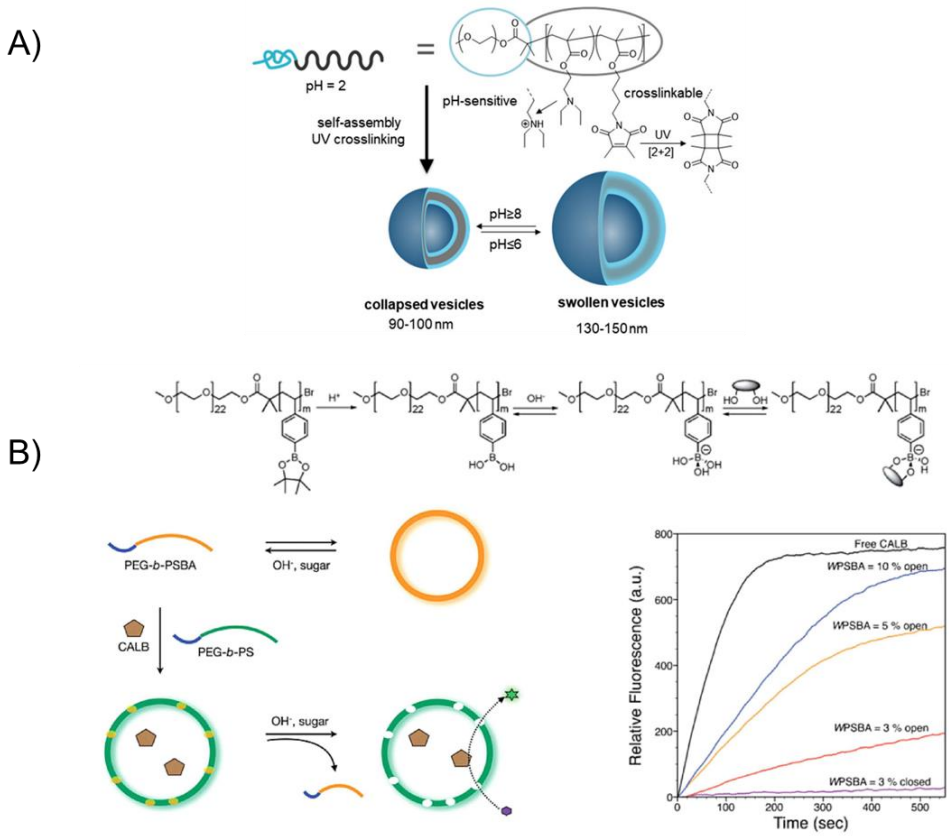

Figure 1-3. (A) Crosslinked pH-responsive polymersomes as bionanoreactors (B) Left: Schematic representation of the formation of polymersome nanoreactors with a permeable membrane utilizing the pH responsiveness of the block copolymer PEG-bPSBA. Right: Activity assay of the bioreactors prepared from the permeable polymersomes with WPSBA 3, 5, and 10%, compared to unencapsulated CALB and the closed polymersomes with WPSBA 3% encapsulating CALB in the inner compartment.

1.1.2. pH-responsive polymersome nanoreactors Inspired by the biomacromolecules using pH gradients in nature, pH-responsive polymersomes can be easily constructed with copolymers with pH-sensitive functionalities. The sensitive functional groups can undergo phase change or morphological transitions, leading to fine-tuning of the membrane permeability. pH-responsive Polymersomes composed of poly(2-(diethylamino)ethyl) methacrylate (PDEAEMA) were reported by Voit et al.[22] These polymersomes have a suitable pKa range for the application in the cellular environment. PEG as the hydrophilic part and PDEAEMA as the hydrophobic part, the polymersomes were self-assembled and pendant 3,4-dimethyl maleic imidoethyl methacrylate (DMIEM,) or 3,4-dimethyl maleic imidobutyl methacrylate (DMIBM) was adopted as cross-linker. The cross-linker help polymersomes can maintain their morphology regardless of pH conditions and enhance mechanical stability. The permeability of the membrane could be finely tuned by the cross-linking degree, shear rate, and pH conditions.

By introducing a portion of sacrificial copolymer with normal amphiphilic copolymer within the polymersomes, we can control the permeability of the polymersome nanoreactors. The sacrificial copolymer has a hydrophobic block with functional groups sensitive to the pH change in the environment. The functional groups become hydrophilic in response to the stimuli and subsequently dissolved into the solution leading to pore generation. Kim et al.[23] demonstrated this strategy by adopting a blending of two polymers: PEG-b-PS as the inert part and PEG-poly(styreneboronic acid) (PSBA) as pH-responsive part. In the basic condition and following the addition of saccharides such as glucose or fructose, the boronic acid forms a complex with saccharides with increased solubility of the PSBA block in water. Dissolution of the PSBA part led to the pore generation from

the polymersome bilayer. Owing to the inertness of PEG-PS under the basic condition and saccharides, Only PEG-PS was left and maintained the structure of polymersomes. The reaction kinetics of enzymatic reactions can be adjusted depending on the degree of porosity by varying the blending ratio between PEG-b-PSBA and PEG-b-PS (Figure 1-3).

1.1.2. Light-responsive polymersome nanoreactors Light-responsive undergoes a light-induced conformational change, degradation, and cleavage can be triggered with fast kinetics under simple exposure to light. These light-sensitive moieties have recently applied to self-assembly and gathered considerable attention. Especially, when light-responsive groups were employed in polymersomes, light-induced chemical transformations usually led to permeability changes. There were several reports to regulate the permeability of the polymersome nanoreactor by photoreactions. UV-responsive hydroxyalkylphenone-containing polymers were self-assembled to create photo-sensitive polymersome nanoreactors by Bruns et al.[24] Polymersomes were synthesized with two polymers: α,ω-hydroxy end-capped PMOXA-b-PDMS-b-PMOXA and double bond containing polymers. As double bond containing polymers, α,ω-acrylate end-capped PMOXA-b-PDMS-b-PMOXA, or PEO-b-PB were adopted. Here, water-soluble 2-hydroxy-4-2-(hydroxyethoxy)-2-methylpropiophenone (PP-OH) was used for the radical sources. UV irradiation generated two primary radicals which attacked the double bonds at the main chain blocks. In the proper reaction conditions, PP-OH was added to the hydrophobic polymer domains instead of cross-linking and enhanced the transmembrane permeability. Encapsulated HRP inside the polymersomes showed increased permeability with a light-triggered “ON” state.

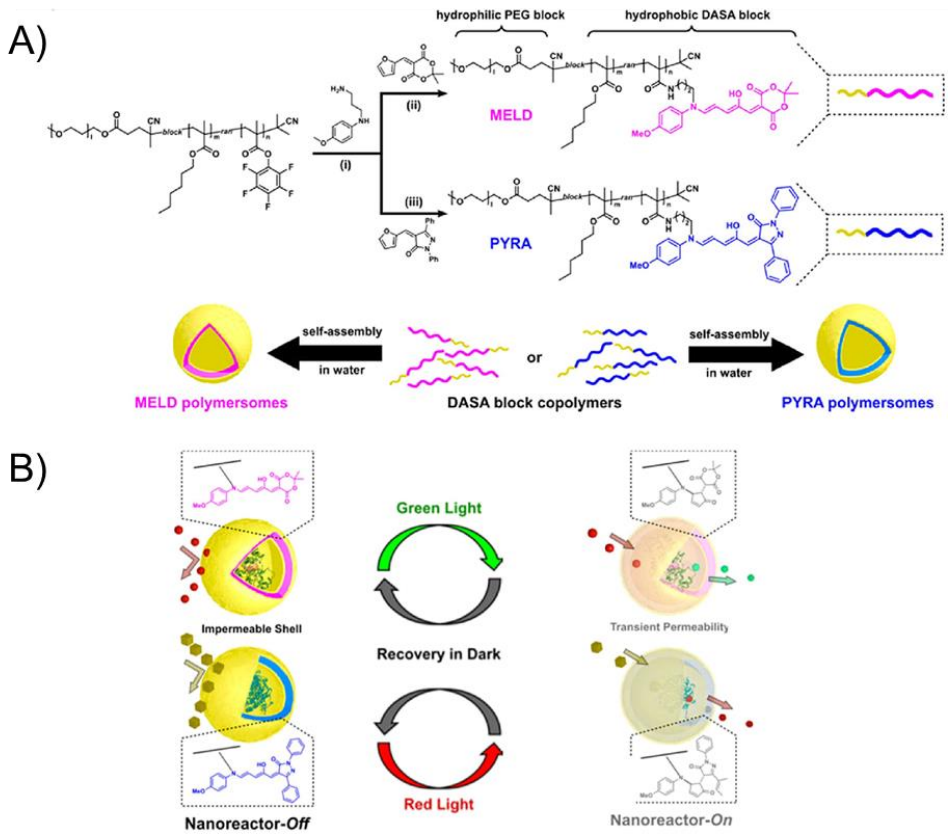

Figure 1-4. (A) Preparation of DASA-functionalized visible light-responsive polymersomes. DASA-functionalized block copolymers MELD and PYRA were synthesized in two steps from an active ester block copolymer. (B) Schematic representation of DASA-bearing visible light-responsive polymersome nanoreactors. Two different DASAs were conjugated with the polymersomes to serve as enzyme-loaded nanoreactors which responded to irradiation with green light and red light respectively. The DASA moieties in the hydrophobic part of the polymer membrane underwent a conformational change upon applying the light stimulus, leading to increased permeability of the polymersome membrane and

activation of the enzyme nanoreactor. The nanoreactors were restored back to their initial impermeable state when the light was turned off.

Recently, Bruns and coworkers reported another interesting research about applying Donor-Acceptor Stenhouse Adducts (DASAs) as photo-sensitive polymersome nanoreactors.[25] They synthesized polymers with PEG as hydrophilic part and poly(pentafluorophenyl methacrylate) (PFPMA) and poly(hexyl methacrylate) (HMA) as hydrophobic part. DASA moieties were randomly distributed along the hydrophobic backbones. DASAs have consisted of the precursor N-(4-methoxyphenyl)-1,3-diaminepropane (MPDP) having aromatic amine and conjugated activated ester. DASAs could isomerize under the visible light irradiation and lead to the permeability change of the polymersome membrane by a conformational change. After the irradiation, triene-enol was converted to cyclopentenone with more polarity. Visible light-triggered polymersomes to an "ON" state that can release the hydrophilic substrates inside the polymersomes and provoke enzymatic reactions. This can be turned off right after the removal of irradiation. Two DASAs having different wavelengths (red and green) were utilized for the polymersome nanoreactors. Two classes of nanoreactors were mixed and showed independent activity with red and green light irradiation conditions. This allowed the one-pot cascade reaction of biocatalysts inside the individual polymersomes under the specific wavelength (Figure 1-4).

1.1.3. Self-adaptive polymersome nanoreactors To make biomimetic systems, it will be an interesting topic to create self-assembly systems that can adapt to the

nature of out-of-equilibrium. Biomolecules usually undergo functional operations after exposure to a specific substrate called “fuel”. These biomimetic fuel-driven out-of-equilibrium systems have been reported from various materials. But there have been limited reports about the self-adaptive polymersome nanoreactors that operate by energy consumption. Van Hest group demonstrated an enzymatic reaction network out of equilibrium through the compartmentalization and autonomous fueling systems.[19] To approach the sustained autonomous movement, the stomatocyte, which can be made from shape transformation of PEG-b-PS vesicles. The osmotic pressure during the self-assembly process led to the bowl-shaped stomatocyte. By encapsulating enzymes, stomatocyte-based nanoreactors were formed. Glucose and phosphoenol pyrvuate (PEP) were used as energy fuels. Glucose is consumed by hexokinase (HK) in the presence of ATP. ATP could be regenerated with Pyruvate Kinase (PK). Here, ATP concentration affected the consumption of glucose. So the conversion rate of glucose in the system was decoupled from the initial concentration of glucose. PK initiated another cycle. PK converted PEP to pyruvate and entered the pyruvate-L-lactate cycle. In this case, pyruvate was consumed by L-lactate dehydrogenase (LDH). Otherwise, L-lactate oxidase (LO) consumed the L-lactate and generate H_2O_2. Subsequent conversion of H_2O_2 to O2 by catalase (CAT) activates the motorcycle and brought out the movement of the stomatocyte (Figure 1-5).

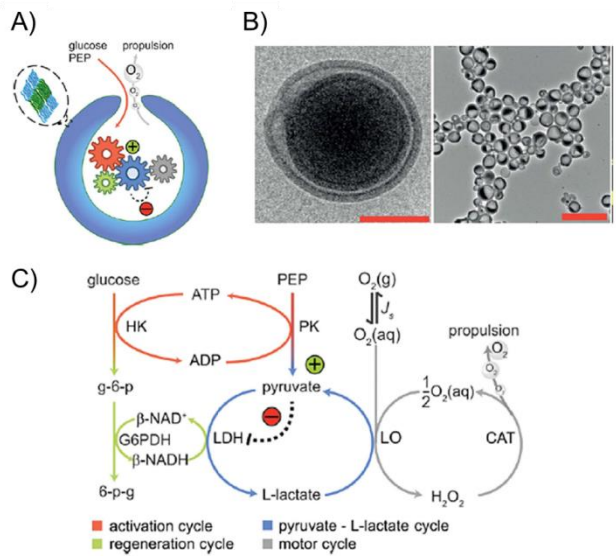

Figure 1-5. (A) Schematic representation of the stomatocyte nanoreactors containing four enzymatic cycles which are utilized to convert glucose and phosphoenolpyruvate (PEP) into movement of the nanoparticles. (b) Cryo-transmission electron microscopy (cryo-TEM, left) and TEM (right) images of the nanoreactors loaded with the enzymatic network. Scale bars 100 nm (left) and 1 μm (right). (c) Rational design of a metabolic pathway for double cycling of natural substrates leading to autonomous movement.

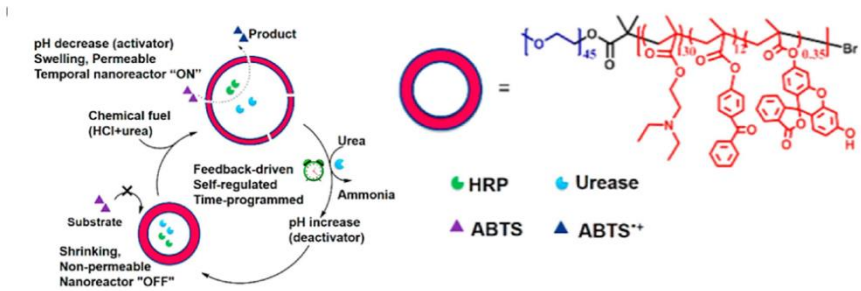

Figure 1-6. (A) Schematic overview of feedback-induced temporal control of polymersome nanoreactors.

More recently, self-regulation of polymersome nanoreactor in a time-programmed manner was also reported in the same group.[20] This time, a "breathing" microgel system was applied at polymersome nanoreactors. Diethylamine which can regulate the swelling rate dependent on the pH was incorporated into a crosslinked polymer network. Urease inside the polymersomes maintains the initial basic condition by changing urea into ammonia which indicated the deswelling of the polymers. Continuous addition of diethylamine as a chemical fuel, the polymersome repeated shrink and relaxed several times. This process endowed the polymersomes with biomimetic "breathing" features (Figure 1-6). The basic strategy of these researches will support the future direction for the engineering of nanoreactors with various features.

1.2 Discrete polymer

Recently, synthetic methods and applications of ultra-precise sequence-defined polymers gathered considerable attention. Many researchers attempted to find new synthetic tools to prepare chemically well-defined polymers including sequences and dispersities.[26-28] Combined with synthetic methodologies, the relation between structure and property endowed various promising applications. Information

storage and decryption with discrete polymers, and self-assembly with precisely defined sequences have fascinated polymer chemists.

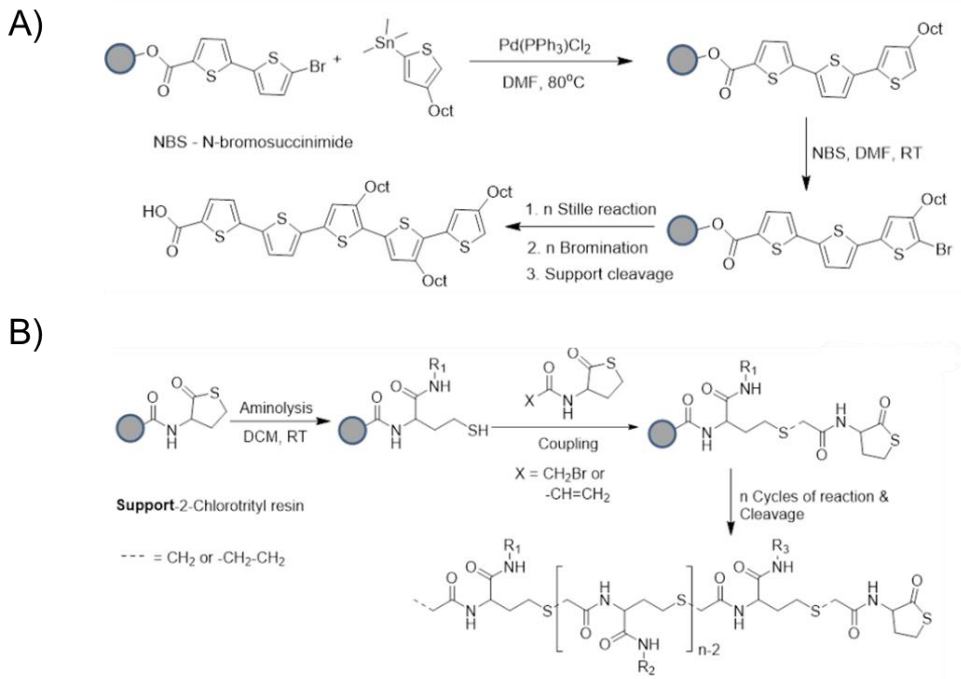

Figure 1-7. (A) Schematic overview of synthesis of solid-supported oligothiophene by stille coupling reaciton (B) Schematic overview of synthesis of solid-supported oligomer with amide-thioether using thiolactone chemistry.

1.2.1. Synthetic approaches One of the representative methods for the synthesis of discrete polymers is solid-phase synthesis (SPS).[29] Even though this strategy was developed for the synthesis of peptides, many researchers adopted SPS for the synthesis of non-natural discrete polymers. the formation of discrete synthetic oligomers. Owing to the facile purification process, many organic reactions for the synthesis of discrete oligomers were demonstrated including stille reaction of

oligothiophenes (Figure 1-7 (A)),[30] copper-catalyzed azide-alkyne cycloadditions,[31] thiolactone chemistry (Figure 1-7 (B)),[32,33] and passerini reactions.[34] But there were some drawbacks such as low reaction rate and aggregation of oligomers. To overcome these problems, soluble supports were utilized to synthesize the discrete oligomers. This strategy improves the reaction rate and ease of stepwise monitoring by analytic tools. Soluble polymers such as polystyrenes or fluorous hydroxyproline supports were used to achieve soluble-supported polymer synthesis.[35,36]

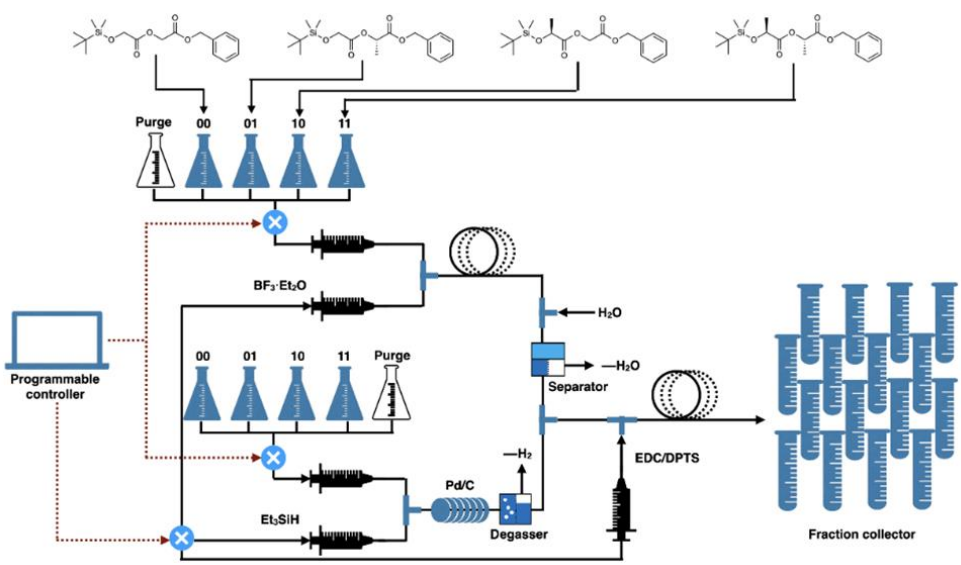

Figure 1-8. (A) Schematic illustrations of the continuous flow process for the iterative exponential growth. Synchronous deprotection of selected dyads and subsequent coupling are performed. All permutations of tetrads are generated by a single continuous flow.

Still, synthesis mainly relies on repeated step-by-step addition of individual monomers which hindered to approaching of the prerequisites of the polymers (scalability and chain length) novel synthetic pathway for the design of chemically well-defined unique polymers was still necessary. Iterative coupling of building blocks has been widely adopted for the synthesis of precisely defined polymers. In this process, afforded coupling product can be transformed into a constituent unit for the next iterative coupling reactions after simple modification steps. Thus, the molecular weight of the resulting polymer can grow exponentially without dispersities. This iterative exponential growth (IEG) provides the drawback for the chain length of the discrete polymers.[37-40] And some reports assisted that high scalability and chain length can be achieved via support-based strategies or continuous flow chemistry. Fuzeon et al.[41] Reported a peptide with 36 repeating units is synthesized on a multiton scale by combining solid and solution phase strategies. And Luts and coworkers synthesized polymers with the degree of polymerization (DP) higher than 100 monomer units using the phosphoramidite approach.[42,43] Recently, Kim group successfully synthesized the sequence-defined PLGA polymers using continuous flow chemistry.[44] Automated and programmable synthesis provided reduced reaction time, and easy scalability. These approaches offer the solution to the limitation of iterative reaction methods (Figure 1-8).

Although there are some examples of breakthroughs, IEG methods still require labor-intensive processes, especially in the purification steps. Hawker et al. published the unique protocol for the purification of monodisperse polymer from the commonly used polymer such as styrene, acrylate, siloxanes, etc.[45] The synthetic availability of discrete oligomers, combined with automated column

chromatography provides opportunities for the simple preparation of discrete oligomers.

1.2.2. Information storage of discrete synthetic polymers Synthetic sequence-defined polymers have recently been gathered attention as information storage media alternatives. Biopolymers such as DNA are regarded as a good candidate for data storage as nature already has optimized the storing and decoding processes over the last decades.[46-49] But some limitations of the biopolymers such as hydrolysis of phosphodiester backbone, limited Shannon capacity,[50] expensive building blocks gave sequence-defined synthetic polymers opportunities as alternatives for the information storage media. Using polymers, denser information storage could potentially be possible by the incorporation of different repeating monomers as individual 'bit' while DNA only composed of four different nucleobases. Boukis and Meier group demonstrated this principle by using 116 different building blocks with the combination of two multicomponent reactions.[51] This strategy allowed them overall 24 bits per unit of data storage. Another example was reported recently using passerini three-component reactions.[52] Two different reagents participate in one passerini reaction and can store individual information. This led to the denser storage capacities than in previous reports. Du Prez group demonstrated a similar method of synthetic sequence-defined oligomers which can encode the QR code.[53] The introduc In this case, they used 15 acrylate units for the building blocks to avoid the need for longer polymer chains. They adopted two-step iterative strategy (aminolysis followed by michael addition) for the synthesis of amide-thioether-based polymer by using thiolactone building blocks. Of course, macromolecules with longer polymer chains were demonstrated as data storage media. Another strategy to enhance the information storage power

is the adoptation of macromolecules composed of the smaller molecular alphabet (i.e. binary code). However, it requires labor-intensive synthetic steps. But there were recently reported examples that can attenuate the difficulties. Kim and co-workers demonstrated the scalable synthesis of high molecular weight binary encoded polyester up to 38 kDa. Cross-convergent synthetic pathways and purification methods using preparative size exclusion chromatography provided facile preparation of high-storage sequence-defined polymers.[54]

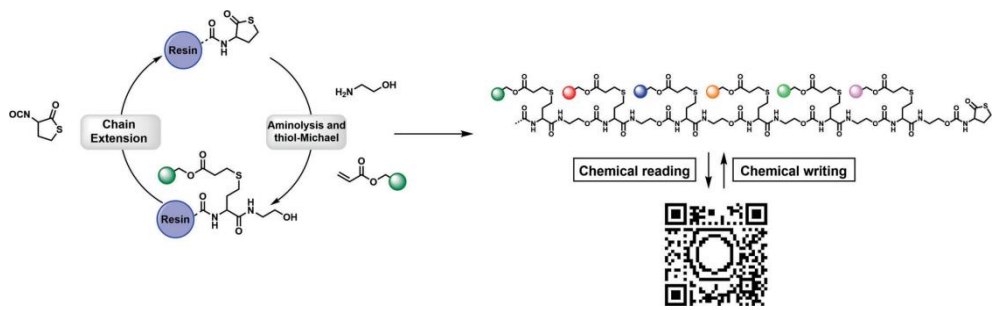

Figure 1-9. (A) Schematic overview of synthesis of solid-supported oligothiophene by stille coupling reaciton (B) Schematic overview of synthesis of solid-supported oligomer with amide-thioether using thiolactone chemistry.

1.2.3. Self-assembly of discrete synthetic polymers Discrete polymers also can be used for self-assembly into high-ordered complex structures. Uncountable examples are having highly-ordered structures induced by the interactions among the building blocks.[55,56] Cellular membranes or coat proteins covering the viruses can be typical examples. Theoretical models of the molecular self-assembly of small amphiphilic molecules have already been extensively studied to predict the behavior.[57] We can predict that a similar tendency of assembly will occur from the block copolymers. But dispersity of the actual

polymers usually hampers the sophisticated self-assembly behavior. Fortunately, continuous development of the synthetic methodologies enabled the synthesis of sequence-controlled polymers without dispersity. Hawker and Meijer have reported that self-assembly behavior ia dramatically affected by dispersity.[58] In their work, they synthesized discrete poly(dimethylsiloxane-b-lactic acid) PDMS-b-PLA block copolymers that have a high χ-parameter between the blocks. Discrete block copolymers with a molecular weight below 7 kDa and the volume fraction of lactic acid from 025 to 0.5 were self-assembled. Except the low fraction of lactic acid BCPs, distinct bulk morphologies were observed different from the disperse polymer groups. Hawker group published similar experimental reports with poly(dimethylsiloxane-b-methyl methacrylate) (PDMS-b-PMMA).[38] When the polymer has crystalline domains, the effect of uniformity gets further highlighted. Compared to BCPs composed of atactic lactic acid, crystalline (l)-lactic acid containing BCPs showed more uniform domain spacing and ordering. Meijer and coworkers also reported the self-assembly behavior not only in the bulk state but also in the solution state with ABA-type BCPs (Figure 1-10).[60] Discrete poly(ethylene glycol-b-(l)-lactic acid) (PEG-b-PLLA) showed gel-like properties in the water, while dispersed BCPs with similar molecular weight and block ratio dissolve in the same condition. Johnson et al. developed an innovative synthetic method called iterative exponential growth (IEG) for the synthesis of sequence-defined polymers.[61,62] They used copper-catalyzed azide-alkyne cycloaddition (CuAAC) to couple the building blocks. Epoxide rings were used to introduce the azide anion into the backbones. By introducing allyl groups as pendant groups, they can introduce various side chains via radical thiol-ene reactions. Dependent on the side chains, the polymers showed different self-assembly behavior. Polymers

undergo microphase separation at bulk state to form hexagonally packed cylinders with domain sizes that directly correlate with their molecular structures.

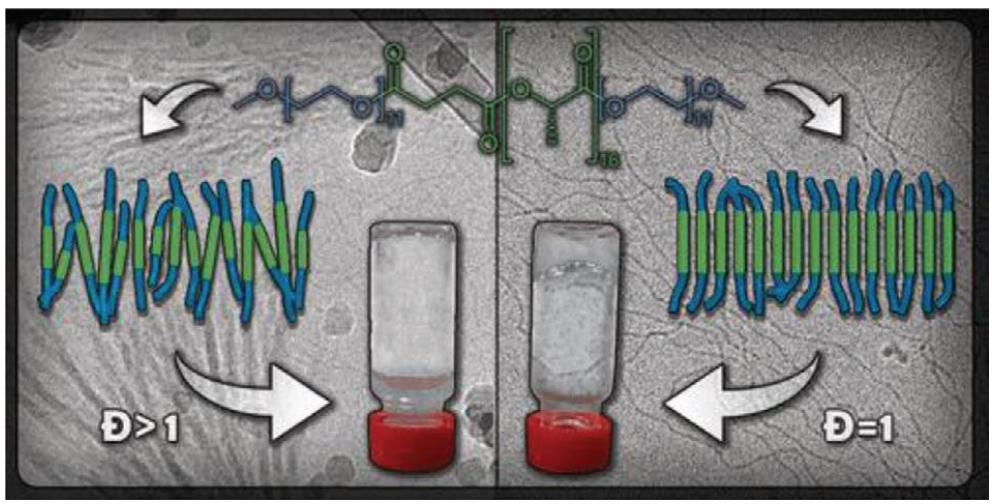

Figure 1-10. (A) Discrete ABA-type block copolymer with ethylene glycol and (l)-lactic acid blocks studied by Meijer and co-workers formed a transparentgel in water. Introduction of chain length variation (Đ = 1.2) in the (l)-lactic acid block inhibited the self-assembly and led to solubility under the same conditions.

Biomacromolecules which can interact with each other with programmed sequences showed predictable and higher-ordered structures. Indeed, DNAs or proteins having certain sequences self-assembled to uniform structures. Of course, synthetic macromolecules equipped with complementary recognition units, have the potential to form sequence-selective duplexes. But there have been a limited number of reports using molecular interactions between the sequence-defined polymers. Polymers having a rigid backbone composed of m-terphenyl-diacetylene

were well known to form double helices.[63] By introducing side chains capable of molecular interactions, these rigid oligomers can form duplexes. Salt bridges between amidine and carboxylic acid groups at the pendant groups connected each oligomer and formed duplexes. A rigid backbone hampered the intramolecular folding and assisted the preparation of hetero-oligomers. A similar duplex formation can also be accomplished with the introduction of hydrogen bond donor and phosphine oxide as hydrogen bond acceptor as pendant groups (Figure 1-11).

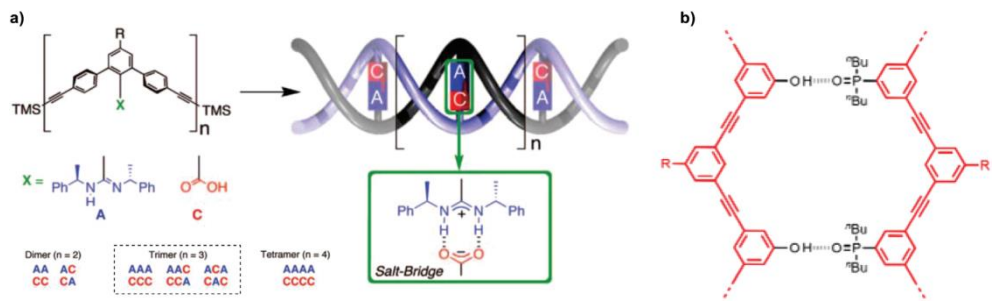

Figure 1-11. (A) Schematic overview of synthesis of solid-supported oligothiophene by stille coupling reaciton (B) Schematic overview of synthesis of solid-supported oligomer with amide-thioether using thiolactone chemistry.

Duplex formation with a more flexible backbone was also reported from Hunter and co-workers.[64] Strong hydrogen bond acceptors such as phosphine oxide, pyridine, and pyridine oxide were utilized in combination with phenol as hydrogen bond donors. It was demonstrated that a flexible property of the backbone hampers the duplex formation between the oligomers as intramolecular fording can compete with complexation between the functional moieties. These dynamic nature of the non-covalent interactions can be also substituted with dynamic covalent chemistry. Scott group adopted dynamic covalent Scandium-catalyzed imine metathesis for

the formation of duplexes in a sequence-selective manner.[65-67] They used peptoid as backbone owing to the synthetic efficiency using the submonomer strategy and the facile introduction of side groups. Σ-strand of peptoid backbone is expected to make corona-like side chains that can easily form an imine bond between the aldehyde and amine moieties. A catalytic amount of scandium triflate with the same length of oligomer pairs generated the duplexes. Although initially formed imine bonds result in misaligned duplexes, reshuffling among the dynamic covalent bonds led to the thermodynamically stable duplexes. In a later study, sequence-selective hybridization of mixed sequence oligomers containing dynamic covalent imine bonds was investigated.[67] Three pairs of sequence-complementary oligomers were prepared and mixed together. Dependent on the scandium triflate catalyst concentration, the equilibrium could be shifted. After the reshuffling among the pairs, catalyst removal by aqueous extraction led to the annealed oligomers with sequence-specific duplexes (Figure 1-12).

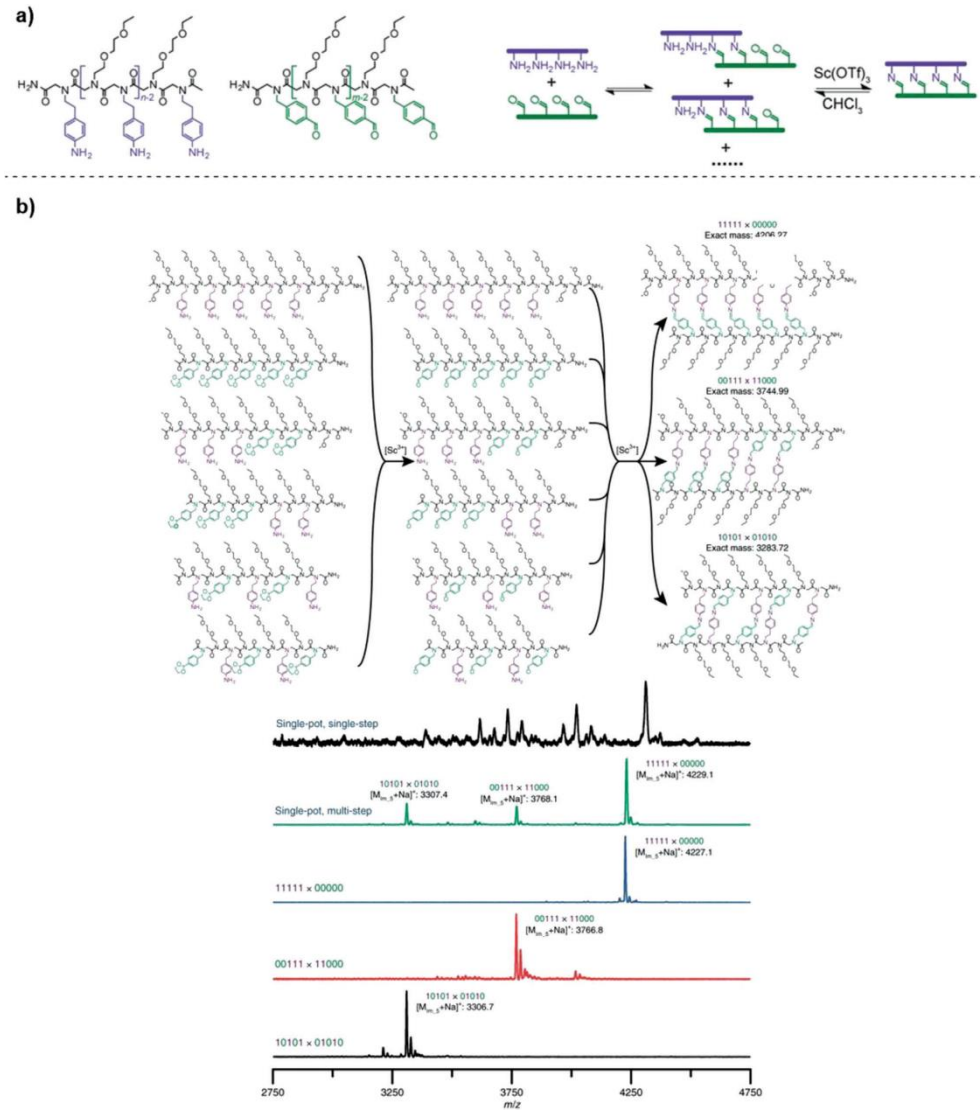

Figure 1-12. (A) Schematic overview of synthesis of solid-supported oligothiophene by stille coupling reaciton (B) Schematic overview of synthesis of solid-supported oligomer with amide-thioether using thiolactone chemistry.

1.4 Summary of thesis

This dissertation reports the synthesis of block copolymers containing different functionalities and charactertistics. The molecular structures of these copolymers directly affected the self-assembly structures. Well-defined self-assembly structures require precisely determined chemical structures. Monomers with specific functionality or characteristics directly polymerized with various polymerization techniques such as RAFT polymerization, ATRP, KCTP, and Iterative exponential growth. Prepared polymers showed different self-assembly behaviors dependent on the various factors including oxidation responsiveness, crystallinity of conjugated polymers, and dispersity (discrete polymer), ionic interaction between hydrophilic groups. I expect the self-assembly behaviors of the polymers will enable elaborate construction of the structures with prediction.

Chapter 2 reported a method for controlling the permeability of the polymersomes of the binary blend of (PEG-*b*-PS) and stimuli-responsive poly(ethylene glycol)-b-poly(acrylbenzylborate) (PEG-*b*-PABB). The presence of H_2O_2 in the medium triggers the oxidation of benzyl borate pendants of PABB to form poly(acrylic acid) (PAA). This transformation results in the pore generation of the compartmentalizing membrane of polymersomes by the dissolution of PEG-b-PAA domains embedded in the inert PEG-b-PS matrix. By controlling the composition of the stimuli-responsive block copolymer, the polymersomes of the binary blend exhibit size-selective permeability without losing the structural integrity. Release of fluorescent guests with different sizes can be controlled by tuning the composition of blended polymersomes. Selective permeability of the membrane provides protection of the encapsulated enzymes from external

proteases present in the medium, resulting in the one-pot synthesis of small molecules via cascades of chemical reactions. The nanoparticular catalysts are also encapsulated within the permeable polymersomes, serving as modular reactors for the conversion of organic compounds via a cascade of reactions.

Chapter 3 demonstrated the preparation method for the poly(3-hexylthiophene) (P3HT) based nanofibers with controllable lengths and enhanced solubility. Conventional P3HT has high crystallinity thereby reflecting the efficient electrical properties. But this property is accompanied by brittleness and low solubility. To overcome the disadvantages of P3HT, we synthesized a conjugated block copolymer composed of crystalline P3HT with amorphous Poly(3-etyhlhexylthiophene) P3EHT (P(3HT-*b*-3EHT)). The amorphous P3EHT corona enhanced the solubility of the block copolymer and enabled living CDSA in volatile cyclohexane. The block copolymer can be self-assembled to form 1D nanofibers and their lengths can be controlled with self-seeding method. In TEM image, entanglement and bendage of the nanofiber were observed owing to the amorphous corona. Through simple evaporation of nanofiber dispersion, we demonstrated the fabrication of flexible P(3HT-*b*-3EHT) nanofiber films.

In Chapter 4, we demonstrated unique faceted vesicles with charged ionic block copolymer complex. We used the convergent method to synthesize monodisperse and precisely defined block co-oligomers (BCOs) having the tetramers of L-malic acid or (s)-4-amino-2-hydroxybutyric acid as a hydrophilic block and oligo(lactic acid) as a hydrophobic block. These oppositely charged BCOs, with an absolutely defined number of cations or anions were mixed for the co-assembly in water. Indeed, ionic interaction between assembled block co-oligomers opposes the

membrane's natural curvature and leads to the faceting of the membranes. The self-assembled structures were characterized by Cryo-TEM and DLS.

Excerpts from the following chapters have already been published:

Chapter 2: Kim, J.; Jeong, S.; Shin, K.; Kim, K. T. Cross-linked Polymersomes with Reversible Deformability and Oxygen Transportability. Biomacromolecules 2019, 20, 2430–2439.

1.5 References

1. Vicini, P.; Incerti, M.; La Colla, P.; Loddo, R. Anti-HIV evaluation of benzo[d]isothiazole hydrazones. *Eur. J. Med. Chem.* **2009**, *44*, 1801−1807.
2. Lehn, J. -M. Perspectives in Chemistry-Steps towards Complex Matter. *Angew. Chem. Int. Ed*. **2013**, *52*, 2836−2850.
3. Zhou, X. -P.; Wu, Y.; Li, D. Polyhedral Metal-Imidazolate Cages: Control of Self-Assembly and Cage to Cage Transformation. *J. Am. Chem. Soc*. **2013**, *135*, 16062−16065.
4. van Hest, J. C. M.; Delnoye, D. A. P.; Baars, M. H. P.; van Genderen, M. H. P. Meijer, E. W. Polystyrene-Dendrimer Amphiphilic Block Copolymers with a Generation-Dependent Aggregation. *Science* **1995**, *268*, 1592−1595.
5. Zhang, L.; Eisenberg, A. Multiple Morphologies of "Crew-Cut" Aggregates of Polystyrene-b-poly(acrylic acid) Block Copolymers. *Science* **1995**, *268*, 1728−1731.

6. Kim, K. T.; Meeuwissen, S. A.; Nolte, R. J. M.; van Hest, J. C. M. Smart nanocontainers and nanoreactors. *Nanoscale* **2010**, *2*, 844−858.

7. Renggli, K.; Baumann, P.; Langowska, K.; Onaca, O.; Bruns, N.; Meier, W. Selective and Responsive Nanoreactors. *Adv. Funct. Mater*. **2011**, *21*, 1241−1259.

8. Brinkhuis, R. P.; Rutjes, F. P. J. T.; van Hest, J. C. M. Polymeric vesicles in biomedical applications. *Polym. Chem*. **2011**, *2*, 1449−1462.

9. Massignani, M.; Lopresti, C.; Blanazs, A.; Madsen, J.; Armes, S. P.; Lewis, A. L.; Battaglia, G. *Small* **2009**, *5*, 2424−2432.

10. Onaca, O; Enea, R.; Hughes, D. W.; Meier, W. *Macromol. Biosci.* **2009**, 9, 129−139.

11. Zhang, L.; Yu, K.; Eisenberg, A. *Science* **1996**, *272*, 1777−1779.

12. Zhang, L.; Eisenberg, *J. Am. Chem. Soc.* **1996**, *118*, 3168−3181.

13. La, Y.; An, T. H.; Shin, T. J.; Park, C.; Lee, E.; Kim, K. T. *Angew. Chem. Int. Ed*. **2015**, *54*, 10483−10487.

14. Discher, D. E.; Eisenberg, A. *Science* **2002,** *297*, 967–973

15. Vriezema, D. M.; Garcia, P. M.; Sancho Oltra, N.; Hatzakis, N. S.; Kuiper, S. M.; Nolte, R. J.; Rowan, A. E.; van Hest, J. C. M. *Angew. Chem. Int. Ed.* **2007**, *119*, 7522–7526

16. Vriezema, D. M.: Hoogboom, J.; Velonia, K.; Takazawa, K.; Christianen, P. C.; Maan, J. C.; Rowan, A. E.; Nolte, R. J. *Angew. Chem. Int. Ed.* **2003**, *42*, 772–776

17. Kumar, M.; Grzelakowski, M.; Zilles, J.; Clark, M.; Meier, W. *Proc. Mont. Acad. Sci*. **2007**, *104*, 20719–20724

18. Langowska, K.; Palivan, C. G.;Meier, W. *Chem. Commun*. **2013**, *49*, 128–130.

19. Nijemeisland, M.; Abdelmohsen, L. K.; Huck, W. T.; Wilson, D. A.; van Hest, J. C. M. *ACS Cent. Sci.* **2016**, *2*, 843–849.

20. Che, H.; Cao, S.; van Hest, J. C. M. *J. Am. Chem. Soc*. **2018**, *140*, 5356–5359.

21. Peters, R. J.; Marguet, M.; Marais, S.; Faraaije, M. W.; Van Hest, J. C. M.; Lecommandous, S. *Angew. Chem. Int. Ed*. **2014**, *126*, 150–154.

22. Gaitzsch, J.; Appelhans, D.; Wang, L.; Battaglia, G.; Voit, B. *Angew. Chem. Int. Ed*. **2012**, *51*, 4448–4451;

23. Kim, K. T.; Cornelissen, J. J. L. M.; Nolte, R. J. M.; van Hest, J. C. M. *Adv. Mater.* **2009**, *21*, 2787–2791.

24. Spulber, M.; Najer, A.; Winkelbach, K.; Glaied,O.; Waser, M.; Pieles, U.; Meier, W.; Bruns, N. *J. Am. Chem. Soc.* **2013**, *135*, 9204–9212.

25. Rifaie-Graham, O.; Ulrich, S.; Galensowske, N. F. B.; Balog, S.; Chami, M.; Rentsch, D.; Hemmer, J. R.; Read de Alaniz, J.; Boesel, L. F.; Bruns, N. *J. Am. Chem. Soc.* **2018**, *140*, 8027–8036.

26. Solleder, S. C.; Schneider, R. V.; Wetzel, K. S.; Boukis,A. C.; Meier, M. A. R. *Macromol. Rapid Commun.* **2017**, *38*, 1600711.

27. Ouahabi, A. Al.; Charles, L.; Lutz, J. F. *J. Am. Chem. Soc.* **2015**, *137*, 5629.

28. Li, J.; Leclercq, M.; Fossepré, M.; Surin, M.; Glinel, K.; Jonas, A. M.; Fernandes, A. E. *Polym. Chem.* **2020**, *11*, 4040.

29. Merrifield, R. B. *J. Am. Chem. Soc.* **1963**, *85*, 2149.

30. Malenfant, P. R. L.; Frechet, J. M. J. *Chem. Commun.* **1998**, 2657-2658.

31. Pfeifer, S.; Zarafshani, Z.; Badi, N.; Lutz, J.-F. *J. Am. Chem. Soc.* **2009**, *131*, 9195.

32. Espeel, P.; Carrette, L. L. G.; Capenberghs, K. Bury, S.; Martins, J. C.; Du prez F. E.; Madder, A. *Angew. Chem. Int. Ed.* **2013**, *52*, 13261-13264.

33. Trinh, T. T. Laure C.; Lutz, J. F. *Macromol. Chem. Phys.* **2015**, *216*, 1498-1506.

34. Hill, S. A.; Gerke, C.; Hartmann, L.; *Chem. - Asian J*. **2018**, *13*, 3611

35. Amrane, M. I.; Chouikhi, D.; Badi, N.; Lutz, J. F. *Macromol. Chem. Phys.* **2014**, *215*, 1984.

36. Porel, M.; Alabi, C. A. *J. Am. Chem. Soc.* **2014**, *136*, 13162.

37. Barnes, J. C.; Ehrlich, D. J. C.; Gao, A.; X. Leibfarth, F. A.; Jiang, Y.; Zhou, E.; Jamison, T. F.; Johnson, J. A. *Nat. Chem.* **2015**, *7*, 810–815

38. van Genebeck, B.; De Waal, B. F. M.; Gosens, M. M. J.; Pitet, L. M.; Palmans, A. R. A. *J. Am. Chem. Soc.* **2016,** *138*, 4210–4218

39. Takizawa, K.; Tang, C.; Hawker, C. J. *J. Am. Chem. Soc.* **2008**, *130*, 1718–1726

40. Amir, F.; Jia, Z.; Monteiro, M. J. *J. Am. Chem. Soc*. **2016** ,*138*, 16600–16603

41. Bruckdorfer, T.; Marder, O.; Albericio, F. *Curr. Pharm. Biotechnol*. **2004**, *5*, 29

42. Al Ouahabi, A.; Kotera, M.; Charles, L.; Lutz, J. F. *ACS Macro Lett*. **2015**, *4*, 1077.

43. Zhang, Y.; Antunez, P. M.; Fortuin, L.; Andren, O. C. J.; Malkoch, M. *Biomacromolecules* **2020**, *21*, 4294

44. Lee, J. M.; Kwon, J.; Lee, S. J.; Jang, H.; Kim, D.; Song, J.; Kim, K. T. *Sci. Adv.* **2022**, *8*, eabl8614

45. Lawrence, J.; Lee, S.-H.; Abdilla, A.; Nothling, M. D.; Ren, J. M.; Knight, A. S.; Fleischmann, C.; Li, Y.; Abrams, A. S.; Schmidt, B. V. K. J.; Hawker, M. C.; Connal, L. A.; McGrath, A. J.; Clark, P. G.; Gutekunst, W. R.; Hawker, C. J. *J. Am Chem. Soc*. **2016**, *138*, 6306-6310

46. Erlich, Y.; Zielinski, D. *Science* **2017**, *355*, 950.

47. Newman, S.; Stephenson, A. P.; Willsey, M.; Nguyen, B. H.; Takahashi, C. N.; Strauss, K.; Ceze, L. *Nat. Commun*. **2019**, *10*, 1706.

48. Ceze, L.; Nivala, J.; Strauss, K. *Nat. Rev. Genet.* **2019**, *20*, 456.

49. Anavy, L.; Vaknin, I.; Atar, O.; Amit, R.; Yakhini, Z. *Nat. Biotechnol*. **2019**, *37*, 1229.

50. Azzarito, V.; Long, K.; Murphy, N. S.; Wilson, A. J. *Nat. Chem.* **2013**, *5*, 161.

51. Boukis, A. C.; Meier, M. A. R. *Eur. Polym. J*. **2018**, *104*, 32.

52. Wetzel, K. S.; Frölich, M.; Solleder, S. C.; Nickisch, R.; Treu, P.; Meier, M. A. R. *Commun. Chem*. **2020**, *3*, 63.

53. Martens, A.; Landuyt, P.; Espeel, B.; Devreese, P.; Dawyndt, F. Du Prez, *Nat. Commun*. **2018**, *9*, 4451.

54. Lee, J. M.; Koo, M. B.; Lee, S. W.; Lee, H.; Kwon, J.; Shim, Y. H.; Kim, S. Y.; Kim, K. T. *Nat. Commun*. **2020**, *11*, 56.

55. Liu, Z.; Qiao, J.; Niu, Z.; Wang, Q. *Chem. Soc. Rev.* **2012**, *41*, 6178.

56. Mendes, A. C.; Baran, E. T.; Reis, R. L.; Azevedo, H. S. *Wiley Interdiscip. Rev.: Nanomed. Nanobiotechnol*. **2013**, *5*, 582.

57. Lombardo, D.; Kiselev, M. A.; Magazù, S.; Calandra, P. *Adv. Condens. Matter Phys.* **2015**, *2015*, 151683

58. Oschmann, B.; Lawrence, J.; Schulze, M. W.; Ren, J. M.; Anastasaki, A.; Luo, Y.; Nothling, M. D.; Pester, C. W.; Delaney, K. T.; Connal, L. A.; McGrath, A. J.; Clark, P. G.; Bates, C. M.; Hawker, C. J. *ACS Macro Lett.* **2017**, *6*, 668.

59. Das, A.; Petkau-Milroy, K.; Klerks, G.; van Genabeek, B.; Lafleur, R. P. M.; Palmans, A. R. A.; Meijer, E. W. *ACS Macro Lett*. **2018**, *7*, 546.

60. Jiang, Y.; Golder, M. R.; Nguyen, H. V. T.; Wang, Y.; Zhong, M.; Barnes, J. C.; Ehrlich, D. J. C.; Johnson, J. A. *J. Am. Chem. Soc.* **2016**, *138*, 9369.

61. Barnes, J. C.; Ehrlich, D. J. C.; Gao, A. X.; Leibfarth, F. A.; Jiang, Y.; Zhou, E.; Jamison, T. F.; Johnson, J. A. *Nat. Chem*. **2015**, *7*, 810

62. Swain, J. A.; Iadevaia, G.; Hunter, C. A. *J. Am. Chem. Soc*. **2018**, *140,* 11526.

63. Stross, A. E; Iadevaia, G.; Hunter, C. A. *Chem. Sci*. **2016**, *7*, 94

64. Wei, T. Jung, J. H.; Scott, T. F. *J. Am. Chem. Soc*. **2015**, *137*, 16196.

65. Wei, T.; Furgal, J. C.; Scott, T. F. *Chem. Commun*. **2017**, *53*, 3874.

66. Leguizamon, S. C.; Scott, T. F. *Nat. Commun*. **2020**, *11*, 784.

Chapter 2. Polymersome-based modular nanoreactors with size-selective transmembrane permeability

2.1 Abstract

Polymersome nanoreactors encapsulating the enzymes or particulate catalysts attract interest because of their potential use as modular reactors to synthesize complex compounds via a cascade of chemical reactions in a single batch. To achieve these goals, a key requirement is the tunable permeability of the polymersome membrane, which allows the size-selective transportation of reagents and products while protecting the encapsulated catalysts during the chemical reaction. We report here a stimuli-responsive route for controlling the permeability of the polymersomes of the binary blend of poly(ethylene glycol)-*b*-polystyrene (PEG-*b*-PS) and poly(ethylene glycol)-*b*-poly(acrylbenzylborate) (PEG-*b*-PABB). The presence of H_2O_2 (1 mM) in the medium (0.1M PBS, pH 7.4) triggers the oxidation of benzyl borate pendants of PABB to form poly(acrylic acid) (PAA). This transformation results in the perforation of the compartmentalizing membrane of polymersomes by the dissolution of PEG-*b*-PAA domains embedded in the inert PEG-*b*-PS matrix. By controlling the composition of the stimuli-responsive block copolymer, the polymersomes of the binary blend exhibit size-selective permeability without losing the structural integrity. Release of fluorescent guests with different sizes (Fluorescein, PEG2k-Cm, PEG5k-Rho) can be controlled by tuning the composition (PEG-*b*-PS/PEG-*b*-PABB = 100/0 ~ 80/20) of blended

polymersomes. Selective permeability of the membrane provides protection of the encapsulated enzymes from external proteases present in the medium, resulting in the one-pot synthesis of small molecules via cascades of chemical reactions. The nanoparticular catalysts are also encapsulated within the permeable polymersomes, serving as modular reactors for the conversion of organic compounds via a cascade of reactions.

2.2 Introduction

Polymer nanocapsules can store and transport guest molecules within a nanoscale compartment that is separated from the surroundings by polymer membranes. When the compartmentalizing polymer membranes possess controlled porosity, these structures can serve as chemical and biochemical nanoreactors by allowing reactions in the confinement encapsulating the catalysts or enzymes.[1–5] The spatial confinement of the reaction site within the nanoscale compartment of polymersomes provides longevity of the catalytic activities by protecting the encapsulated catalysts from contamination or hydrolytic degradation.[6–8] Of particular interest are the cascade reactions for one-pot synthesis of complex products requiring multi-step preparation, without the purification of intermediates. In addition, the individual reaction is carried out within the compartment encapsulating the catalyst, such that the incompatible reaction conditions co-exist in a reaction medium.[9–13] Molecular cages and metal-organic nanocages have been used as modular reactors to conduct multi-step reactions by employing the catalytic moieties within the cages.[14–16] However, the nanocages with large compartments that allow the encapsulation of macromolecular or nanoparticulate catalysts have rarely been used as modular reactors for one-pot reaction cascades.

Polymersomes are promising candidates for nanoreactors owing to the tunability of their sizes, shapes, and physicochemical properties arising from the chemical diversity of block copolymer (BCP) building blocks.[17,18] Compared to liposomes, the compartmentalizing membranes of polymersomes exhibit superior physical stability under harsh conditions because of the high molecular weight of hydrophobic polymer chains forming the membrane.[19,20] However, this robustness reduces the permeability of guest molecules through the compartmentalizing membranes of polymersomes. Although polymersomes composed of intrinsically permeable membranes have been reported,[21–23] most polymersomes require pore generators (porogens) embedded within the membranes to afford transmembrane permeability. These porogens include biomimicries such as channel proteins, outer membrane porins,[24–26] and DNA nanopores.[27] Other porogens are based on the functionalization of polymer membrane that induced the stimuli-responsive actuator or pore generators,[28–33] and sacrificial components at the polymersome membrane.[34–36] Furthermore, researches about polymersomes with tunable porosity were published recently with great interest.[37–40]

Previous studies reported that phase-separation can drive domain formation and control the surface topology of the membrane of the vesicles.[41–44] When co-assembled with an inert BCP to form polymersomes, a stimuli-responsive BCP used as a minor component in the BCP blend serves a functional or sacrificial porogen by switching its solubility in water upon exposure to the external stimulants.[36,45] After the selective removal of sacrificial porogens, the resulting compartmentalizing membrane that is only composed of an inert BCP exhibits transmembrane permeability due to the generation of pores while maintaining the structural integrity of polymersomes. This pore generation by the sacrificial

porogen is based on the phase separation between the two hydrophobic polymer blocks within the bilayer of the polymersomes. One remaining challenge is to control the permeability of the compartmentalizing membranes of polymersomes with respect to the composition ratio of the block copolymer blend. The size-selective permeability of the polymersome membrane can guarantee the free access of encapsulated catalysts by reagents while protecting the catalysts from contamination or deterioration by size-selective exclusion of external pollutants.

Here we report a stimuli-responsive route to control the permeability of polymersomes by the generation of pores in the compartmentalizing membrane. The pore generation and control of the pore size were achieved by adjusting the content of a stimuli-responsive BCP, poly(ethylene glycol)-*b*-poly(acrylbenzylborate) (PEG-*b*-PABB), in the binary blend with inert PEG-*b*-polystyrene (PEG-*b*-PS). In the presence of 1 mM H_2O_2 (0.1M PBS, pH 7.4), the benzylborate pendants on the PABB block oxidatively degraded to carboxylic acids, which converted the hydrophobic PABB block into water-soluble poly(acrylic acid) (PAA).[35,46−48] This resulted in the extraction of the porogenic BCP from the compartmentalizing membrane of polymersome. Size-selective permeability of the polymersome membrane was achieved by adjusting the content of the stimuli-responsive porogenic BCP in the binary BCP blend (Figure 1). The perforated membrane selectively released the encapsulated PEGs with different molecular weights depending on the composition of the binary blend. Utilizing this size-selective permeability, it is demonstrated that these polymersomes with size-selective permeabilities can serve as modular nanoreactors protecting the encapsulated enzymes from external proteases present in the medium, resulting in the one-pot synthesis of small molecules via cascades of chemical reactions. The

nanoparticular catalysts could also be encapsulated within the permeable polymersomes, acting as modular reactors for the conversion of organic compounds via a cascade of reactions.

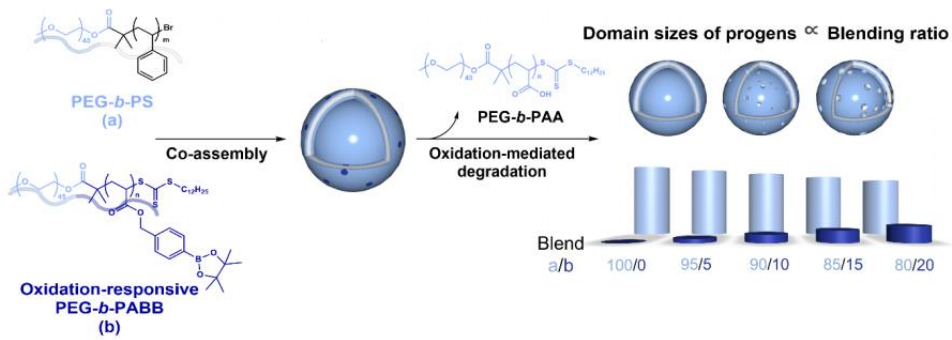

Figure 2-1. Schematic of the synthetic process of polymersomes with size-selective permeability achieved by controlling the composition ratio of a BCP blend.

2.3 Experimental Section

2.3.1. Materials. All reagents and chemicals were purchased from Sigma Aldrich, Alfa Aesar, and TCI and used as received. To remove the stabilizer, styrene was passed through basic alumina oxide before polymerization. CH_2Cl_2 was dried (using CaH_2 under a N_2 atmosphere) and distilled. Tetrahydrofuran (THF) was refluxed with Na and benzophenone under a N_2 atmosphere and distilled before use. All reactions were performed in an inert atmosphere.

2.3.2.Preparation of polymersomes.

Polymerization of PEG-b-PABB. A 5 ml glass vial equipped with a magnetic stirring bar and fitted with a TFE/SIL screw cap was charged with $mPeg_{45}$-DDMAT (60 mg, 0.025 mmol), (4-(4,4,5,5-tetramethyl-1,3,2-dioxaborolan-2-yl)benzyl acrylate (ABB) (500 mg, 1.74 mmol), Tris[2-phenylphridinato-C^2,*N*]iridium(III) ($Ir(ppy)_3$) (0.0083 mg, 0.0127 μmol), 1 ml of DMSO. The mixture was covered in aluminum foil and degassed by N_2 for 20 min. Under a N_2 atmosphere, the reaction mixture was stirred with irradiation under blue LED light (4.8 Watts, λ_{max} = 435 nm) at room temperature. Aliquots were withdrawn by nitrogen- perged syringes from the reaction at predetermined interval times and analyzed by ^1H NMR ($CDCl_3$) and GPC (THF) to measure the conversions, number average molecular weights (M_n), and dispersities (M_w/M_n, $Đ$). The final solution was decanted and redissolved CH_2Cl_2 precipitated in hexane. The yellow precipitate was collected, re-dissolved in a minimal amount of THF, and precipitated in water. The precipitate was then collected and freeze-dried to give desired products.

Self-Assembly of Block Copolymer. 1,4-dioxane solution of the mixture of two block copolymers was prepared by mixing two stock solutions (concentration of 10 mg/ml) of the block copolymers. The resulting solution of BCP mixture was allowed to equilibrate for 24 h at room temperature. The BCP blend (10 mg) was initially dissolved in 1,4-dioxane (total 2 ml, 2 wt %) in a capped vial and the solution was stirred for 24 h at room temperature. Water (total 2 ml) was added at a controlled rate (4 ml/h) to the solution via a syringe pump with vigorous stirring (850 rpm). The resulting suspension was dialyzed (molecular weight cutoff (MWCO) = 12-14 kDa, SpectraPor) against water for 1 day to remove the organic solvent.

2.3.3. Size-dependent permeability analysis with dye encapsulated polymersomes. Proper weight ratio of mixed polymer (10 mg) was dissolved in 1,4-dioxane (1 ml) in a 20ml capped vial with a magnetic bar. The solution was stirred for 1 h at room temperature (765 rpm). A syringe pump was calibrated to deliver 0.5 mM aqueous solution of fluorescein, PEG attached coumarin (PEG-Cm) and PEG attached rhodamine (PEG-Rho) at a speed of 2 ml h^{-1}. The vial cap was replaced by a rubber septum, and water was added to the polymer solution for 30 min using a syringe pump with 6 ml syringe equipped with a steel needle. The resulting suspension was subjected to dialysis (molecular weight cutoff 12-14 kDa (SpectraPor, Rancho Dominguez, CA)) against water for 24 h. All process was carefully proceeded in the dark. The residual dye was removed by centrifugation and size exclusion chromatography (SEC) (Sephadex G-200). Collected suspension was re-concentrated by centrifugation and diluted with 100 μg of 10 mM H_2O_2 0.1 M pH 7.4 PBS buffer. After 24 h, dyes spilled out of the pore were collected by centrifugation using a Amicon Ultra Free-MC centrifugal filter (MW cutoff: 100 kDa) and analyzed with Fluorophotometer. CLSM images were taken with suspension of polymersomes before the filtration.

2.3.4. Preparation of enzyme encapsulated polymersomes. PK, GOX, HRP or CAL (2.5 mg ml^{-1} for each enzyme) was dissolved in 0.1 M pH 7.4 Phosphaste-Buffered Saline (PBS). Blended polymer was dissolved in Acetone or dioxane. A syringe pump was calibrated to deliver each enzyme solution at a speed of 2 ml h^{-1}. After self-assembly, suspension was centrifuged to remove the organic solvents and re-dispersed in PBS buffer. The suspension was then transferred to an Amicon Ultra Free-MC centrifugal filter with a cutoff of 100 kDa and centrifuged to dryness. The polymersomes were re-dispersed in PBS buffer and then centrifuged

again. This step was repeated six times (to remove the residual enzymes). To generate the membrane pores, each enzyme encapsulated polymersomes were centrifuged and was transferred to 0.1 M pH 7.4 PBS buffer with 1 mM of H_2O_2 and left for 4 h and re-dispersed with 0.1 M pH 7.4 PBS buffer using a Amicon Ultra Free-MC centrifugal filter (MW cutoff : 100 kDa).

2.3.5. Preparation of AuNPs containing nanoreactor. Commercial gold nanoparticle (AuNP, Sigma-Aldrich, 50 nm diameter, OD 1, stabilized suspension in citrate buffer) solution was diluted 10 times with 0.1 mM PBS. The AuNP solution (1 ml) was dropped into the blended polymersome containing 1,4-dioxane solution (10 mg ml^{-1}, 1 ml) instead of the D.I water. The AuNP solution was added at a controlled rate (2 ml h^{-1}) to the polymer solution with a syringe pump with vigorous stirring (850 rpm). The resulting suspension was purified with centrifugation and SEC (Sephadex G-200) to remove the residual free AuNPs. Collected suspension was concentrated by centrifugation and diluted with 100 μg of 10 mM H_2O_2 0.1M pH 7.4 PBS buffer for the pore generation at the membrane of the polymersomes. After 24 h, polymersomes were concentrated by centrifugation and dispersed with 0.1 mM PBS.

2.3.6. Enzyme activity assay Stock solution of 1,2,3,4-Tetra-*O*-acetyl-β-D-glucopyranose (β-D-glucopyranose, 1 M of β-D-glucopyranose in 0.1 M PBS, pH 7.4) and ABTS (4 mM of ABTS in 0.1 M PBS, pH 7.4) were freshly prepared before UV-vis spectrometry measurements. A dispersion of enzyme encapsulated polymersomes (40 μl) or an aliquot of control solution (40 μl) was placed in micro quartz cuvette cell, followed by the stock solutions of β-D-glucopyranose (20 μl) and ABTS (20 μl). Monitoring the formation of the radical cation of ABTS by its

absorption at 405 nm was started immediately after mixing. Resistance of nanoreactors was monitored after addition of 5 μl of 0.1 M PBS buffer containing proteinase K (1 mg/ml)

2.3.7. One pot synthesis of 4-aminophenol. To NaH_2PO_4 pH 7 buffer (0.025 M; 45 μl), the solution of 4-NPA in ACN (0.1 M; 5 μl) was added under magnetic stirring at 25 °C and let to homogenize. After that, CAL encapsulated polymersome (25 μl) aqueous suspension was added. The reaction was kept on gentle stirring until complete conversion of substrate 4-NPA to 4-NP. Subsequently, AuNP encapsulated polymersome (25 μl) and $NaBH_4$ (0.04 mmol, 1.52 mg) was directly added to initialize the catalyzed reduction of 4-NP to 4-AP. The reaction progress was monitored by the absorption spectrum between 600 and 200 nm in a quartz cuvette.

2.4 Result and Discussion

2.4.1 Synthesis of stimuli-responsive BCPs. PEG-*b*-PABB was synthesized as a pore-generating BCP because of the facile oxidative decomposition of the benzylborate pendants of PABB block in the presence of H_2O_2 as an oxidant. Pinacol-protected benzylborate acrylate (**1**) was synthesized following the procedure reported by Li and coworkers.[46,49,50] The polymerization of **1** was achieved via atom-transfer radical polymerization (ATRP) with a PEG-macroinitiator (M_n = 2000 g/mol) and CuBr, which afforded polymers with large dispersities ($Đ$ > 1.3). Reversible addition-fragmentation chain transfer (RAFT)

polymerization of **1** with a PEG chain transfer agent and 2,2′-Azobis(2-methylpropionitrile) (AIBN) as a radical source resulted in a low conversion (< 40%), yielding a limited control over the molecular weight and dispersity. Therefore, the method of polymerization was changed to the photo-induced electron/energy transfer-RAFT (PET-RAFT) polymerization with *fac*-[$Ir(ppy)_3$] as a photocatalyst and 2-(dodecylthiocarbonothioylthio)-2-methylpropionic acid as a chain transfer agent (CTA) (Figure 2A) under visible light irradiation (λ = 435 nm).[51,52]

Under the PET-RAFT polymerization conditions, 75% conversion of **1** was achieved at room temperature in 3 h, resulting in the formation of homopolymer $PABB_{66}$ **2b** with the target molecular weight (M_n = 19000 g/mol) and low dispersity ($Đ$ = 1.07). The stimuli-responsive BCPs were synthesized using a macromolecular PEG-CTA (M_n(PEG) = 2000 g/mol) under identical polymerization conditions, which produced the BCP, PEG_{45}-*b*-$PABB_{51}$ (**4b**, M_n = 16800 g mol^{-1}, $Đ$ = 1.12). PET-RAFT polymerization of **1** exhibited first-order kinetics showing a linear increase of M_n with an increase in the duration of visible light irradiation (Figure 2B). The dispersity of the synthesized polymer remained low throughout the polymerization. As an inert BCP, PEG-*b*-PS was synthesized by ATRP with a PEG macroinitiator.[36]

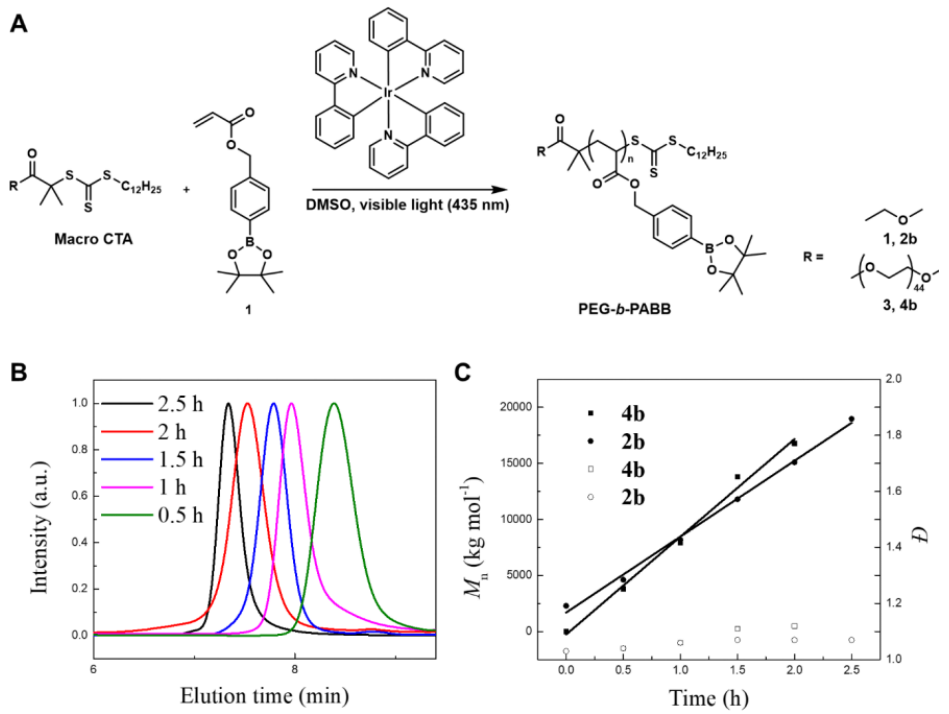

Figure 2-2. (A) PET-RAFT polymerization of PABB and PEG-*b*-PABB. (B) Time-trace of gel permeation chromatography (GPC) results for PET-RAFT polymerization of **1** to **4b**. (C) Plots of polymerization time vs number-average molecular weight (M_n) and polydispersity index ($Đ$) for **2b** and **4b**. Filled squares and circles indicate M_n values, and open squares and circles indicate $Đ$ values.

2.4.2 H_2O_2-responsive behavior of PABB. Pinacol-protected benzyl borate pendants of PABB were oxidatively degraded to quinone methide in the presence of H_2O_2, which converted the hydrophobic PABB to hydrophilic poly(acrylic acid) (PAA).[35,46,47] The oxidative conversion of benzyl borate was studied by ^{1}H NMR, which showed a complete conversion of PEG_{45}-*b*-$PABB_{40}$ (**3b**, M_n = 13700 g mol^{-1}, $Đ$ = 1.06) to PEG_{45}-*b*-PAA_{40} in the presence of H_2O_2 (10 mM) (Figures 3A and S2,

Supporting Information). Subsequently, the disassembly of the polymersomes of PEG-*b*-PABB triggered by the presence of H_2O_2 was investigated. **3b** was allowed to self-assemble into polymersomes in water via the co-solvent method using dioxane as a common solvent for the BCP. The morphology and diameter of the polymersomes of PEG_{45}-*b*-$PABB_{40}$ were examined by transmission electron microscopy (TEM) and dynamic light scattering (DLS), which showed an average diameter of 427 nm for the polymersomes (Figures S3 and S4, Supporting Information). After changing the dispersion medium from water to PBS (pH 7.4), H_2O_2 (10 mM) was introduced into the polymersomes dispersed in PBS. The transmittance of the dispersion was monitored at 580 nm, which showed a rapid increase from 4.8 % to 78.7 % in 24 h. This indicated the disassembly of light-scattering polymersomes into molecularly dissolved BCP (Figure 3B). When the concentration of H_2O_2 was reduced to 1 mM, the transmittance of the dispersed solution (observed at 580 nm) gradually increased from 5.1 % to 22 % within 400 min reached a plateau. The TEM images of an aliquot of this solution showed that the polymersomes were partially disrupted (Figure 3C), presumably due to the incomplete conversion of PABB block to PAA at a low H_2O_2 concentration.

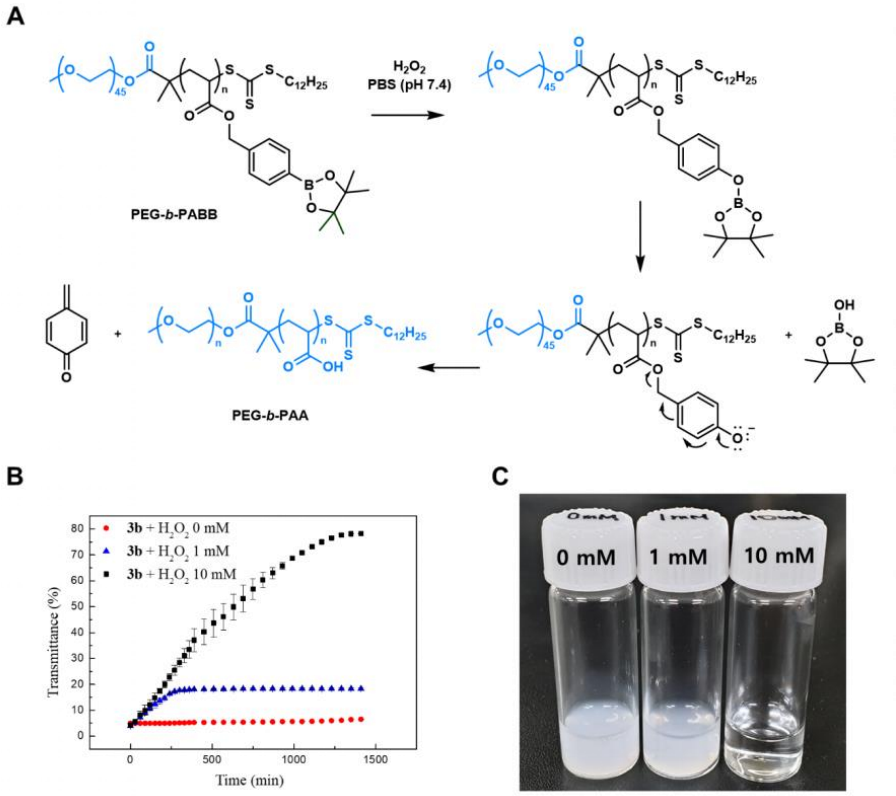

Figure 2-3. (A) Mechanism of oxidation-mediated degradation of PEG-*b*-PABB. (B) Transmittance spectra of PEG_{45}-*b*-$PABB_{40}$ (**3b**) polymersomes after the addition of H_2O_2. (C) Digital photographs of PEG-*b*-PABB polymersomes after the addition of different concentrations of H_2O_2.

2.4.3 Phase separation of PABB and PS. When the two BCPs with chemically distinct hydrophobic blocks were mixed and co-assembled to form polymersomes, the hydrophobic polymer blocks underwent phase separation within the hydrophobic compartment of the membrane. It was speculated that the stimuli-responsive PEG-*b*-PABB could be used as a minor component to form a BCP blend

with inert PEG-*b*-PS. Upon self-assembly to form the bilayer membranes of the polymersomes, the phase-separated PABB domains formed islands dispersed in the PS matrix. It was assumed that the composition ratio between the two BCPs could be translated to the size of the PABB islands embedded in the bilayer membrane, resulting in the permeability of the polymersomes being proportional to the weight fraction of PEG-*b*-PABB in the BCP blend.

To confirm the phase separation between PS and PABB, a series of binary solution blends were prepared with varying compositions of PS_{95} (**1a**, M_n = 10000 g mol^{-1}, $Đ$ = 1.05) and $PABB_{35}$ (**1b**, M_n = 10000 g mol^{-1}, $Đ$ = 1.06). The PS and PABB blend in dioxane (2 wt%) was cast on a silicon wafer by spin-coating of the blend solution.[51] Atomic force microscopy (AFM) images of the film of the binary blend, **1a**/**1b (**50/50) (**1a**:**1b** = 50:50 w/w), showed the presence of large islands (mean grain size of 498 nm) dispersed in the PS matrix covering 46.7 % of the surface, which indicated the microphase separation of two polymers via the nucleation-and-growth mechanism (Figure 4B). Subsequently, the blend film cast on the silicon wafer was immersed in PBS buffer containing 10 mM H_2O_2 for 8 h and rinsed with water. The AFM images of the H_2O_2-treated film showed that the islands were removed from the matrix, leaving large wells in the PS matrix (Figure S5, Supporting Information). This result indicated that the phase-separated domains of PABB were removed from the PS matrix by the H_2O_2-triggered conversion of PABB to PAA, which was soluble in PBS.

By controlling the compositions of the two BCPs, the structural parameters of the porous nanostructures could be efficiently tuned. To investigate the relationship between the sizes of the PABB islands and the composition of the binary blend, a

thin film of the binary blend containing a modified composition of PABB (**1a**/**1b** (80/20) and **1a**/**1b** (90/10)) was prepared. The AFM images of the resulting films with modified composition of the binary blends showed that the mean grain sizes of the PABB islands were reduced to 228 nm for a blend **1a**/**1b (**80/20) and 105.3 nm for **1a**/**1b** (90/10). The fraction of the surface area of the PABB-domain on the films were reduced from 46.7% for **1a**/**1b** (50/50) to 20.5 % for **1a**/**1b** (80/20) and 9 % for **1a**/**1b** (90/10), which was consistent with the compositions of PABB used in the blend (Figures 4C and 4D, Figure S6, Supporting Information). These results strongly suggested that the permeability of the film of the binary blend of PS and PABB could be modified by varying the composition of the stimuli-responsive polymer in the blend.

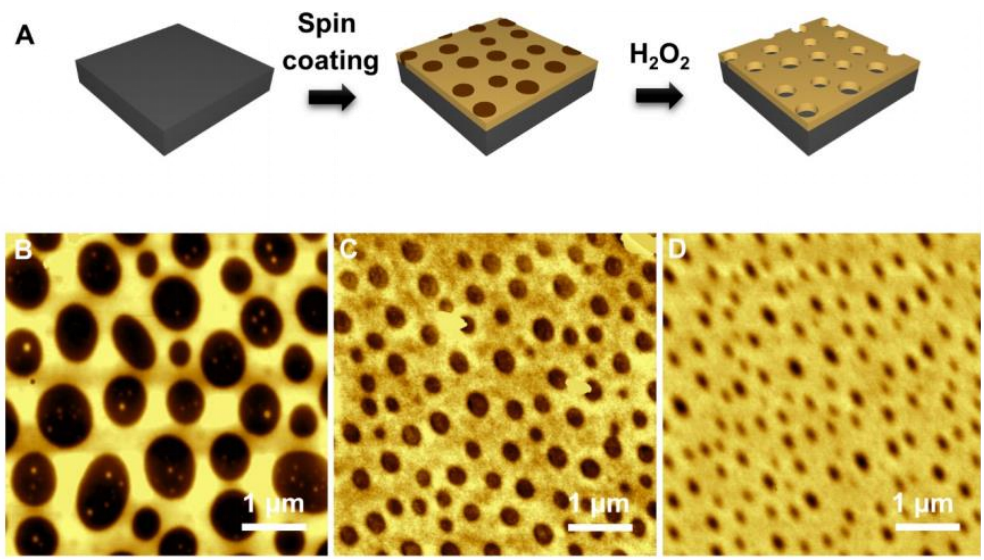

Figure 2-4. (A) Schematic of the fabrication of PS and PABB polymer blended film. AFM images of spin-coated binary blended BCP films on silicon wafer. Size-

ratio proportional formation of PABB islands on the film: (B) **1a**/**1b** (50/50), (C) **1a**/**1b** (80/20), and (D) **1a**/**1b** (90/10). Scale bar = 1 μm.

2.4.4 Size-selective permeability of the polymersomes of BCP blends. A binary blend of the BCPs was used for the formation of permeable polymersomes. For the BCP blends, two diblock copolymers were selected, PEG_{45}-*b*-PS_{110} (**2a**, M_n = 13600 g mol^{-1}, $Đ$ = 1.06) and PEG_{45}-*b*-$PABB_{40}$ (**3b**, M_n = 13700 g mol^{-1}, $Đ$ = 1.07). When self-assembled separately, these BCPs formed polymersomes with similar average diameters (~ 430 nm). The two BCPs were dissolved in dioxane (2 wt%) at different compositions of **2a** and **3b** (**2a**:**3b** = 100:0, 90:10 and 80:20 w/w) to form a series of BCP blends. After self-assembly, the polymersomes of these BCP blends were treated with 10 mM H_2O_2 in PBS (pH 7.4). In all cases, the scattered light intensity of the polymersome solution did not change noticeably after H_2O_2 treatment, which suggested that the two BCPs co-assembled to form polymersomes without forming the polymersomes of each BCP independently (Figures S7, Supporting Information).

The morphologies of the polymersomes after H_2O_2-triggered perforation of the membrane were examined using TEM. The TEM images of the perforated polymersomes of **2a**/**3b** (70/30) and **2a**/**3b** (60/40) showed the collapse of the membrane caused by the removal of large domains occupied by **3b** from the membranes of the polymersomes (Figure 5C~F, Figures S7). The complete disappearance of **3b** from the polymersome was confirmed by the ^{1}H NMR spectrum of the freeze-dried polymersomes with 70/30 blend after perforation (Figure S8). The polymersomes prepared from the BCP blends **2a**/**3b** (90/10) and **2a**/**3b** (80/20) showed the retention of the structural integrity of polymersomes

(Figure 5A, 5B, and Figure S7, Supporting Information). Interestingly, the cryo-TEM images showed the shape transformation of the spherical polymersomes to kippah polymersomes when the perforation was performed in a buffer medium of high ionic strength (~0.1 M PBS).[54] This shape transition was presumably due to the decrease in the internal volumes of the polymersomes caused by the osmotic pressure-driven rejection of water through the perforated membrane (Figure 5H), which could be prevented by matching the ionic concentration of both sides of the membrane in the buffer medium. [55]

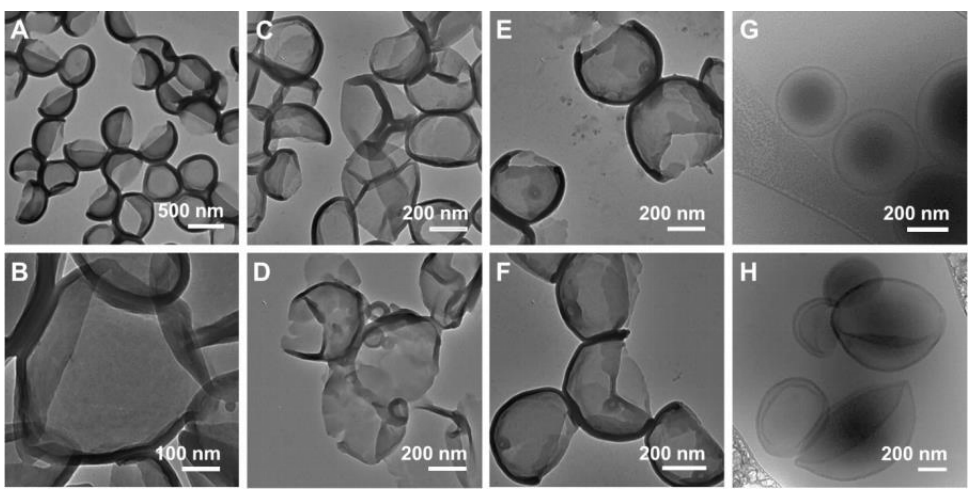

Figure 2-5. TEM images of the PEG-*b*-PS and PEG-*b*-PABB binary blended polymersomes (A, B) **2a**/**3b** = 80/20, (C, D) **2a**/**3b** = 70/30, and (E, F) **2a**/**3b** = 60/40 after treating with 10 mM H_2O_2 in 0.1 M PBS buffer (pH 7.4). (G, H) Cryo-TEM images of the **2a**/**3b** = 80/20 binary blended polymersomes after treating with 10 mM H_2O_2 in 0.1 M PBS buffer (pH 7.4). Aqueous solution conditions: (G) 0.1 M PBS buffer (pH 7.4) and (H) DI water.

The controllability of the membrane permeability of the perforated polymersomes was investigated by adjusting the composition of the BCP blend. To examine the size-selectivity of the perforated polymersome membrane, the fluorescently labeled macromolecular guests including coumarin-labeled PEG, PEG2K-Cm (M_n(PEG) = 2000 g mol^{-1}), and rhodamine-labeled PEG, PEG5K-Rho (M_n(PEG) = 5000 g mol^{-1}), were synthesized.[56,57] These guest molecules with different molecular weights and sizes (fluorescein (λ_{em} = 512 nm), PEG2k-Cm (λ_{em} = 472 nm), and PEG5k-Rho (λ_{em} =585 nm)) were encapsulated in the polymersomes of a blend of **2a** and **3b**. Before perforation, confocal laser scanning microscopy (CLSM) of the polymersome of **2a**/**3b** showed that all three guest molecules were encapsulated in the water-filled inner compartments of the polymersomes (Figure 6A–C). The observed fluorescence intensity of PEG2k-Cm was reduced due to the Förster resonance energy transfer (FRET) between coumarin and fluorescein within the inner compartments of the polymersomes (Figure 6D).[58]

The polymersomes of **2a**/**3b** (95/5) only released fluorescein and retained the polymeric guest molecules, PEG2k-Cm and PEG5k-Rho, within the polymersomes. Upon the removal of fluorescein from the inner compartment, the fluorescence intensity of PEG2k-Cm increased, indicating the absence of FRET absorber in the polymersomes. When the amount of **3b** in the blend increased from **2a**/**3b** (95/5) to **2a**/**3b** (90/10), the perforated polymersomes released fluorescein and PEG2k-Cm, while retaining PEG5k-Rho within the inner compartment, indicating the size-selective release of guest molecules through the perforated membranes. PEG5k-

Rho was released from the polymersomes when the composition of the BCP blend was changed to **2a**/**3b** = 80/20 (w/w). The release of the encapsulated guest molecules from the perforated polymersomes was confirmed by checking the fluorescence of the medium after the removal of polymersomes by centrifugal filtration (Figure 6 H, L, and P).

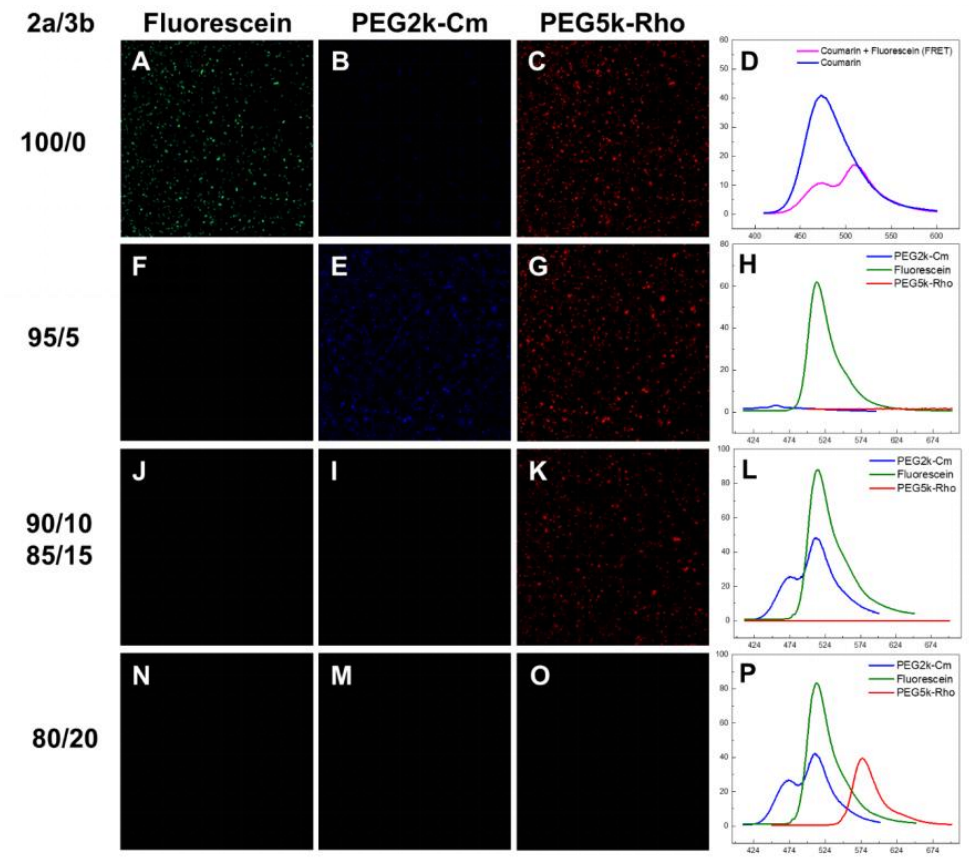

Figure 2-6. CLSM images of **2a** and **3b** blended polymersomes after oxidation-mediated pore development with fluorescein (green), PEG2k-Cm (blue), PEG5k-Rho (red) as encapsulants. **2a**/**3b** = 100/0 (A–C); **2a**/**3b** = 95/5 (E–G); **2a**/**3b** =

90/10, 85/15 (I–K); **2a**/**3b** = 80/20 (M–O). (D) Fluorescence spectra of FRET between coumarin and fluorescein. Fluorescence spectra of filtered solution after H_2O_2-mediated dissolution of **3b.** (H) **2a**/**3b** = 95/5; (L) **2a**/**3b** = 90/10, 85/15; (P) **2a**/**3b** = 80/20. Y-axis: normalized fluorescence intensity (a.u.), x-axis: wavelength (nm).

2.4.5. Polymersome nanoreactors encapsulating enzymes and particulate catalysts for one-pot transformation. *3.5.1 Tandem reaction of compartmentalized nanoreactors having controllable permeability*. Polymersome nanoreactors encapsulating large catalysts such as enzymes and nanoparticles can be used in tandem for the one-pot synthesis of complex compounds via a cascade of reactions. These nanoreactors can potentially perform the complex transformation of molecules involving multiple conversions of reagents by isolating the sites of the reactions without exposing the encapsulated catalysts to other catalysts and external contaminants. A tandem reaction was performed with polymersome nanoreactors incorporating glucose oxidase (GOx), and horseradish peroxidase (HRP) at 37 °C (Figure S9 and S10, Detailed information about Encapsulation Efficiency (EE%) of each enzyme was on Supporting Information). GOx and HRP were incorporated into the nanoreactors and β-glucose was added into the reaction medium as a reagent. which was subsequently oxidized by GOx to produce H_2O_2. The cascade of enzymatic reactions was confirmed by the appearance of radical cations of ABTS ($ABTS^{\bullet+}$), which were formed by the oxidation of ABTS by HRP in the presence of H_2O_2. The absence of the nanoreactor encapsulating the GOx or HRP in the reaction mixture did not result in

the conversion of ABTS, indicating that the cascade of enzymatic reactions could be performed by using the polymersome nanoreactors in tandem (Figure 7C).The polymersome nanoreactors with different blending compositions were introduced for the cascade reaction. After the treatment of H_2O_2 (1 mM), domains composed of **3b** dissolved followed by the gradual increase of the enzyme activity that indicates the permeability enhancement of the polymersomes. After a certain period, the slope of the activity turned to negative due to the denaturation of enzymes at a high concentration of H_2O_2. The polymersome nanoreactors with the composition of **2a**/**3b** = 85/15 showed maximum enzyme activity (at 4000 seconds) after 4 h of exposure to H_2O_2 (Figure 7D). To minimize the denaturation, nanoreactors quickly purified with centrifugal filter (MW cutoff: 100 kDa) to remove the H_2O_2. Nanoreactors exhibited recyclability after purification (Figure S11). During the reaction, proteinase K (PK, 28.9 kDa) was introduced into the reaction medium at a specific point of time. The reaction medium containing unencapsulated GOx and HRP exhibited the immediate loss of enzymatic activities upon the addition of PK, indicating the hydrolytic degradation of enzymes caused by PK. In contrast, the polymersome nanoreactors did not show any deterioration of reactivity in the presence of PK, suggesting that the access of PK to the inner compartment of the nanoreactor was prevented due to the size-selective permeability of the polymersome membrane (Figure 7E).

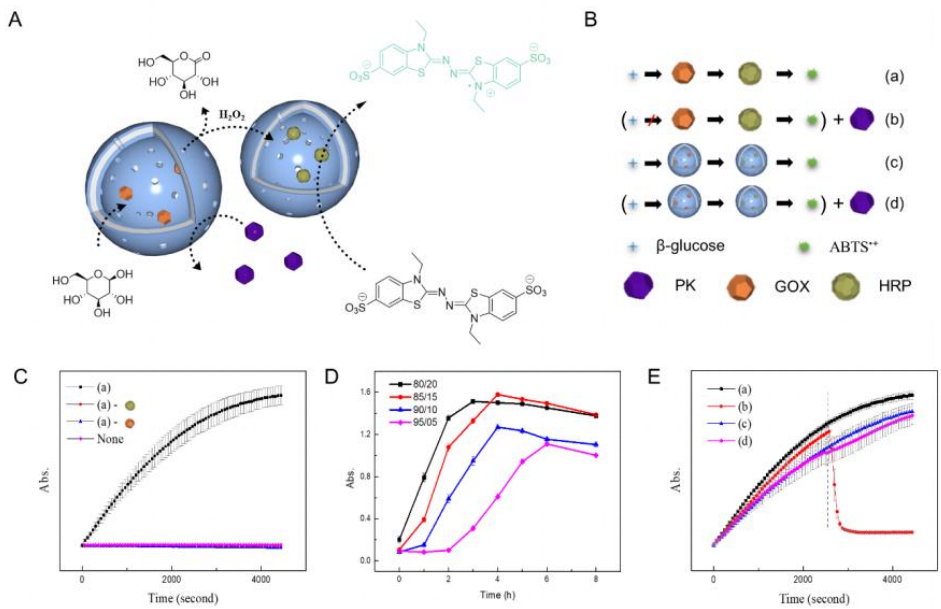

Figure 2-7. (A) Schematic of the cascade reaction of polymersome nanoreactors with GOx and HRP as encapsulants. (B) Graphical representation of the utilized cascade systems in (E). (C) Fluorescence measurements of the tandem reactions of nanoreactors at 37 °C. (D) Time-dependent enzyme activity of the nanoreactors with different blending ratios. (E) Fluorescence measurements of the tandem reactions of free enzymes and nanoreactors. PK is added as external stimuli at the marked time. All graphs are normalized based on the maximum conversion of the reaction of (a).

2.4.6. Three enzyme cascade reaction of modular nanoreactors encapsulating incompatible enzymes. High diffusivity without losing the ability to confine the catalysts within the compartmentalizing membrane is highly required for the

development of polymersome nanoreactors. Confined enzymes in different compartments have to serve as an independent catalyst without unnecessary reactions among catalysts. Here, a cascade of enzymatic reaction was exhibited with three different batches of polymersome nanoreactors to demonstrate complex multistep reactions in the compartmentalized system. 1,2,3,4-Tetra-*O*-acetyl-β-D-glucopyranose (β-glucopyranose, 1 M) was introduced into the solution, resulting in the production of β-D-glucose due to hydrolysis by PK. After the hydrolysis, desired $ABTS^{\bullet+}$ was detected at the UV-vis spectrometry which indicated that two incompatible enzymes, GOx and PK, functioned appropriately inside the modular polymersomes. PK not only induced the hydrolysis of β-glucopyranose but could also catalyze the proteolysis reaction. The cascade reaction of the nanoreactors containing totally incompatible enzymes at the same medium indicates successful cut-off between the enzymes owing to the size-selective permeability. The absence of the nanoreactor encapsulating the enzymes in the reaction mixture did not result in the conversion of ABTS, indicating the proteolysis of GOx and HRP by PK (Figure 8C).

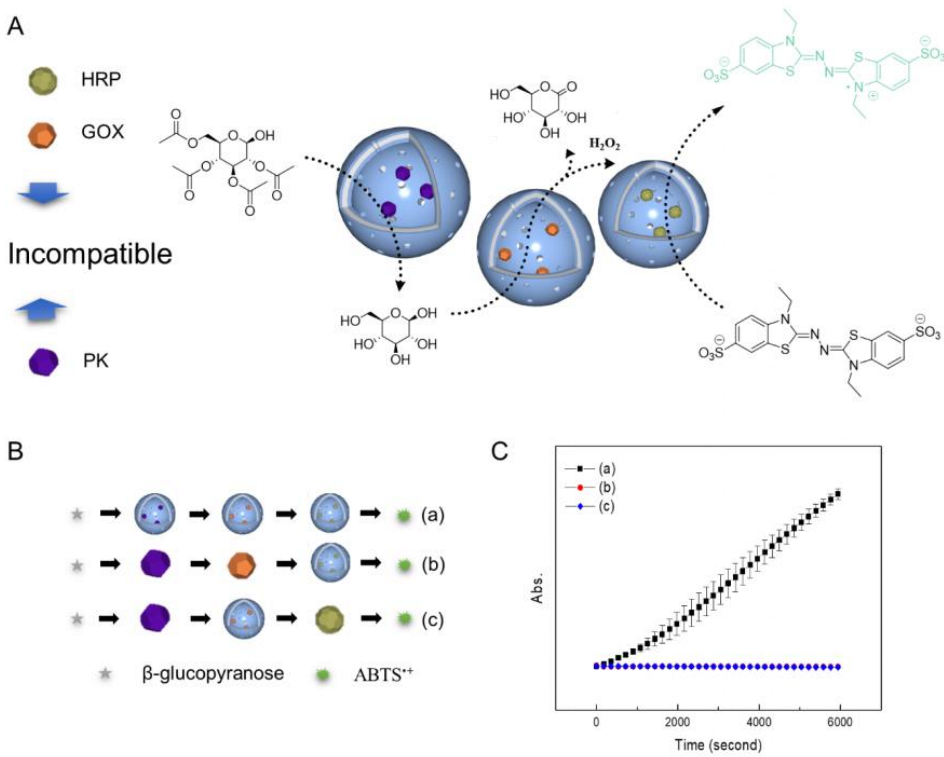

Figure 2-8. (A) Schematic of the cascade reaction of polymersome nanoreactors with PK, GOx, and HRP as encapsulants. (B) Graphical representation of the utilized cascade systems in (C). (C) Fluorescence measurements of the one-pot cascade reaction at 37 °C. Conversions are normalized based on the maximum conversion of the reaction of (a).

2.4.7. Tandem reaction with transition metal encapsulated polymersomes. Transition metal catalysts inside the hollow nano or microstructures are important in the pursuit of novel chemical reactions.[59] A two-step conversion of 4-nitrophenyl acetate (4-NPA) to 4-aminophenol (4-AP) was performed via a cascade of hydrolysis reaction catalyzed by *Candida antarctica* lipase (CAL) and reduction by

Au-nanoparticles (AuNPs, diameter = 50 nm). CAL and AuNPs were separately encapsulated in the polymersomes of **2a/3b** (90/10), which were used in tandem for the conversion (Figure S12, Detailed information about Encapsulation Efficiency (EE%) of AuNP was on Supporting Information). CAL was encapsulated using the same procedure as that for the enzyme capturing nanoreactors. AuNPs with an average diameter of 50 nm were encapsulated inside the polymersomes and purified with centrifugation and size-exclusion chromatography (Sephadex G−200) to remove the unencapsulated AuNPs.[60,61] The conversion of 4-NPA was monitored by UV−Vis spectroscopy.[62,63] The absorbance of 4-NPA at 271 nm gradually decreased and a new peak emerged at 314 nm, which indicated the conversion of 4-NPA to 4-nitrophenol (4-NP) (Figure 9C). After the addition of excess amount of $NaBH_4$, 4-NP was ionized to afford 4-nitrophenolate (λ_{max} = 400 nm). Immediate addition of the nanoreactors containing the AuNPs resulted in a decrease in the absorbance of 4-NP and an increase in the absorbance peak of 4-AP (Figure 9D). The proposed systems successfully demonstrated that the facile pore generation process of the polymersomes afforded smart nanoreactors with various catalytic guest molecules.

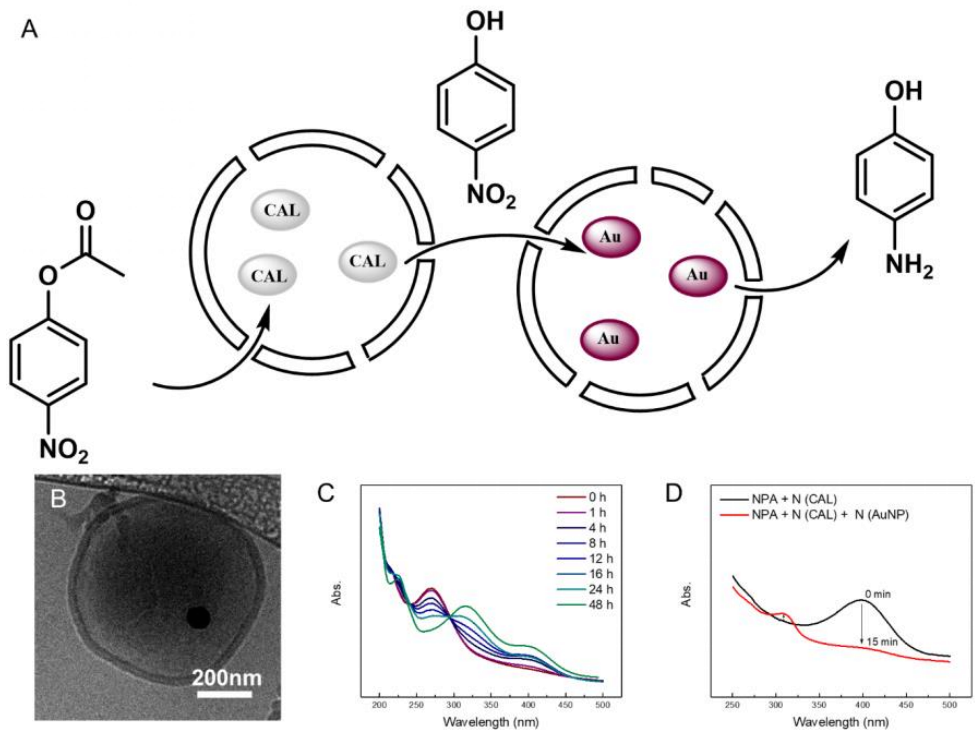

Figure 2-9. (A) Schematic of the cascade reaction of polymersome nanoreactors with CAL and AuNPs as encapsulants. (B) Cryo−TEM images of polymersomes (**2a**/**3b** = 90/10) encapsulating AuNP (50 nm). (C) UV−Vis spectroscopy data for time-dependent hydrolysis of 4-NPA into 4-NP with nanoreactors encapsulating CAL. (D) Absorbance measurements before and after the reduction of 4-NP into 4-AP with nanoreactors encapsulating AuNPs. N indicates polymersome nanoreactors encapsulating catalysts between the brackets.

2.5 Conclusion

To overcome the severe permeability deficiency of typical polymersome membranes, two discrete BCPs, PEG-*b*-PS and PEG-*b*-PABB, were synthesized. Distinct reactivity of each polymer toward H_2O_2 was employed to induce the permeability of the polymersomes. Binary blending of two polymers and subsequent self-assembly afforded the blended polymersomes. The phase separation occurred at the hydrophobic membrane of the polymersomes and was kinetically trapped due to the high crystallinity of each block. In the presence of H_2O_2, only the inert PEG-*b*-PS remained after the complete dissolution of porogenic PEG-*b*-PABB islands, which resulted in pore generation at the membranes of the polymersomes. The pore size could be altered through a facile modulation of the blending ratio. Selective permeability depending on the blending ratios was observed with different sizes of fluorescent guest molecules. The polymersomes could be transformed into nanoreactors owing to the selective permeability. The cascade reaction was successfully performed with polymersome nanoreactors encapsulating PK, GOx, and HRP by employing the selectivity toward large external stimuli outside the polymersomes. One-pot synthesis of 4-AP was also performed with a modular nanoreactor independently encapsulating the metal nanoparticles and enzymes. This system provides a new strategy for the facile preparation of porogenic stable nanocarriers and affords a novel route for a more efficient preparation of permeable polymersomes. The porogenic polymersome system reported herein can be a powerful tool for the development of nanoreactors or delivery vehicles in future.

2.7 References

1. Kuchler, A.; Yoshimoto, M.; Luginbuhl, S.; Mavelli, F.; Walde, P. Enzymatic Reactions in Confined Environments. *Nat. Nanotechnol.* **2016,** *11* (5), 409-20.

2. Brooks, W. L.; Sumerlin, B. S. Synthesis and Applications of Boronic Acid-Containing Polymers: From Materials to Medicine. *Chem. Rev.* **2016,** *116* (3), 1375-97.

3. LoPresti, C.; Lomas, H.; Massignani, M.; Smart, T.; Battaglia, G. Polymersomes: Nature Inspired Nanometer Sized Compartments. *J. Mater. Chem.* **2009,** *19* (22).

4. Peters, R. J.; Marguet, M.; Marais, S.; Fraaije, M. W.; van Hest, J. C.; Lecommandoux, S. Cascade Reactions in Multicompartmentalized Polymersomes. *Angew. Chem. Int. Ed.* **2014,** *53* (1), 146-50.

5. Nishimura, T.; Akiyoshi, K. Biotransporting Biocatalytic Reactors toward Therapeutic Nanofactories. *Adv. Sci.* **2018,** *5* (11), 1800801.

6. Spulber, M.; Najer, A.; Winkelbach, K.; Glaied, O.; Waser, M.; Pieles, U.; Meier, W.; Bruns, N. Photoreaction of a Hydroxyalkyphenone with the Membrane of Polymersomes: A Versatile Method to Generate Semipermeable Nanoreactors. *J. Am. Chem. Soc.* **2013,** *135* (24), 9204-9212.

7. Thambi, T.; Park, J. H.; Lee, D. S. Stimuli-Responsive Polymersomes for Cancer Therapy. *Biomater. Sci.* **2016,** *4* (1), 55-69.

8. Peters, R. J. R. W.; Louzao, I.; van Hest, J. C. M. From Polymeric Nanoreactors to Artificial Organelles. *Chem. Sci.* **2012,** *3* (2), 335-342.

9. Marguet, M.; Bonduelle, C.; Lecommandoux, S. Multicompartmentalized Polymeric Systems: towards Biomimetic Cellular Structure and Function. *Chem. Soc. Rev.* **2013,** *42* (2), 512-29.

10. Vriezema, D. M.; Garcia, P. M.; Sancho Oltra, N.; Hatzakis, N. S.; Kuiper, S. M.; Nolte, R. J.; Rowan, A. E.; van Hest, J. C. Positional Assembly of Enzymes in Polymersome Nanoreactors for Cascade Reactions. *Angew. Chem. Int. Ed.* **2007,** *46* (39), 7378-82.

11. van Dongen, S. F.; Nallani, M.; Cornelissen, J. J.; Nolte, R. J.; van Hest, J. C. A Three-Enzyme Cascade Reaction through Positional Assembly of Enzymes in a Polymersome Nanoreactor. *Chemistry* **2009,** *15* (5), 1107-14.

12. Renggli, K.; Baumann, P.; Langowska, K.; Onaca, O.; Bruns, N.; Meier, W. Selective and Responsive Nanoreactors. *Adv. Func. Mater.* **2011,** *21* (7), 1241-1259.

13. Xu, Z.; Xiao, G.; Li, H.; Shen, Y.; Zhang, J.; Pan, T.; Chen, X.; Zheng, B.; Wu, J.; Li, S.; Zhang, W.; Huang, W.; Huo, F. Compartmentalization within Self-Assembled Metal-Organic Framework Nanoparticles for Tandem Reactions. *Adv. Func. Mater.* **2018,** *28* (34).

14. Ueda, Y.; Ito, H.; Fujita, D.; Fujita, M. Permeable Self-Assembled Molecular Containers for Catalyst Isolation Enabling Two-Step Cascade Reactions. *J. Am. Chem. Soc.* **2017,** *139* (17), 6090-6093.

15. Jiao, J.; Tan, C.; Li, Z.; Liu, Y.; Han, X.; Cui, Y. Design and Assembly of Chiral Coordination Cages for Asymmetric Sequential Reactions. *J. Am. Chem. Soc.* **2018,** *140* (6), 2251-2259.

16. Salles, A. G., Jr.; Zarra, S.; Turner, R. M.; Nitschke, J. R. A Self-Organizing Chemical Assembly Line. *J. Am. Chem. Soc.* **2013,** *135* (51), 19143-6.

17. Gaitzsch, J.; Huang, X.; Voit, B. Engineering Functional Polymer Capsules toward Smart Nanoreactors. *Chem. Rev.* **2016,** *116* (3), 1053-93.

18. Che, H.; van Hest, J. C. M. Adaptive Polymersome Nanoreactors. *ChemNanoMat* **2019,** *5* (9), 1092-1109.

19. Discher, D. E.; Ahmed, F. Polymersomes. *Annu. Rev. Biomed. Eng.* **2006,** *8*, 323-41.

20. Tanner, P.; Baumann, P.; Enea, R.; Onaca, O.; Palivan, C.; Meier, W. Polymeric Vesicles: From Drug Carriers to Nanoreactors and Artificial Organelles. *Accounts of Chemical Research* **2011,** *44* (10), 1039-1049.

21. Kuiper, S. M.; Nallani, M.; Vriezema, D. M.; Cornelissen, J. J.; van Hest, J. C.; Nolte, R. J.; Rowan, A. E. Enzymes Containing Porous Polymersomes as Nano Reaction Vessels for Cascade Reactions. *Org. Biomol. Chem.* **2008,** *6* (23), 4315-8.

22. Nishimura, T.; Sasaki, Y.; Akiyoshi, K. Biotransporting Self-Assembled Nanofactories Using Polymer Vesicles with Molecular Permeability for Enzyme Prodrug Cancer Therapy. *Adv. Mater.* **2017,** *29* (36).

23. Blackman, L. D.; Varlas, S.; Arno, M. C.; Fayter, A.; Gibson, M. I.; O'Reilly, R. K. Permeable Protein-Loaded Polymersome Cascade Nanoreactors by Polymerization-Induced Self-Assembly. ACS Macro Lett 2017, 6 (11), 1263-1267.

24. Kumar, M.; Grzelakowski, M.; Zilles, J.; Clark, M.; Meier, W. Highly Permeable Polymeric Membranes Based on the Incorporation of the Functional Water Channel Protein Aquaporin Z. *Proc. Natl. Acad. Sci. U.S.A* **2007,** *104* (52), 20719.

25. Garni, M.; Thamboo, S.; Schoenenberger, C. A.; Palivan, C. G. Biopores/Membrane Proteins in Synthetic Polymer Membranes. *Biochim Biophys Acta Biomembr* **2017,** *1859* (4), 619-638.

26. Sauer, M.; Haefele, T.; Graff, A.; Nardin, C.; Meier, W. Ion-Carrier Controlled Precipitation of Calcium Phosphate in Giant ABA Triblock Copolymer Vesicles. *Chem. Commun.* **2001,** (23), 2452-2453.

27. Messager, L.; Burns, J. R.; Kim, J.; Cecchin, D.; Hindley, J.; Pyne, A. L.; Gaitzsch, J.; Battaglia, G.; Howorka, S. Biomimetic Hybrid Nanocontainers with Selective Permeability. *Angew. Chem. Int. Ed.* **2016,** *55* (37), 11106-9.

28. Chiu, H. C.; Lin, Y. W.; Huang, Y. F.; Chuang, C. K.; Chern, C. S. Polymer Vesicles Containing Small Vesicles within Interior Aqueous Compartments and pH-Responsive Transmembrane Channels. *Angew. Chem. Int. Ed.* **2008,** *47* (10), 1875-8.

29. Molla, M. R.; Rangadurai, P.; Antony, L.; Swaminathan, S.; de Pablo, J. J.; Thayumanavan, S. Dynamic Actuation of Glassy Polymersomes through Isomerization of a Single Azobenzene Unit at the Block Copolymer Interface. *Nat. Chem.* **2018,** *10* (6), 659-666.

30. Yan, Q.; Wang, J.; Yin, Y.; Yuan, J. Breathing Polymersomes: CO_2-Tuning Membrane Permeability for Size-Selective Release, Separation, and Reaction.

Angew. Chem. Int. Ed. **2013,** *52* (19), 5070-3.

31. Amstad, E.; Kim, S. H.; Weitz, D. A. Photo- and Thermoresponsive Polymersomes for Triggered Release. *Angew. Chem. Int. Ed.* **2012,** *51* (50), 12499-503.

32. Wang, X.; Hu, J.; Liu, G.; Tian, J.; Wang, H.; Gong, M.; Liu, S. Reversibly Switching Bilayer Permeability and Release Modules of Photochromic Polymersomes Stabilized by Cooperative Noncovalent Interactions. *J. Am. Chem. Soc.* **2015,** *137* (48), 15262-75.

33. Rifaie-Graham, O.; Ulrich, S.; Galensowske, N. F. B.; Balog, S.; Chami, M.; Rentsch, D.; Hemmer, J. R.; Read de Alaniz, J.; Boesel, L. F.; Bruns, N. Wavelength-Selective Light-Responsive DASA-Functionalized Polymersome Nanoreactors. *J. Am. Chem. Soc.* **2018,** *140* (25), 8027-8036.

34. Kim, H.; Kang, Y. J.; Kang, S.; Kim, K. T. Monosaccharide-Responsive Release of Insulin from Polymersomes of Polyboroxole Block Copolymers at Neutral pH. *J. Am. Chem. Soc.* **2012,** *134* (9), 4030-3.

35. Hu, X.; Yu, J.; Qian, C.; Lu, Y.; Kahkoska, A. R.; Xie, Z.; Jing, X.; Buse, J. B.; Gu, Z. H2O2-Responsive Vesicles Integrated with Transcutaneous Patches for Glucose-Mediated Insulin Delivery. *ACS Nano* **2017,** *11* (1), 613-620.

36. Kim, K. T.; Cornelissen, J. J. L. M.; Nolte, R. J. M.; van Hest, J. C. M. A Polymersome Nanoreactor with Controllable Permeability Induced by Stimuli-Responsive Block Copolymers. *Adv. Mater.* **2009,** *21* (27), 2787-2791.

37. Che, H.; Cao, S.; van Hest, J. C. M. Feedback-Induced Temporal Control of "Breathing" Polymersomes To Create Self-Adaptive Nanoreactors. *J. Am.*

Chem. Soc. **2018,** *140* (16), 5356-5359.

38. Liu, X.; Appelhans, D.; Voit, B. Hollow Capsules with Multiresponsive Valves for Controlled Enzymatic Reactions. *J. Am. Chem. Soc.* **2018,** *140* (47), 16106-16114.

39. Li, J.; Liang, L.; Liang, J.; Wu, W.; Zhou, H.; Guo, J. Constructing Asymmetric Polyion Complex Vesicles via Template Assembling Strategy: Formulation Control and Tunable Permeability. *Nanomaterials (Basel)* **2017,** *7* (11).

40. Feng, A.; Liang, J.; Ji, J.; Dou, J.; Wang, S.; Yuan, J. CO_2-Breathing and Piercing Polymersomes as Tunable and Reversible Nanocarriers. *Sci. Rep.* **2016,** *6*, 23624.

41. Christian, D. A.; Tian, A.; Ellenbroek, W. G.; Levental, I.; Rajagopal, K.; Janmey, P. A.; Liu, A. J.; Baumgart, T.; Discher, D. E. Spotted Vesicles, Striped Micelles and Janus Assemblies Induced by Ligand Binding. *Nat. Mater.* **2009,** *8* (10), 843-849.

42. LoPresti, C.; Massignani, M.; Fernyhough, C.; Blanazs, A.; Ryan, A. J.; Madsen, J.; Warren, N. J.; Armes, S. P.; Lewis, A. L.; Chirasatitsin, S.; Engler, A. J.; Battaglia, G. Controlling Polymersome Surface Topology at the Nanoscale by Membrane Confined Polymer/Polymer Phase Separation. *ACS Nano* **2011,** *5* (3), 1775-1784.

43. Massignani, M.; LoPresti, C.; Blanazs, A.; Madsen, J.; Armes, S. P.; Lewis, A. L.; Battaglia, G. Controlling Cellular Uptake by Surface Chemistry, Size, and Surface Topology at the Nanoscale. *Small* **2009,** *5* (21), 2424-32.

44. Ruiz-Pérez, L.; Messager, L.; Gaitzsch, J.; Joseph, A.; Sutto, L.; Gervasio, F. L.; Battaglia, G. Molecular Engineering of Polymersome Surface Topology. *Sci. Adv.* **2016,** *2* (4), e1500948.

45. Rahman, M. M.; Ueda, M.; Hirose, T.; Ito, Y. Spontaneous Formation of Gating Lipid Domain in Uniform-Size Peptide Vesicles for Controlled Release. *J. Am. Chem. Soc.* **2018,** *140* (51), 17956-17961.

46. Song, C.-C.; Ji, R.; Du, F.-S.; Liang, D.-H.; Li, Z.-C. Oxidation-Accelerated Hydrolysis of the Ortho Ester-Containing Acid-Labile Polymers. *Acs Macro Lett.* **2013,** *2* (3), 273-277.

47. de Gracia Lux, C.; Joshi-Barr, S.; Nguyen, T.; Mahmoud, E.; Schopf, E.; Fomina, N.; Almutairi, A. Biocompatible Polymeric Nanoparticles Degrade and Release Cargo in Response to Biologically Relevant Levels of Hydrogen Peroxide. *J. Am. Chem. Soc.* **2012,** *134* (38), 15758-64.

48. Cui, Y.; Zhang, M.; Du, F.-S.; Li, Z.-C. Facile Synthesis of H_2O_2-Cleavable Poly(ester-amide)s by Passerini Multicomponent Polymerization. *ACS Macro Lett.* **2016,** *6* (1), 11-15.

49. Hagen, H.; Marzenell, P.; Jentzsch, E.; Wenz, F.; Veldwijk, M. R.; Mokhir, A. Aminoferrocene-Based Prodrugs Activated by Reactive Oxygen Species. *J. Med. Chem.* **2012,** *55* (2), 924-34.

50. Zheng, N.; Armstrong, J. D.; Eng, K. K.; Keller, J.; Liu, T.; Purick, R.; Lynch, J.; Hartner, F. W.; Volante, R. P. A Convergent Asymmetric Synthesis of a Growth Hormone Secretagogue. *Tetrahedron: Asymmetry* **2003,** *14* (22), 3435-3446.

51. Shanmugam, S.; Xu, J.; Boyer, C. Photoinduced Electron Transfer–Reversible Addition–Fragmentation Chain Transfer (PET-RAFT) Polymerization of Vinyl Acetate and N-Vinylpyrrolidinone: Kinetic and Oxygen Tolerance Study. *Macromolecules* **2014,** *47* (15), 4930-4942.

52. Xu, J.; Jung, K.; Atme, A.; Shanmugam, S.; Boyer, C. A Robust and Versatile Photoinduced Living Polymerization of Conjugated and Unconjugated Monomers and Its Oxygen Tolerance. *J. Am. Chem. Soc.* **2014,** *136* (14), 5508-5519.

53. Guo, X.; Liu, L.; Zhuang, Z.; Chen, X.; Ni, M.; Li, Y.; Cui, Y.; Zhan, P.; Yuan, C.; Ge, H.; Wang, Z.; Chen, Y. A New Strategy of Lithography Based on Phase Separation of Polymer Blends. *Sci. Rep.* **2015,** *5*, 15947.

54. Mai, Y.; Eisenberg, A. Self-Assembly of Block Copolymers. Chem. Soc. Rev. 2012, 41 (18), 5969-85.

55. Wong, C. K.; Stenzel, M. H.; Thordarson, P. Non-Spherical Polymersomes: Formation and Characterization. Chem. Soc. Rev. 2019, 48 (15), 4019-4035.

56. Sivakumar, K.; Xie, F.; Cash, B. M.; Long, S.; Barnhill, H. N.; Wang, Q. A Fluorogenic 1,3-Dipolar Cycloaddition Reaction of 3-Azidocoumarins and Acetylenes. *Org. Lett.* **2004,** *6* (24), 4603-4606.

57. Wei, X.; Chen, W.; Chen, X.; Russell, T. P. Disorder-to-Order Transition of Diblock Copolymers Induced by Alkyne/Azide Click Chemistry. *Macromolecules* **2010,** *43* (14), 6234-6236.

58. Widmer, S.; Dorrestijn, M.; Camerlo, A.; Urek, S. K.; Lobnik, A.; Housecroft, C. E.; Constable, E. C.; Scherer, L. J. Coumarin Meets Fluorescein: A Forster

Resonance Energy Transfer Enhanced Optical Ammonia Gas Sensor. *Analyst* **2014,** *139* (17), 4335-42.

59. Prieto, G.; Tuysuz, H.; Duyckaerts, N.; Knossalla, J.; Wang, G. H.; Schuth, F. Hollow Nano- and Microstructures as Catalysts. *Chem. Rev.* **2016,** *116* (22), 14056-14119.

60. Mai, Y.; Eisenberg, A. Controlled Incorporation of Particles into the Central Portion of Vesicle Walls. *J. Am. Chem. Soc.* **2010,** *132* (29), 10078-10084.

61. Jaskiewicz, K.; Larsen, A.; Schaeffel, D.; Koynov, K.; Lieberwirth, I.; Fytas, G.; Landfester, K.; Kroeger, A. Incorporation of Nanoparticles into Polymersomes: Size and Concentration Effects. *ACS Nano* **2012,** *6* (8), 7254-7262.

62. Filice, M.; Marciello, M.; Morales Mdel, P.; Palomo, J. M. Synthesis of Heterogeneous Enzyme-Metal Nanoparticle Biohybrids in Aqueous Media and Their Applications in C-C Bond Formation and Tandem Catalysis. *Chem Commun (Camb)* **2013,** *49* (61), 6876-8.

63. Aditya, T.; Pal, A.; Pal, T. Nitroarene Reduction: A Trusted Model Reaction to Test Nanoparticle Catalysts. *Chem. Commun.* **2015,** *51* (46), 9410-31.

Chapter 3. Nanofiber organogel of all-conjugated block copolymers

3.1 Abstract

All conjugated block copolymers having controlled molecular weights in constituting polymer blocks can self-assemble into 1-dimensional nanostructures with controlled lengths and widths via crystallization-driven self-assembly in a block selective solvent. The resulting worm-like micelles having semi-conductive cores have attracted recent interest as organic nanowires showing enhanced charge carrier mobility with respect to the length of the micelles. In this report, all-conjugated diblock and triblock copolymers having poly(3-hexylthiophene) (P3HT) as a regioregular block and poly(3-(2-ethylhexyl)-thiophene) (P3EHT) as a stereo-irregular block were synthesized via a successive Grignard metathesis polymerization of the corresponding monomers using Kumada catalysts. The pseudo-living nature of this polymerization yielded diblock and triblock copolymers composed of polythiophene backbones differing in the solubility of constituting blocks in solvents depending on the solubilizing side chains at the 3-position of the repeating units. The self-seeding of P3HT-*b*-P3EHT and P3EHT-*b*-P3HT-*b*-P3EHT in anisole produced long 1-D nanofibers having controlled lengths depending on the growth temperature of the solution. Owing to solubilizing block (P3EHT), 1-D nanofibers were also obtained in the volatile cyclohexane. The introduction of triblock copolymer P3HT-b-P3EHT-b-P3HT to the crystallization-

driven self-assembly of P3HT-b-P3EHT induced the formation of organogels by non-covalent cross-linking of nanofibers. High concentration (>1 wt%) of triblock copolymer also induced the nanofiber organogels. The thiophene-based nanofiber organogel could be weaved to form porous foam by removing the solvent by freeze drying pocesses. These porous foam could be utilized as thermoelectric devices.

3.2 Introduction

Self-assembly of block copolymers (BCPs) in solution localizes the distinguished polymer domain within the core of the low dimensional structures such as spherical and worm-like micelles. When the BCP self-assembles into worm-like micelles, the solvent-insoluble polymer block forms the core that is surrounded by the solvent-soluble polymer block. This spontaneous process creates polymer nanowires having the shielded polymer domain with desired chemical and physical properties originating from the chemical structures of the core-forming polymer block.[1-4] In this regard, BCPs having conjugated polymers as a core-forming block have been highly anticipated to form self-assembled nanowires having semi-conductive core surrounded by solvent-soluble polymer blocks.[5-11] The crystallinity of the core-forming conjugated polymer block has been utilized to create polymer nanowires having conductivity by the crystallization-driven self-assembly (CDSA) in solution.[8,12-15] The CDSA of BCPs having conjugated core-forming blocks has allowed the length of the worm-like micelles of BCPs to be controlled with a narrow size distribution. In addition, the width of the conductive core of the micelle could be changed in relation to the well-controlled molecular weight of the conjugated polymer block. Manners and coworkers demonstrated that the semi-conducting nanowires created by the self-assembly of BCPs exhibited

enhanced charge carrier mobility in relation to the length of the polymer nanowire.[16-26]

All conjugated BCPs possess the extended conjugation of electrons throughout the backbone of the polymer chain without disruption. These BCPs have been highlighted as self-assembling building blocks to form nano-scaled heterojunction materials, which could be promising nanostructured materials for photovoltaics, or thermoelectrics. In particular, all-conjugated BCPs composed of amorphous and crystalline polymer blocks are highly interesting as they could form one-dimensional nanostructures with controlled lengths and aspect ratios via self-assembly driven by the association of the crystallizable conjugated polymer blocks stabilized by amorphous conjugated polymer blocks in solution.[27-29] Manners and coworkers have shown that the length of the self-assembled nanowires affects the crystallinity of the conjugated polymer core, which leads to enhanced conductivity through the nanowire.[8] In comparison to the BCP composed of a conjugated block and non-conjugated polymer block, these block copolymers would form nanowires having the conjugated polymer domains surrounding semi-conductive core of the micelles. The resulting nanowires of all-conjugated BCPs could be beneficial in the formation of weaved films as the semi-conducting corona of worm-like micelles having conjugated jacket surrounding the conductive core could be weaved to form macroscopic films.[30-34] When the resulting nanowires were weaved to macroscopic films, the conjugated polymer domain surrounding the semi-conductive core of nanowires

In this report, all-conjugated diblock and triblock copolymers having poly(3-hexylthiophene) (P3HT) as a regioregular block and poly(3-(2-ethylhexyl)-thiophene) (P3EHT) as a stereo-irregular block were synthesized via a successive

Grignard metathesis polymerization of the corresponding monomers using Kumada catalysts. The pseudo-living nature of this polymerization yielded diblock and triblock copolymers composed of polythiophene backbones differing in the solubility of constituting blocks in solvents depending on the solubilizing side chains at the 3-position of the repeating units. The seeded growth of P3HT-b-P3EHT and P3EHT-b-P3HT-b-P3EHT in anisole produced long 1-D nanofibers having controlled lengths depending on the growth temperature of the solution. The introduction of triblock copolymer P3HT-b-P3EHT-b-P3HT to the crystallization-driven self-assembly of P3HT-*b*-P3EHT induced the formation of organogels by non-covalent cross-linking of nanofibers. The nanofiber organogel of P3HT-b-P3EHT could be transfromed to porous foam. These porous foam-type materials could be utilized as thermoelectric devices.

3.3 Experimental Section

3.3.1 Materials. All reagents and chemicals were purchased from Sigma Aldrich, Alfa Aesar, and TCI and used as received. 3-Hexylthiophene, 2-bromo-3-hexylthiophene, 2-bromo-3-hexyl4-iodothiophene and poly(3-hexylthiophene) were synthesized as previously reported. Tetrahydrofuran (THF) was refluxed with Na and benzophenone under a N_2 atmosphere and distilled before use. All reactions were performed in an inert atmosphere.

3.3.2 Synthesis of 3-(2-Ethylhexyl)thiophene. To a mixture of magnesium turnings (4.9 g, 0.204 mol), anhydrous THF (20 mL) and a small amount of iodine

in a 250 mL schlenk flask, a solution of 2-ethylhexylbromide (38.5 g, 0.200 mol) in anhydrous THF (50 mL) was added slowly at 0 °C under N_2. After refluxing for 1 h, the solution was added dropwise to a mixture of 3-bromothiophene (25 g, 0.153 mol), Ni(dppp)Cl2 (0.83 g, 1.53 mmol) and anhydrous THF (50 mL) placed in a 250 mL schlenk flask at 0 °C. After the mixture was stirred overnight at room temperature, the reaction was quenched with HCl aq. (1 M) into the mixture. The product was extracted with $CHCl_3$ and dried over anhydrous Mg_2SO_4. The crude product was further purified by column chromatography using hexane as the eluent to give a clear liquid (25 g, 83 %). ^{1}H NMR ($CDCl_3$, 400 MHz): 7.21-7.22 (m, 1H), 6.89-6.90 (m, 2H), 2.56 (d, J = 6.7 Hz, 2H), 1.55-1.56 (m, 1H), 1.19-1.32 (m, 8H), 0.82-0.91 (m, 6H).

3.3.3 Synthesis of 2-Bromo-3-(2-ethylhexyl)thiophene. To 150 mL of THF solution of 1 (5.89 g, 30 mmol), N-bromosuccinimide (5.34 g, 30 mmol) was added at 0 °C and the mixture was stirred at R.T. After evaporation of THF, the organic fraction was extracted with water and MC, washed with $NaHCO_3$ aq., and dried over anhydrous Mg_2SO_4. Further purification by Kugelrohr distillation gave a transparent oil (8.16 g, 99%). ^{1}H NMR ($CDCl_3$, 400 MHz): 7.17-7.18 (d, 1H), 6.75-6.77 (d, 1H), 2.49-2.52 (d, 2H), 1.54-1.61 (1H), 1.23-1.32 (8H), 0.82-0.91 (6H).

3.3.4 Synthesis of 2-Bromo-3-(2-ethylhexyl)-5-iodothiophene To a solution of 2-Bromo-3-(2-ethylhexyl)thiophene (5 g, 18.17 mmol) in CH_2Cl_2 (100 mL), iodine (2,30 g, 18.1 mmol) and iodobenzene diacetate (2.92 g, 9.1 mmol) were successively added at 0 °C. The mixture was stirred at R.T. for 5 h. After 10% $Na_2S_2O_3$ aq. was added, the mixture was extracted with Et_2O. The organic layer

was collected and dried over anhydrous $MgSO_4$. After filtration, the organic solvents and iodobenzene were removed by evaporation under reduced pressure. The residue was purified by silica gel column chromatography using hexane as the eluent (6.91 g, 95%). ^1H NMR ($CDCl_3$, 400 MHz): 6.93 (s, 1H), 2.42-2.48 (2H), 1.54-1.56 (1H), 1.20-1.31(8H), 0.83-0.91 (6H)

3.3.5 Synthesis of Poly(3-hexylthiophene-block-3-(2-ethylhexyl)thiophene-block-3-hexylthiophene) P(3HT-*b*-3EHT-*b*-3HT). The feed molar ratio and molecular weights of 3-hexylthiophene and 3-(2-ethylhexyl)thiophene were controlled by fixing the ratio of the amount of Ni catalyst to the total monomer. Three shlenk tubes were dried by heating under reduced pressure and cooled to room temperature. 2-Bromo3-hexyl-5-iodothiophene was splitted and (1g, 2.68 mmol) placed in two flasks under N_2, and then evacuated under reduced pressure to remove water and oxygen inside. After adding dry THF (10 mL) into the flask via a syringe, the solution was mixed at 0 °C. 1.3M solution of i-PrMgCl,LiCl in THF (2.02 mL, 2.62 mmol) was added via a syringe, and the mixture was stirred at 0 °C for 30 min (solution Ax2). In the other flask, 2-Bromo3-ethylhexyl-5-iodothiophene with proper amount dependent on the block ratio was reacted with i-PrMgCl in the same manner (solution B). Solution A was heated up to 35 °C and Ni(dppp)Cl_2 catalyst was added in one portion. After stirring for 1 h, solution B was added to solution A via a syringe, and the resulting solution was stirred for 1 h. And finally, solution A was added to a mixture via a syringe. The reaction was quenched by pouring HCl aq. (50 wt%) into the solution. The crude polymer was successively washed by Soxhlet extraction using methanol and hexane, and finally extracted using $CHCl_3$. The solvent was removed by evaporation to give a purple solid (yield = 81 %). The peaks observed at 6.98 and 6.94 ppm could be assigned

to the sp2 CH of thiophene rings, and the triplet peak at 2.80 ppm and the doublet peak at 2.74 ppm to the sp3 CH2 attached to the thiophene rings in the regioregular P3HT and P3EHT blocks, respectively. From the integration of the peaks in both regions, the molar ratios of the P3HT and P3EHT can be calculated (Fig. 3-2). Diblockcopolymer (P3HT-*b*-P3EHT) was synthesized with exactly same process except the final addition of A soution.

3.3.6 Living CDSA of P(3HT-*b*-3EHT) with controlled length via self-seeding method. To make pristine nanofibers, BCPs were directly dispersed into anisole at a concentration of 1 mg ml^{-1} intightly sealed vials. The solution was heated at 75 °C for 1 h without stirring before cooling down to room temperature. The solutions were bright orange at high temperatures and turned purple in 1 hours after cooling to room temperature. All the pristine fibers formed by the diblock copolymers and homopolymer were longer than 10 μm and were polydisperse in length. The fibers prepared in anisole were subjected to sonication in a sonication bath (160 W) at 0 °C for 60 min to yield seed fibers. The seed solution was heated at different temperatures for 30 min then cooled and aged at room temperature to allow the nanofibers to grow.

3.3.7 CDSA of P(3HT-b-3EHT-b-3HT) network. BCPs were directly dispersed into anisole or cyclohexane at a concentration of 1 mg ml^{-1} intightly sealed vials. The solution was heated at 75 °C for 1 h without stirring before cooling down to room temperature. The solutions were bright orange at high temperatures and turned purple in 1 hours after

cooling to room temperature. To get the organogel of the triBCPs, concentration of the BCP solution was increased to 10 mg ml^{-1}

3.3.8 CDSA of P(3HT-b-3EHT) and P(3HT-b-3EHT-b-3HT) mixed network. Certain ratio of BCPs were directly dispersed into anisole or cyclohexane at a concentration of 1 mg ml^{-1} intightly sealed vials. The solution was heated at 75 °C for 1 h without stirring before cooling down to room temperature. The solutions were bright orange at high temperatures and turned purple in 1 hours after cooling to room temperature. To get the organogel of the triBCPs, concentration of the BCP solution was increased to 10 mg ml^{-1}

3.4 Results and Discussions

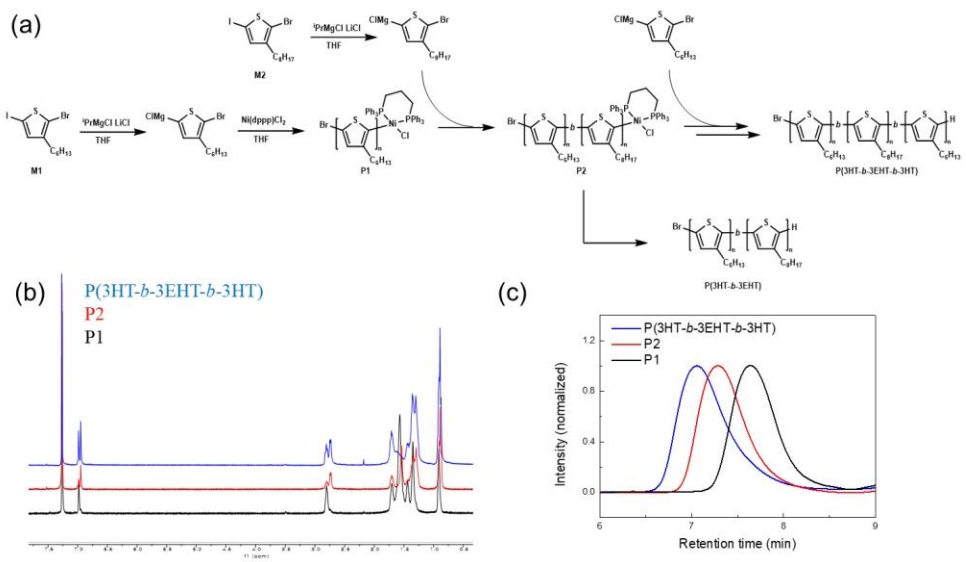

Figure 3-1. (a) Synthetic scheme of BCPs and triBCPs. (b) NMR traces of P(3HT-*b*-3EHT-*b*-3HT), (c) GPC traces of P(3HT-*b*-3EHT-*b*-3HT). The GPC was performed with tetrahydrofuran (THF) as an eluent at a flow rate of 1 mL min^{-1}.

Table 3-1 | Characteristics of homopolythiophenes and block BCPs in this study.

Entry	[M1]:[M2]:[M1]:[cat]	Yield (%)	P1	P2	P3	*Đ*
			$M_n{}^a$ [kDa]	$M_n{}^a$ [kDa]	$M_n{}^a$ [kDa]	
P3HT	60 : 0 : 0 : 1	77	11.2	-	-	1.08
P3EHT	0 : 50 : 0 : 1	68	9.9	-	-	1.12
BCP1	60 : 50 : 0 : 1	75	9.1	12.3	-	1.15
BCP2	120 : 100 : 0 : 1	81	20.5	20.7	-	1.18
BCP3	60 : 100 : 0 : 1	73	8.2	19.8	-	1.19
triBCP	60 : 100 : 60 : 1	66	10.1	24.5	31.2	1.32

[a] Obtained from GPC.

3.4.1 Synthesis of all-conjugated BCPs. Thiophene-based all-conjugated BCPs used in this study were synthesized by Ni(dppp)-mediated Kumada catalyst transfer polymerization (KCTP) of 2-iodo-5-bromothiophenes.[35-38] 3-hexylthiophene (3HT) was used as a monomer for the core-forming crystalline polymer polymer blocks as KCTP produces regioregular poly(3-hexylthiophene) (P3HT). 3-ethylhexylthiphene (3EHT) was adopted for the synthesis of the solvent-soluble conjugated polymer block because stereo-irregular branched alkyl chains on the 3-position of thiophene prevents the crystallization of regioregular P3EHT. 2-bromo-5-iodo derivatives of 3-alkylthiophenes were synthesized to promote regiospecific polymerization of substituted thiphene. Prior to the polymerization with the Ni catalyst, these monomers were activated with i-PrMgCl•LiCl.[39] Initially, the activated 3HT was introduced to the Ni-catalyst solution for the polymerization of the first block, which was allowed to proceed for 1h. The completion of the polymerization was monitored by the GPC analysis. Successive addition of the THF solution of activated 3EHT to the reaction mixture allowed the synthesis of all-conjugated BCPs (for details of the synthesis and purification of BCPS, see the supporting information).[40] The resulting BCPs showed unimodal peaks in the GPC analysis appearing at the retention time corresponding to the expected molecular weights. The molecular weight distribution of the resulting BCP remained low (>

1.18), indicating the pseudo-living nature of the kumada catalyst transfer polymerization (KCTP). Pseudo-controlled nature of KCTP enabled the extension of polymerization to all-conjugated triblock copolymers (triBCPs). We targeted ABA type triblock copolymers having crystalline P3HT as “A” terminal blocks and amorphous P3EHT as “B” block. Three different batches of activated monomers for each block was prepared. Similar to diblock copolymers, monomers were successively introduced to the Ni-catalyst solution. Each polymerization step was traced with GPC analysis. Each polymerization took about 1h for the completion of the polymerization and molecular weights were almost quantitatively grown (Fig 3-1).

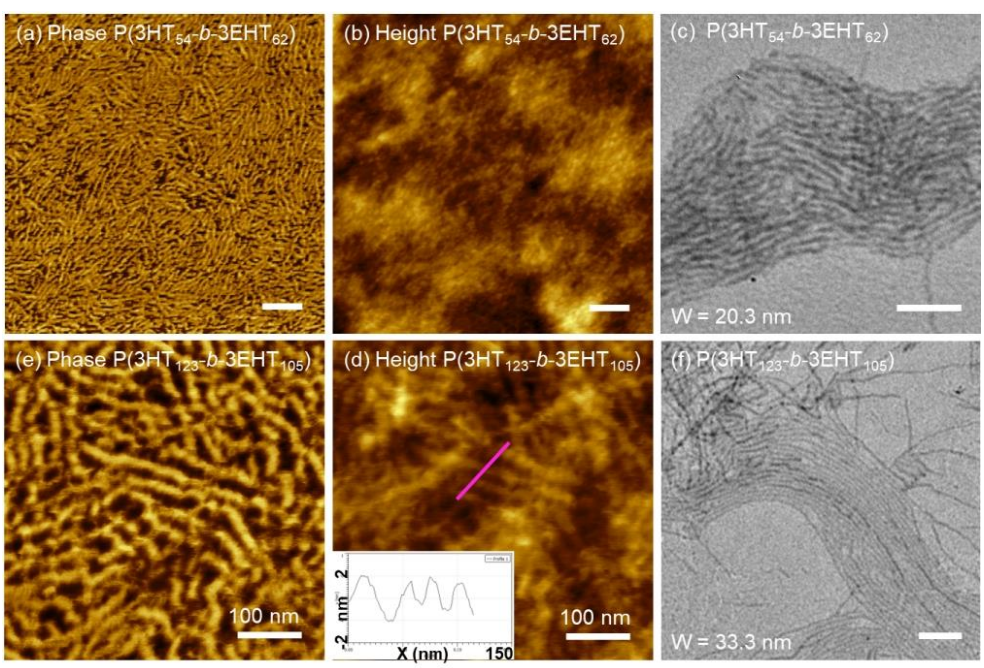

Figure 3-2. (a,b) AFM image of P($3HT_{54}$-*b*-$3EHT_{62}$) fibers (cast from 0.1mg ml^{-1} anisole solution) (a) phase (b) height, (c) TEM image of P($3HT_{54}$-*b*-$3EHT_{62}$) fibers (d,e) AFM image of P($3HT_{123}$-*b*-$3EHT_{105}$) fibers (cast from 0.1mg ml^{-1} anisole solution) (d) phase (e) height, (f) TEM image of P($3HT_{123}$-*b*-$3EHT_{105}$) fibers. Scale bar : 500 nm

3.4.2 Preparation of nanofibers through living CDSA Owing to the solubilizing P3EHT block, CDSA of BCPs in anisole as a solvent successfully afforded the nanofibers with excellent colloidal stability. P($3HT_{54}$-*b*-$3EHT_{62}$) (**BCP1**) and P($3HT_{123}$-*b*-$3EHT_{105}$) (**BCP2**) were turned into polydisperse nanofibers through the conventional CDSA method. BCPs were dissolved to anisole (1 mg ml^{-1}) at 80 °C for 1 h and cooled to room temperature to get the nanofiber of the BCPs (Fig 3-2). The core width of the nanofibers was defined as 20.3 nm for BCP1 and 33.3 nm for BCP2. This indicated that the width of the nanofiber can be tuned depending on the molecular weight of the crystalline P3HT blocks. (Figure 3-2c, e) The height of the nanofibers ranged 2 to 3 nm regardless of the molecular weight of the BCPs.

Precise control of the nanofiber length was demonstrated with the thermally induced self-seeding living CDSA method. .[41-43] This process involved two steps. First, prepared polydisperse nanofibers were fragmented by sonication in anisole at 0 °C for 1h to afford the seed-like nanofibers with short length (Fig. 3-3b). Next,

thermal annealing of the seeds at a desired temperature between 50 °C and 70 °C for 30 min and subsequent cooling to 23 °C initiated the self-seeding processes. Several hours (~ 6 h) of the aging process were necessary for the growth of nanofibers. The length of the nanofibers was kinetically trapped at room temperature and remained the same after 1 week. The average lengths of the nanofibers were calculated from the TEM images. The length of the nanofibers was controllable from 100 nm to 3 μm dependent on the annealing temperature (Fig. 3-3). Above 70 °C, length cannot be estimated due to the bending of the nanofibers. Despite the high crystallinity of the core-forming P3HT block, amorphous P3EHT blocks enable the nanofibers can bend and entangle each other.

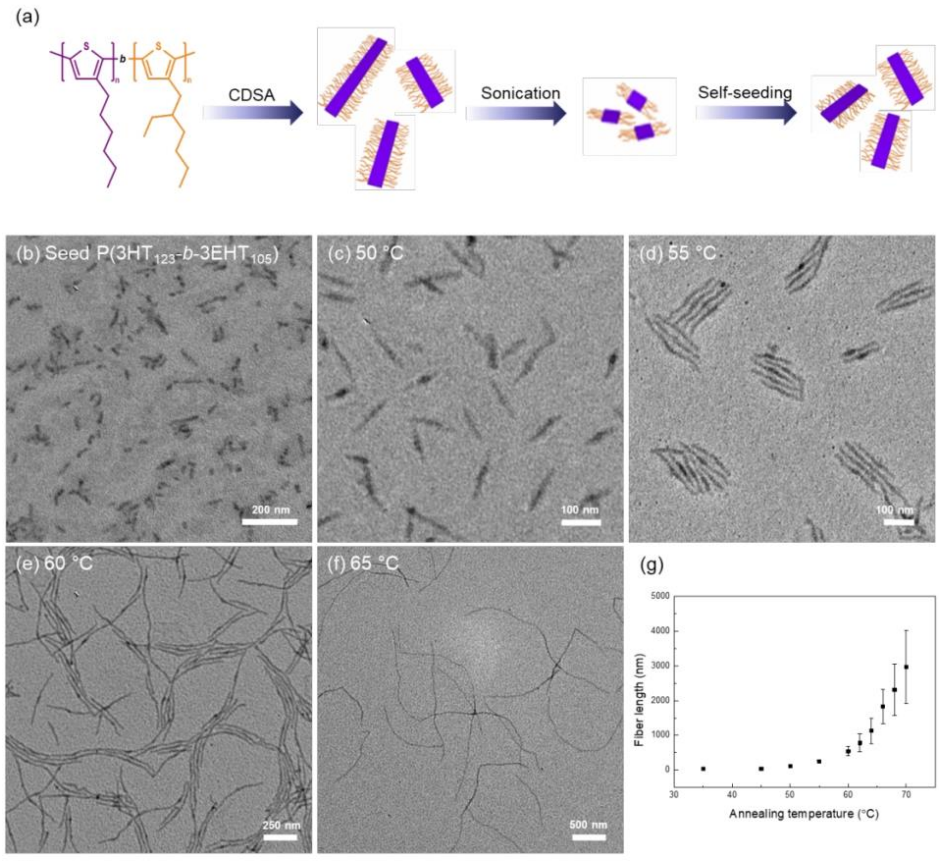

(h)

Temperature (°C)	45	50	55	60	62	64	66	68	70
L_n (nm)	35	113	243	544	780	1134	1826	2312	2970
σ (nm)	5.4	19.3	37.2	136	260	366	495	734	1057
$Đ$	1.07	1.06	1.08	1.09	1.08	1.12	1.13	1.18	1.21

Figure 3-3. (a) Schematic illustration of the living CDSA of P(3HT-b-3EHT) by self seeding method. (b) P($3HT_{123}$-*b*-$3EHT_{105}$) seed after the fragmentation of the nanofibers through sonication for 1h. (c~g) uniform P($3HT_{123}$-*b*-$3EHT_{105}$) nanofibers after the living CDSA at different annealing temperature (for 30 min) and then slowly cooling to 23 °C. (c) 50 °C, (d) 55 °C, (e) 60 °C, (f) 65 °C, (g) Plot

of the L_n of the P($3HT_{123}$-*b*-$3EHT_{105}$) nanofibers vs self-seeding temperature. (h) Nanofiber length analysis summary.

3.4.3 Solvent effect on CDSA behavior of BCPs and network formation of ABA triBCP. The stereogenic center at the alkyl chain of 3-(2-ethylhexyl) thiophene monomer (3-EHT) makes P3EHT amorphous. Differential scanning calorimetry (DSC) analysis of P3EHT proved the amorphous characteristics showing no crystallization peak (S3-1). Low crystallinity of the P3EHT block directly affected the solubility of the BCPS. Increased solubility enabled CDSA of the BCPs not only in the anisole but also in the cyclohexane. Compared to anisole (bp: 153.8°C), cyclohexane (bp: 80.75°C) has a lower boiling point. So, after the CDSA of the BCPs, volatile cyclohexane can be removed through evaporation or freeze-drying method. This advantage enabled the fabrication of nanofiber-based materials such as film or porous foam. BCP2 and triBCP were self-assembled in both solvents. Using BCP2, CDSA in both solvents (1mg/ml) generated nanowires. In anisole (1mg/ml), smooth nanowires were generated and the length of the nanowires could be tuned. But, the structure of the nanowires from cyclohexane (1mg/ml) was undulated and the length of the nanowires was uncontrollable. In the case of ABA triBCP, crystalline P3HT on terminal blocks of the polymer can participate in the CDSA and make intermicellar linkages between the nanowires.[44] Indeed, TEM images after the CDSA of triBCP in anisole and cyclohexane (1mg/ml) revealed nanowires a few micrometers long, with the appearance of several T-junctions among nanowires. Especially in cyclohexane, the undulated structure of the nanowire makes it more favorable for the formation of the links

between the nanowires. At a higher concentration (1wt%), macroscopic gel-like aggregates were observed from the vial containing the sample inside. It indicated that the ABA type triBCP function as linker and induce the formation of nanofiber networks (Fig 3-4).

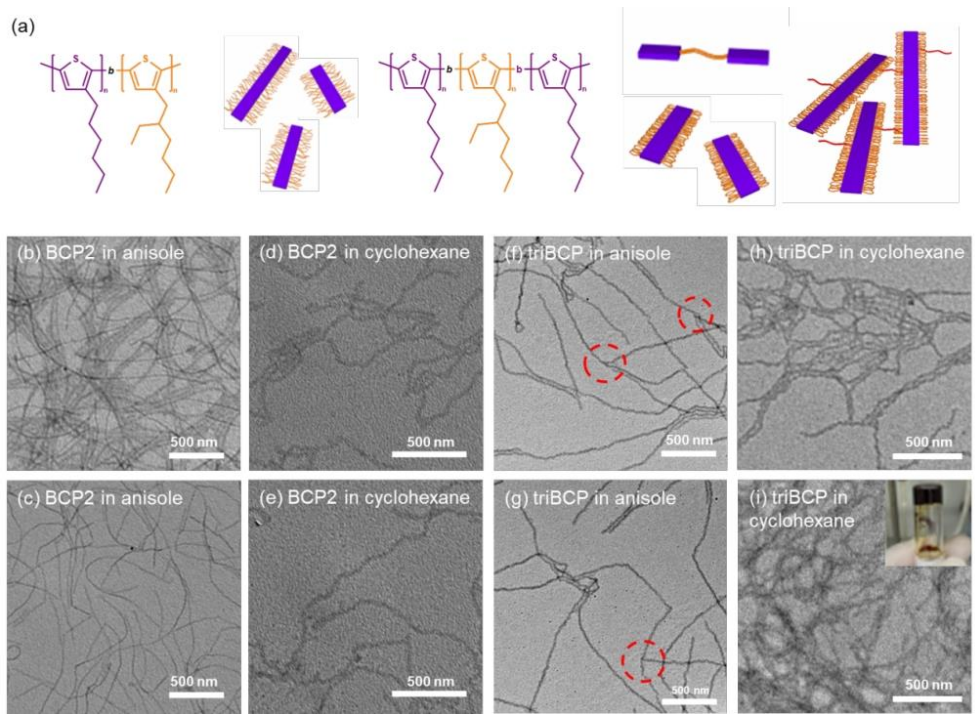

Figure 3-4. (a) Schematic illustration of the CDSA structure from P(3HT-*b*-3EHT) and P(3HT-*b*-3EHT-*b*-3HT). TEM images of (b,c) P($3HT_{123}$-*b*-$3EHT_{105}$) nanowires after CDSA in anisole (1mg/ml). (d,e) P($3HT_{123}$-*b*-$3EHT_{105}$) nanowires after CDSA in cyclohexane (1mg/ml). (f, g) triBCP (P($3HT_{60}$-*b*-$3EHT_{73}$-*b*-$3HT_{40}$)) nanowires after CDSA in anisole (1mg/ml). (h) triBCP (P($3HT_{60}$-*b*-$3EHT_{73}$-*b*-$3HT_{40}$)) nanowires after CDSA in cyclohexane (1mg/ml). (i) triBCP (P($3HT_{60}$-*b*-$3EHT_{73}$-*b*-$3HT_{40}$)) nanowires after CDSA in cyclohexane (10mg/ml) and image of

the vial containing triBCP nanofibers with a intermicellar linking. All samples were diluted to 0.05mg/ml for the TEM analysis.

3.4.4 Network formation of diblock copolymer using ABA triBCP as a linker

ABA triBCP could participate in the CDSA and form intermicellar linkage between the nanowires.[44] The addition of triBCP to the batch of linear nanowires from BCP2 is expected to trigger the formation of nanofiber networks. BCP2 nanowire dispersions were prepared dependent on the solvents (anisole and cyclohexane) and concentrations (1mg/ml, and 10mg/ml). Prior to the addition of triBCP unimer, temperature was kept at 70 °C for 10 min. triBCP unimer was also prepared with different types and concentrations of solvent and kept under 70 °C. triBCP unimer was added to the BCP2 solution with various blending ratios and subsequently cooled to 20 °C, and aged for 24h. At a low concentration of anisole (1mg/ml), macroscopic gel formation was not observed. But, the TEM image of the resulting nanowire revealed the formation of intermicellar networks with the blending ratio of unimer below 15 %. On the other hand, when it comes to the ratio above 20 %, the formation of nanowires was restrained. If the concentration of triBCP unimer exceeds the critical point, unimer hampered the nucleation of BCP2. Highly concentrated (10mg/ml) solution at the ratio of triBCP unimer below 20 %, the viscosity of the solution increased and intermicellar networks fix the nanowires. macroscopic gel formation was visually inspected from the vial. At a 20 % unimer ratio, viscous liquid-like nanowire solution was observed instead of macroscopic gel. When the organic solvent was replaced with cyclohexane, nanowire networks were observed at 5 to 20 % unimer ratios. The formation of the intermicellar

linkage was more favorable due to the undulated surface of the nanowires. Yet, It needed a high concentration (10mg/ml) for the formation of a macroscopic gel (Fig 3-5).

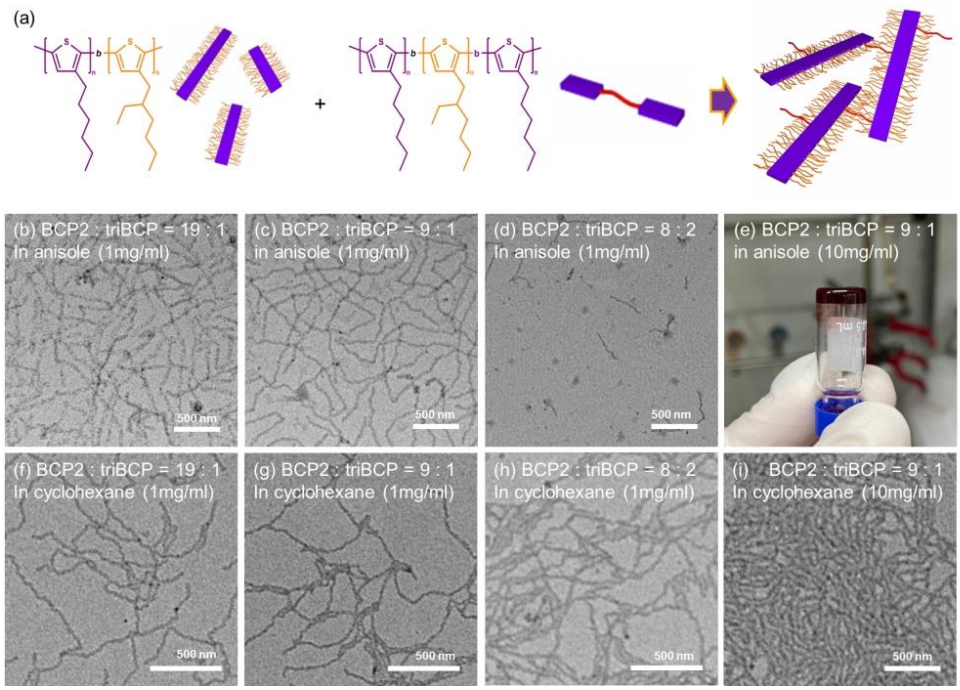

Figure 3-5. (a) Schematic illustration of the network formation from P(3HT-*b*-3EHT) and P(3HT-*b*-3EHT-*b*-3HT). (b, c, d) TEM images of mixture of **BCP2** (P($3HT_{123}$-*b*-$3EHT_{105}$)) and **triBCP (**P($3HT_{60}$-*b*-$3EHT_{73}$-*b*-$3HT_{40}$)) in anisole (1mg/ml) (b) **BCP2**/**triBCP**=19/1, (c) **BCP2**/**triBCP**=9/1, (d) **BCP2**/**triBCP**=8/2. (e) Vial containing the mixture of **BCP2** and **triBCP** with the blending ratio of **BCP2**/**triBCP**=9/1 in anisole (10mg/ml). (f, g, h) TEM images of mixture of **BCP2** (P($3HT_{123}$-*b*-$3EHT_{105}$)) and **triBCP (**P($3HT_{60}$-*b*-$3EHT_{73}$-*b*-$3HT_{40}$) in cyclohexane (1mg/ml) (b) **BCP2**/**triBCP**=19/1, (c) **BCP2**/**triBCP**=9/1, (d)

BCP2/**triBCP**=8/2. (i) TEM images of mixture of **BCP2** (P($3HT_{123}$-*b*-$3EHT_{105}$)) and **triBCP (**P($3HT_{60}$-*b*-$3EHT_{73}$-*b*-$3HT_{40}$)) (**BCP2**/**triBCP**=9/1) in cyclohexane (10mg/ml)

3.4.5 Thermoelectric property of porous foam composed of conducting polymer nanowires Cyclohexane could be removed through evaporation or freeze-drying methods. Using freeze-drying method, we could transform ABA triBCP nanofiber network gel to porous foam. Vial containing macroscopic gel from ABA triBCP in cyclohexane (10mg/ml) was freezed at liquid nitrogen. After the sublimation of cyclohexane through vacuum pump, we could get the dry nanofiber network foam.

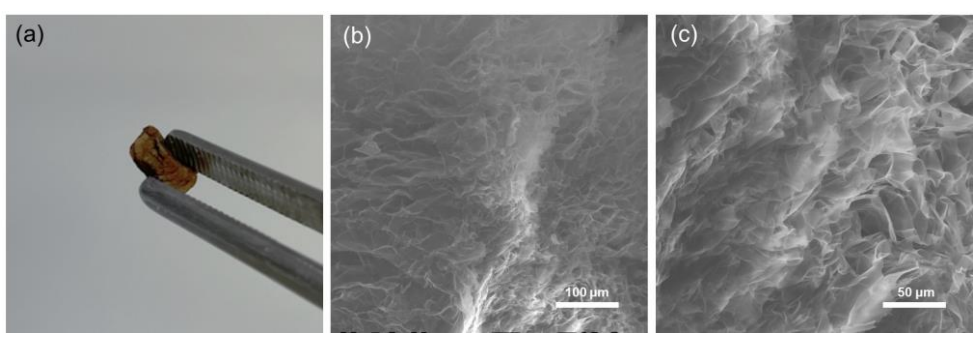

Figure 3-6. (a) Digital image of porous foam from triBCP nanofiber gels. (b, c) SEM image of porous foam

3.5 Conclusions

In summary, we prepared 1D nanofibers through the self-assembly of conjugated P(3HT-*b*-3EHT) and P(3HT-*b*-3EHT-*b*-3HT). P3HT core-forming block induced the stacking of the polymers to nanofiber while P3EHT enhanced the solubility and flexibility. Their preparation by the living CDSA self-seeding method afforded the low dispersity nanofibers with finely controlled lengths. Triblock copolymer form linkage between the nanofibers and generate nanonetworks. At the concentration above 1 wt%, nanofiber nanonetwork fix the movement of the nanofiber and become macroscopic organogel. Organogel could be made by using triblock copolymer as linker or triblock itself as branched nanofibers. After the sublimation of organic solvent, nanofiber organogel became porous foam-type materials. We expect that this foam-type conducting polymer organogel could be used as future thermoelectric materials.

3.6 References

1. Wu, C.; Szymanski, C.; Cain, J.; McNeill, J. *J. Am. Chem. Soc.*, **2007**, *129*, 12904–12905.
2. MacFarlane, L. R.; Shaikh, H.; Garcia-Hernandez, J. D.; Vespa, M.; Fukui, T.; Manners, I. *Nat. Rev. Mater.* **2021**, *6*, 7−26
3. Pecher, J.; Mecking, S. *Chem. Rev.*, **2010**, *110*, 6260–6279.
4. Patel, S. N.; Javier, A. E.; Balsara, N. P. *ACS Nano,* **2013**, *7*, 6056–6068

5. Li, X.; Wang, X. Zhang, L.; Lee, S.; Dai, D. *Science*, **2008**, *319*, 1229–1232.

6. Wang, S.; Pisula, W.; Müllen, K. *J. Mater. Chem.* ***2012***, *22*, 24827−24831

7. Camposeo, A.; Pensack, R. D.; Moffa, M.; Fasano, V.; Altamura, D.; Giannini, C.; Pisignano, D.; Scholes, G. D. *J. Am. Chem. Soc*. **2016**, *138*, 15497−15505

8. Li, X.; Wolanin, P. J.; MacFarlane, L. R.; Harniman, R. L.; Qian, J.; Gould, O. E.; Dane, T. G.; Rudin, J.; Cryan, M. J.; Schmaltz, T. *Nat. Commun*. **2017**, *8*, No. 15909.

9. Grimsdale, A. C.; Chan, K. L.; Martin, R. E.; Jokisz P. G.; Holmes, A. B. *Chem. Rev.*, **2009**, *109*, 897–1091.

10. Liu, C.; Wang, K.; Gong, X.; Heeger, A. J. *Chem. Soc. Rev.* **2016**, *45*, 4825–5846.

11. Zhang, R.; Li, B.; Iovu, M. C.; Jeffries-EL, M.; Sauv`e, G.; Cooper, J.;Jia, S.; Tristram-Nagle, S.; Smilgies, D. M.; Lambeth, D. N.; McCullough, R. D.; Kowalewski, T. *J. Am. Chem. Soc.* **2006**, *128*, 3480–3481.

12. Liu, J.; Arif, M.; Zou, J.; Khondaker S. I.; Zhai, L. *Macromolecules* **2009**, *42*, 9390–9393.

13. Yu,, Z.; Fang, J.; Yan, H.; Zhang, Y.; Lu, K.; Wei, Z. *J. Phys. Chem. C*, **2012**, *116*, 23858–23863.

14. Li, X.; Wolanin, P. J.; MacFarlane, L. R.; Harniman, R. L.; Qian, J.; Gould, O. E. C.; Dane, T. G.; Rudin, J.; Cryan, M. J.; Schmaltz, T.; Frauenrath, H.; Winnik, M. A.; Faul, C. F. J.; Manners, I. *Nat. Commun.* **2017**, *8*, 15909–15916.

15. Jin, X.-H.; Price, M. B.; Finnegan, J. R.; Boott, C. E.; Richter, J. M.; Rao, A.; Menke, S. M.; Friend, R. H.; Whittell, G. R.; Manners, I. *Science*, **2018**, *360*, 897–900.

16. Xu, J.; Zhou, H.; Yu, Q.; Guerin, G.; Manners, I.; Winnik, M. A. *Chem. Sci.* **2019**, *10*, 2280–2284.

17. Qiu, H.; Gao, Y.; Du, V. A.; Harniman, R.; Winnik, M. A.; Manners, I. *J. Am. Chem. Soc.* **2015**, *137*, 2375–2385.

18. He, X.; Hsiao, M.-S.; Boott, C. E.; Harniman, R. L.; Nazemi, A.; Li, X.; Winnik, M. A.; Manners, I. *Nat. Mater.* **2017**, *16*, 481–488.

19. Ganda, S.; Dulle, M.; Drechsler, M.; F¨orster, B.; F¨orster, S.; Stenzel, M. H. *Macromolecules* **2017**, *50*, 8544–8553.

20. Arno, M. C.; Inam, M.; Coe, Z.; Cambridge, G.; Macdougall, L. J.; Keogh, R.; Dove, A. P.; O'Reilly, R. K. *J. Am. Chem. Soc.* **2017**, *139*, 16980–16985.

21. Li, Z.; Liu, R.; Mai, B.; Wang, W.; Wu, Q.; Liang, G.; Gao, H.; Zhu, F. *Polymer* **2013**, *54*, 1663–1670.

22. Schmelz, J.; Schedl, A. E.; Steinlein, C.; Manners, I.; Schmalz, H. *J. Am. Chem. Soc.* **2012**, *134*, 14217–14225.

23. Patra, S. K.; Ahmed, R.; Whittell, G. R.; Lunn, D. J.; Dunphy, E. L.; Winnik, M. A.; Manners, I. *J. Am. Chem. Soc.* **2011**, *133*, 8842–8845.

24. Gilroy, J. B.; Lunn, D. J.; Patra, S. K.; Whittell, G. R.; Winnik, M. A.; Manners, I. *Macromolecules* **2012**, *45*, 5806–5815.

25. Fukui, T.; Garcia-Hernandez, J. D.; MacFarlane, L. R.; Lei, S.; Whittell, G. R.;

Manners, I. *J. Am. Chem. Soc.* **2020**, *142*, 15038−15048.

26. Kynaston, E. L.; Nazemi, A.; MacFarlane, L. R.; Whittell, G. R.; Faul, C. F. J.; Manners, I. *Macromolecules* **2018**, *51*, 1002−1010.

27. Briseno, A. L.; Mannsfeld, S. C. B.; Jenekhe, S. A.; Bao, Z.; Xia, Y. *Mater. Today* **2008**, *11*, 38–47

28. Wang, S.; Kappl, M.; Liebewirth, I.; Muller, M.; Kirchhoff, K.; Pisula, W.; Mullen, K. *Adv. Mater*. **2012**, *24*, 417–420

29. Xiao, C.; Zhao, G.; Zhang, A.; Jiang, W.; Janssen, R. A. J.; Li, W.; Hu, W.; Wang, Z. *Adv. Mater.* **2015**, *27*, 4963–4968

30. Yu, Z.; Fang, J.; Yan, H.; Zhang, Y.; Lu, K.; Wei, Z. *J. Phys. Chem. C* **2012**, *116*, 23858–23863

31. Choi, D.; Chang, M.; Reichmanis, E. *Adv. Funct. Mater*. **2015**, *25*, 920–927

32. Han, L.; Wang, M.; Jia, X.; Chen, W.; Qian, H.; He, F. *Nat. Commun*. **2018**, *9*, 865

33. Kamps, A. C.; Cativo, M. H. M.; Fryd, M.; Park, S.-J. *Macromolecules* **2014**, *47*, 161–164

34. Lee, E.; Hammer, B.; Kim, J.-K.; Page, Z.; Emrick, T.; HAyward, R. C. *J. Am. Chem. Soc*. **2011**, *133*, 10390–10393

35. Yang, S.; Choi, T.-L. *Chem. Sci.*, **2020**, *11*, 8416

36. Zhang, Y.; Tajima, K.; Hirota, K.; Hashimoto, K. *J. Am. Chem. Soc*. **2008**, *130*, 7812–7813

37. Scherf, U.; Gutacker, A; Koenen, N. *Acc. Chem. Res*. **2008**, *41*, 1086–1097

38. Zhang, U.; Tajima, K.; Hirota, K.; Hashimoto, K. *J. Am. Chem. Soc*. **2008**, *130*, 7812-7813

39. Zhang, Y.; Tajima, K.; Hashimoto, K. *Macromolecules* **2009**, *42*, 7008-7015

40. Bao, R, L-Y.; Zhaoa R.; Shi, L. *Chem. Commun*. **2015**, *51*, 6884-6900

41. Gilroy, J. B.; Gat, T.; Whittel, G. R; Chabanne, L.; Mitchels, J. M.; Richardson, R. M.; Winnik, M. A.; Manners, I. A *Nat. Chem.* **2010**, *2*, 566–570

42. . Hudson, Z. M.; Boott, C. E.; Robinson, M. E.; Rupar, P. A.; Winnik, M. A.; Manners, I. *Nat. Chem.* **2014**, *6*, 893–898

43. Qiu, H.; Gao, Y.; Boott, C. E.; Gould, O C.; Harniman, R. L.; Miles, M. J.; Web, S. E. D.; Winnik, M. A.; Manners. I. *Science* **2016**, *352*, 697–701

44. Garcia-Hernandez, J. D.; Kang, Y.; Fukui, T.; Finnegan, J. R.; Manners, I. *Macromolecules* **2022**, *55*, 3821-3830

Chapter 4. Self-assembly of Oppositely Charged Ionic Block Copolymer Complex with Discrete Molecular Weight

4.1 Abstract

When the oppositely charged amphiphilic molecules are mixed, they self-assemble into unusual structures with periodic ionic lattices on their membrane via self-organization due to the electrostatic interactions. Oppositely charged block copolymers have seldom been used to mimic such behavior due to the synthetic difficulty and ill-defined chemical structures. Here we report the self-assembly of oppositely charged ionic block copolymer complex to highly ordered structures. We used the convergent method to synthesize monodisperse and precisely defined block co-oligomers (BCOs) having the tetramers of L-malic acid or (s)-4-amino-2-hydroxybutyric acid as a hydrophilic block and oligo(lactic acid) as a hydrophobic block. These oppositely charged BCOs, with an absolutely defined number of cations or anions were mixed for the co-assembly in water. Indeed, ionic interaction between assembled block co-oligomers opposes the membrane's natural curvature and leads to the faceting of the membranes. The self-assembled structures were characterized by Cryo-TEM and DLS.

4.2 Introduction

One of the ultimate goals in the field of macromolecular chemistry is building the highly ordered self-assembled structures from small molecules by understanding the roles and interactions between the molecules. To solve this grand challenge, it is necessary to understand the function of building units constituting the ordered nanostructures. In this respect, unusual self-assembled structures have drawn the attention of many scientists including stomatocytes,[1,2] cubosomes,[3,4] Janus particles,[5,6] etc. Among them, polyhedral structures with faceted membranes have attracted us. In the past, Thomas and coworkers discovered the faceting of the vesicle membrane composed of charged surfactant complexes which induced the formation of polyhedral structures.[7] Samuel and Olvera established the theory through computational simulations.[8-10] Pall demonstrated that the shape transformation of polymersomes from sphere to polyhedron shapes could also be induced through the aggregation of perylene moieties.[11] However, to utilize the faceted vesicles for further application, we still need to advance the understanding of the faceted structures.

We tried to access the faceting of the membrane from the absolutely defined polymer sequences. When oppositely charged amphiphilic molecules come together, attractive and repulsive forces of the functional units led to unusual consequential structures to avoid charge accumulation. It results in the formation of ionic crystalline structures like flat, cylindrical structures,[13] and 3D structures with faceted surfaces. Especially, mixtures of anionic and cationic surfactants generate buckling of the vesicle membrane and form icosahedral-shaped vesicles.[8-10,12] We hypothesized that the ionic crystalline structures would favorably induce the

faceting of the membranes which cannot be done due to ill-defined chemical structures of polymers and synthetic complexities. But recently, various synthetic strategies have been provided for the synthesis of discrete polymers with sequential accuracies such as solid-phase synthesis,[14-18] Cherry picking of polymers with column chromatography,[19] and iterative exponential growth of polymers.[20,21] We recently published the synthesis of poly(α-hydroxy acid) (PAH) with an absolutely defined aperiodic sequence and molecular weight using the iterative exponential growth method.[22] A subsequent study about intramolecular cyclization of PAHs was also successfully achieved by functionalization of end groups.[23] However, the options for functional hydrophilic monomers are seriously limited.

Here, we report amphiphilic block copolymers with ionic functionalities composed of newly synthesized two distinct monomers containing ionic functional groups. Both monomers contain hydroxy and carboxylic acid groups and additional functional groups. Each monomer can participate in the iterative convergent method with other α-hydroxy acids and make discrete oligomers. Afforded oligomers can be precursors for the preparation of amphiphilic block copolymers with ionic functionalities. Combined with discrete polylactic acid which can serve as a hydrophobic part, we synthesized a series of discrete amphiphilic block copolymers. Through the solvent-switch self-assembly,[11] we observed faceted polymersomes with the mixture of discrete cationic polymer **AHBA**$_4$-*b*-**LA**$_8$-tz and discrete anionic polymer **MA**$_4$-*b*-**LA**$_8$-tp. The self-assembled structures were characterized by cryo-TEM and DLS.

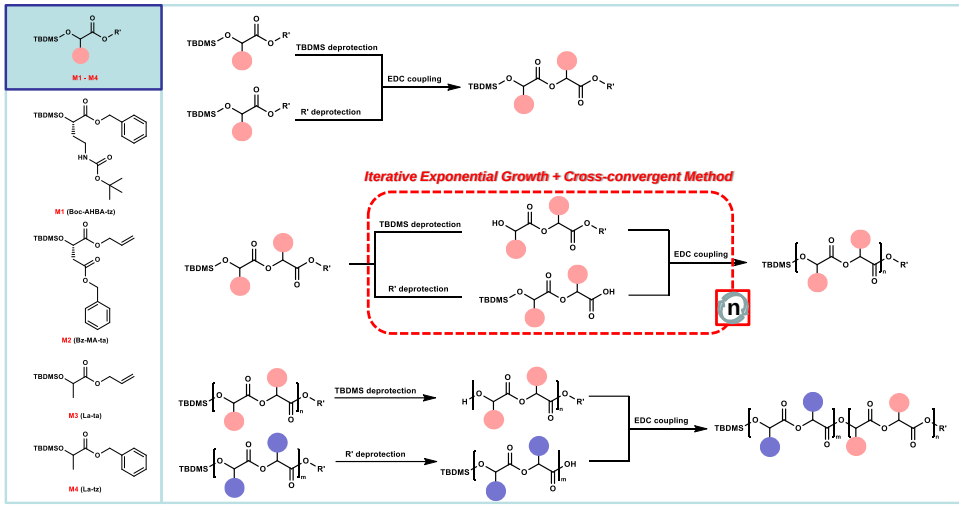

Figure 4-1. Schematic of the Iterative convergent synthesis of discrete ionic block copolymers.

4.3 Experimental Sections

4.3.1 Materials. All reagents and chemicals were purchased from Sigma Aldrich, Alfa Aesar, and TCI and used as received. CH_2Cl_2 was dried (using CaH_2 under a N_2 atmosphere) and distilled. Tetrahydrofuran (THF) was refluxed with Na and benzophenone under a N_2 atmosphere and distilled before use. All reactions were performed in an inert atmosphere.

4.3.2 Synthesis of hydrophilic monomers. *(S)-4-((tert-butoxycarbonyl)amino)-2-hydroxybutanoic acid (**N-boc-AHBA**).* Commercially available (S)-4-amino-2-hydroxybutanoic acid (1.790 g, 15.03 mmol) was dissolved in a solution of K_2CO_3 (5.193 g, 37.6 mmol) in water (50 mL) and treated with a solution of di-tert-butyl dicarbonate (3.815 g, 17.48 mmol) in 1,4-dioxane (20 mL). After stirring at room

temp. for 24 h, the solution was extracted twice with Et_2O. The aqueous phase was acidified to pH = 1 with HCl (1M), treated with solid NaCl to saturate it and extracted five times with AcOEt. The organic phases were concentrated to dryness to give *N-boc-AHBA*, pure enough for further use (3.226 g, 98%). ^{1}H NMR [400 MHz, DMSO-d6]: d δ 6.75 (t, 1H), 3.93 (dd, 1H), 3.00 (m, 2H), 1.77 (m, 1H), 1.57 (m, 1H), 1.36 (s, 9H); HRMS (MM: ESI–APCI) calcd for $C_9H_{17}NO_5$ $[M+Na]^+$ 242.0999, found 242.0997

*(benzyl (S)-4-((tert-butoxycarbonyl)amino)-2-hydroxybutanoate (**N-boc-AHBA-z**)*. A two-neck round bottom flask (RBF) was charged with (S)-4-((tert-butoxycarbonyl)amino)-2-hydroxybutanoic acid (N-boc-AHBA) (10 g, 45.61 mmol), triethylamine (TEA, 68.42 mmol), benzyl chloride (68.42 mmol), and ethyl acetate (100 mL). The reaction flask was connected to a condenser and was refluxed for 24 h. Upon completion of the reaction, the reaction mixture was washed with water and brine. The combined organic layer was dried over MgSO4, and the solvent was removed under reduced pressure. The crude mixture was purified by column chromatography using n-hexane/EA (7:3 v/v) as an eluent. The product was further purified with recrystallization (n-hexane, EA) and obtained as white crystal (12.3g, 87%); 1H NMR (400MHz, $CDCl_3$): δ 7.27-7.2 (s, 5H), 6.68 (s, 1H), 5.37 (s, 1H), 5.01 (s, 2H), 3.99 (dd, 1H), 2.9 (m, 2H), 1.73-1.63, 1.55-1.46 (m, 2H), 1.25 (s, 9H).

*Benzyl (S)-4-((tert-butoxycarbonyl)amino)-2-((tert-butyldimethylsilyl)oxy)butanoate (**N-boc-AHBA-tz, M1**)*. ((benzyl (S)-4-((tert-butoxycarbonyl)amino)-2-hydroxybutanoate (N-boc-AHBA-z) (3 g, 9.70 mmol) was dissolved in dry DMF (40 mL). To this solution, imidazole (19.40 mmol) and

TBDMSCl (12.61 mmol) were added. The reaction mixture was stirred at room temperature for 12 h. Upon completion of the reaction, the reaction was quenched with saturated $NaHCO_3$ (15 mL), followed by dilution with water (30 mL). The resulting mixture was extracted with MC. The combined organic layer was washed with brine and dried over $MgSO_4$, and the solvent was removed under reduced pressure. Colorless liquid (3.20 g, 78%); ^{1}H NMR (400MHz, CDCl3): δ 7.35-7.32 (s, 5H), 5.15 (s, 2H), 4.91 (s, 1H), 4.34 (t, 1H), 3.23 (m, 2H), 1.94 (q, 2H), 1.42 (s, 9H), 0.91 (s, 9H), 0.1 (s, 6H).

2-[2,2-Dimethyl-5-oxo-1,3-dioxolan-4-yl]acetic Acid ***(1)***. To a mixture of L-malic acid (20 g, 0.15 mol) and 2,2-dimethoxypropane (74 mL, 0.60 mol) in a Schlenk tube under nitrogen was added p-toluenesulfonic acid monohydrate (0.29 g, 1.5 mmol), and the solution was stirred at room temperature for 3.5 h. H2O (100 mL) containing NaHCO3 (0.13 g, 1.5 mmol) was added to the solution before the aqueous layer was separated and extracted with DCM (5 × 100 mL). The combined organic layers were dried with NaSO4 and filtered, and the solvent was removed under reduced pressure. The resulting solid was recrystallized from Et2O, yielding a white solid (16.89 g, 65%). ^{1}H NMR (400MHz, $CDCl_3$): δ 11.02 (s, 1H,), 4.71 (dd, 1H), 3.00 (dd, 1H), 2.86 (dd, 1H), 1.62 (s, 3H), 1.57 (s, 3H).

2-[2,2-Dimethyl-5-oxo-1,3-dioxolan-4-yl]acetic acid benzyl ester ***(2)***. To a solution of 2-[2,2-Dimethyl-5-oxo-1,3-dioxolan-4-yl]acetic Acid (10 g, 61 mmol) in dry acetone under nitrogen was added dry NEt3 (10.2 mL, 73 mmol) followed by benzyl bromide (8.9 mL, 75 mmol). The solution was refluxed for 60 h at 50 °C before being cooled to room temperature. The solids were removed by filtration and washed with acetone before the volatile organic solvents were removed under

reduced pressure. The resulting residue was dissolved in EtOAc (300 mL) and H_2O (150 mL). The aqueous layer was further extracted with EtOAc (2 × 100 mL) before the combined organic layers were dried with MgSO4, filtered, and reduced in vacuo. The resultant solid was recrystallized from Et2O to yield white crystals (12.14 g, 80%). ^{1}H NMR (400 MHz, $CDCl_{3)}$ δ 7.36 (m, 5H), 5.18 (d, 2H), 4.74 (dd, 1H), 2.98 (dd, 1H), 2.84 (dd, 1H), 1.58 (s, 3H), 1.56 (s, 3H).

*2-[2,2-Dimethyl-5-oxo-1,3-dioxolan-4-yl]acetic acid benzyl ester (**Bz-MA-a**)*. Ground K_2CO_3 (12.3 g, 89.2 mmol) and tetrabutyl ammonium bromide (2.40 g, 7.43 mmol) were suspended in DMF (150 mL), and 2-[2,2-Dimethyl-5-oxo-1,3-dioxolan-4-yl]acetic acid benzyl ester (16.7 g, 74.3 mmol) and allyl bromide (7.55 mL, 89.2 mmol) were added. The mixture was stirred at room temp. After 4 h, it was concentrated (at ca. 1 mbar; 35 °C) to a quarter of its initial volume and Et_2O (250 mL), 5% aq. citric acid solution (150 mL) and water (50 mL) were added. The aqueous phase was separated and extracted with Et2O. The combined organic phases were washed with 5% NaHCO3 and sat. NaCl solutions, dried (MgSO4), and concentrated. Purification by flash chromatography (Et2O/pentane 1:1) gave product (18.0 g, 92%) as a colorless, oily liquid. ^{1}H NMR (400 MHz, $CDCl_{3)}$ δ 7.36 (m, 5H), 5.90 (m, 1H), 5.28 (dd, 2H), 5,15 (t, 2H), 4.66 (d, 2H), 4.54 (dd, 1H), 3.18 (d, 1H), 2.89 (m, 2H).

*1-allyl 4-benzyl (S)-2-((tert-butyldimethylsilyl)oxy)succinate (**Bz-MA-ta, M2**)* (Bz-MA-a) (3 g, 8.87 mmol) was dissolved in dry DMF (40 mL). To this solution, imidazole (11.53 mmol) and TBDMSCl (17.74 mmol) were added. The reaction

mixture was stirred at room temperature for 12 h. Upon completion of the reaction, the reaction was quenched with saturated $NaHCO_3$ (15 mL), followed by dilution with water (30 mL). The resulting mixture was extracted with MC. The combined organic layer was washed with brine and dried over $MgSO_4$, and the solvent was removed under reduced pressure. Colorless liquid (3.28 g, 98%) ^{1}H NMR (400 MHz, $CDCl_3$) δ 7.36 (m, 5H), 5.90 (m, 1H), 5.27 (dd, 2H), 5,13 (t, 2H), 4.66 (t, 2H), 4.59 (m, 1H), 2.89 (m, 2H), 0.88 (s, 9H), 0.075 (d, 6H).

4.3.3 Deprotection of functional groups.

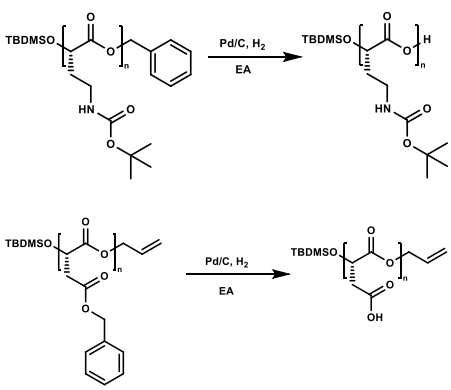

,

General procedure for the deprotection of benzyl group from N-Boc-AHBA$_m$-tz and Bz-MA$_4$-b-LA$_n$-ta by hydrogenation. A compound protected with tert-butyldimethylsilyl (TBDMS) and benzyl groups was dissolved in ethyl acetate. Palladium on activated charcoal (10% Pd/C, 0.03~0.2 eq.) was added to the solution, and the suspension was purged with argon for 15 minutes. The argon atmosphere was then replaced with hydrogen atmosphere, and the reaction mixture was stirred at room temperature. The reaction was monitored by thin layer chromatography (TLC) analysis. Upon completion of the reaction, the suspension

was filtered through a Celite cake to remove Pd/C. The product was obtained by removing the solvent from the filtrates under reduced pressure.

N-Boc-AHBA$_2$-t. Colorless oil; ; ^{1}H NMR (400MHz, $CDCl_3$): δ 5.28-5.13 (t, 1H, O-C**H**(CH_2CH_2N)-C=O), 4.41 (t, 1H, SiO-C**H**(CH_2CH_2N)-C=O), 3.4-3.1 (m, 4H, C**H**$_2$N), 2.19-1.97 (m, 4H, C**H**$_2$$CH_2N$), 1.43 (s, 18H, O-C(C**H**$_3$)$_3$), 0.91 (s, 9H, (C**H**$_3$)$_3$C-Si), 0.09 (dd, 6H, $(CH_3)_3$C-Si(C**H**$_3$)$_2$-O) ppm; Yield: 5.2 g, 99%

N-Boc-AHBA$_4$-t. Colorless viscous oil; ; ^{1}H NMR (400MHz, $CDCl_3$): δ 5.28-4.94 (m, 7H, O-C**H**(CH_2CH_2N)-C=O, and N**H**), 4.41 (t, 1H, SiO-C**H**(CH_2CH_2N)-C=O), 3.4-3.1 (m, 8H, C**H**$_2$N), 2.19-1.96 (m, 8H, C**H**$_2$$CH_2N$), 1.43 (s, 36H, O-C(C**H**$_3$)$_3$), 0.91 (s, 9H, (C**H**$_3$)$_3$C-Si), 0.09 (dd, 6H, $(CH_3)_3$C-Si(C**H**$_3$)$_2$-O) ppm; Yield: 1.2 g, 98%

MA$_4$-b-LA$_8$-tp. Colorless viscous oil; ; ^{1}H NMR (400MHz, $CDCl_3$): δ 5.61-5.47 (m, 3H), 5.23-5.07 (m, 8H), 4.7 (t, 1H), 4.15-4.04 (m, 2H), 3.2-2.70 (m, 8H), 1.69-1.61 (m, 2H), 1.61-1.45 (m, 24H), 0.93 (t, 3H), 0.89 (s, 9H), 0.09 (d, 6H) ppm; MS (MALDI-TOF): m/z calcd for [M+Na]+: 1236.36; found 1236.87. Yield: 268 mg , 98%

MA$_4$-b-LA$_{16}$-tp. White solid; ; ^{1}H NMR (400MHz, $CDCl_3$): δ 7.37-7.28 (m, 5H), 5.86-5.39 (m, 1H), 5.52-5.61 (m, 3H), 5.07-5.36 (m, 27H) 4.69-4.74 (m, 1H), 4.62 (d, 2H), 2.70-3.05 (m, 8H), 1.45-1.6 (m, 48H), 0.91 (s, 9H), 0.09 (d, 6H) ppm; MS (MALDI-TOF): m/z calcd for [M+Na]+: 1594.53; found 1595.13. Yield: 342 mg , 99%

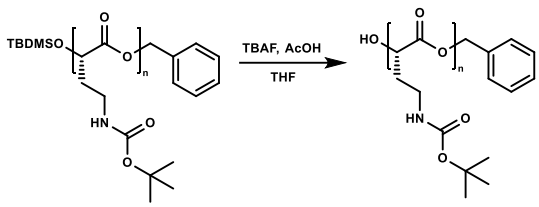

General procedure for the deprotection of TBDMS group on N-Boc-AHBA$_n$-tz with TBAF A compound protected with TBDMS and benzyl groups was dissolved in dry tetrahydrofuran (0.05M in THF). After the addition of AcOH (2 eq to starting material (S.M.)), the mixture was stirred for 10 min. and TBAF (1M solution in THF, 3 eq to S.M.) was added dropwisely. The reaction mixture was stirred at room temperature for 3 h. The reaction was monitored by TLC analysis. Upon completion of the reaction, the reaction was quenched with saturated NaHCO3 followed by dilution with water. THF was evaporated with vacuum evaporator and aqueous solution was extracted with MC (3 times). The organic layer was separated and washed with brine. The combined organic layer was dried over MgSO4, and the solvent was removed under reduced pressure. The crude product was purified by column chromatography.

N-Boc-AHBA$_2$-z. Colorless oil; ; ^{1}H NMR (400MHz, $CDCl_3$): δ 7.40-7.32 (m, 5H, Ph-**H**), 5.17-5.13 (m, 3H, O-C**H**(CH_2CH_2N)-C=O and Ph-C**H**$_2$-O), 4.93, 4.75 (s, 2H, N**H**), 4.33 (t, 1H, HO-C**H**(CH_2CH_2N)-C=O), 3.33-3.18 (m, 4H, C**H**$_2$N), 2.10-1.99, 1.83 (m, 4H, C**H**$_2$$CH_2N$), 1.42 (s, 18H, O-C(C**H**$_3$)$_3$) ppm; Yield: 6.5 g, 86%

N-Boc-AHBA$_4$-z. Colorless viscous oil; ; ^{1}H NMR (400MHz, $CDCl_3$): δ 7.40-7.32 (m, 5H, Ph-**H**), 5.26-4.77 (m, 8H, O-C**H**(CH_2CH_2N)-C=O, and Ph-C**H**$_2$-O), 4.36 (t,

1H, HO-C**H**(CH_2CH_2N)-C=O), 3.42-3.1 (m, 8H, C**H**$_2$N), 2.24-1.86 (m, 8H, C**H**$_2$$CH_2N$), 1.43 (s, 36H, O-C(C**H**$_3$)$_3$) ppm; Yield: 600 mg, 65%

General procedure for the deprotection of allyl group on Bz-MAn-ta.

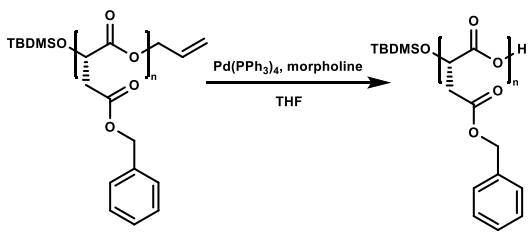

A schlenk flask was charged with $Pd(PPh_3)_4$ (0.1 mol. eq.) and THF under a nitrogen atmosphere. The Bz-MA_n-ta (1.0 mol. eq.) was added into the reaction mixture. The reaction mixture was stirred at 0 °C. Morpholine (1.05 mol. eq.) was added to the solution dropwise at 0 °C and monitored by TLC. After the reaction was complete, the solvent was removed under reduced pressure. The crude was dissolved in dichloromethane and washed three times with 1M HCl (aq). The extracted organic layer was dried with anhydrous $MgSO_4$ and filtered. The solvent was removed under reduced pressure. Crude mixture was redissolved in Et_2O and filtered through a Celite cake. The product was obtained by removing the solvent from the filtrates under reduced pressure.

Bz-MA$_2$-t. Colorless oil; ; ^{1}H NMR (400MHz, $CDCl_3$): δ 7.38-7.29 (m, 10H), 5.62 (m, 1H), 5.14 (t, 4H), 4.62 (q, 1H), 2.98 (d, 2H), 2.89-2.74 (m, 2H), 0.91 (s, 9H), 0.09 (d, 6H) ppm; Yield: 3.17 g, 94%

Bz-MA$_4$-t. Colorless viscous oil; ; δ 7.38-7.29 (m, 20H), 5.57 (m, 3H), 5.17-5.04 (m, 8H), 4.71 (q, 1H), 2.98 (d, 2H), 3.03-2.74 (m, 2H), 0.91 (s, 9H), 0.09 (d, 6H) ppm; Yield: 896 mg, 89%

General procedure for the deprotection of TBDMS group on Bz-MAn-ta with BF3•Et2O

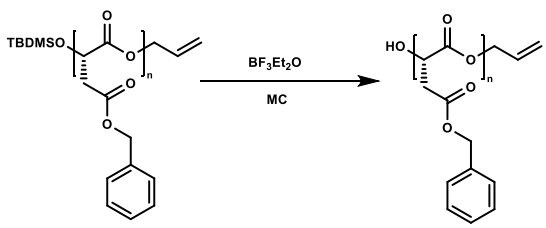

A compound protected with TBDMS and benzyl groups was dissolved in dry dichloromethane (DCM). The solution was cooled to 0ºC on an ice bath, and boron trifluoride diethyl etherate (BF3•Et2O) was added dropwise. The reaction mixture was stirred at room temperature for 4 h. The reaction was monitored by TLC analysis. Upon completion of the reaction, the reaction was quenched with saturated NaHCO3 followed by dilution with water. The organic layer was separated and washed with brine. The combined organic layer was dried over MgSO4, and the solvent was removed under reduced pressure. The crude product was purified by automated column chromatography.

Bz-MA$_2$-a. Colorless viscous oil; ; ^{1}H NMR (400MHz, $CDCl_3$): δ 7.38-7.29 (m, 10H), 5.83 (m, 1H), 5.62 (m, 1H), 5.34-5.09 (m, 6H), 4.62-4.53 (m, 3H), 3.09 (m, 1H), 2.98-2.74 (m, 4H) ppm; . Yield: 1.71 g , 98%

Bz-MA4-a. colorless viscous oil; ^{1}H NMR (400MHz, $CDCl_3$): δ 7.38-7.29 (m, 20H), 5.81 (m, 1H), 5.63-5.50 (m, 3H), 5.34-5.09 (m, 10H), 4.62-4.53 (m, 3H), 3.13-2.86 (m, 9H) ppm; . Yield: 1.14 g , 98%

General procedure for the deprotection of N-Boc groups on N-Boc-AHBAn-LAm-tz with TFA. Compound was dissolved in dry MC (5 wt%). TFA was added dropwisely with 40 wt% to MC. The reaction mixture was stirred at room temperature for 1 h. The reaction was monitored by TLC analysis and NMR. Upon completion of the reaction, solvent and TFA were removed with evaporator. The crude mixture was redissolved with small amount of EA and polymer was precipitated to cold hexane. After 3 times of centrifugation with 4500 rpm for 5h, residue solvents were removed with evaporator.

AHBA$_4$-b-LA$_8$-tz. Viscous white solid; ; ^{1}H NMR (400MHz, $CDCl_3$): δ 8.12-7.65 (m, 8H) 7.38-7.31 (m, 5H), 5.41-5.06 (m, 11H), 4.49 (m, 1H), 3.37-2.97 (m, 8H) 2.51-2.08 (m, 8H), 1.6-1.48(m, 24H), 0.91 (s, 9H), 0.09 (d, 6H) ppm; Yield: 201 mg , 71%

AHBA$_4$-b-LA$_{16}$-tz. White solid; ; ^{1}H NMR (400MHz, $CDCl_3$): δ 8.12-7.65 (m, 16H) 7.38-7.31 (m, 5H), 5.41-5.06 (m, 21H), 4.49 (m, 1H), 3.37-2.97 (m, 8H) 2.51-2.08 (m, 8H), 1.6-1.48(m, 48H), 0.91 (s, 9H), 0.09 (d, 6H) ppm; Yield: 314 mg, 92%

4.3.4 Coupling reaction of monomers and oligomers.

General procedure for esterification reactions

Alcohol and carboxylic acid (1.05 eq.) were dissolved in dry DCM, and the mixture was cooled to 0 oC on an ice bath. To the mixture, 4-(Dimethylamino)pyridinium 4-toluenesulfonate (DPTS, 0.2 eq.) and 1-(3-dimethylaminopropyl)- 3-ethylcarbodiimide hydrochloride (EDC•HCl, 1.4 eq.) were added. The reaction mixture was stirred overnight at room temperature, and the reaction was monitored by TLC analysis. Upon completion of the reaction, the reaction mixture was washed with water and brine. The combined organic layer was dried over MgSO4, and the solvent was removed under reduced pressure. The crude product was purified by automated column chromatography. Block oligomers were purified by preparative-size exclusion chromatography (prep-SEC) with a series of columns using chloroform as an eluent.

Synthesis of discrete oligo((S)-(-)-4-amino-2-hydroxybutyric acid). N-Boc-AHBAn-t and N-Boc-AHBAn-z were dissolved in dry DCM under argon and cooled to 0 °C in ice bath. To the solution, 4-(dimethylamino)pyridinium 4-toluenesulfonate (DPTS, 0.2 eq.) and 1-(3-dimethylaminopropyl)-3-ethylcarbodiimide hydrochloride (EDC•HCl, 1.5 eq.) were added. The reaction mixture was stirred overnight at room temperature. After completion, the reaction

mixture was washed with water and brine. The organic layer was dried with MgSO4, filtered, and concentrated under reduced pressure. The crude product was purified by automated column chromatography using hexane/ethyl acetate as eluent. (N-Boc-AHBAn-t and N-Boc-AHBAn-z were prepared by the debenzylation and desilylation of according to the described general procedure)

N-Boc-AHBA$_2$-tz. Colorless oil; ; ^{1}H NMR (400MHz, $CDCl_3$): δ 7.40-7.32 (m, 5H, Ph-**H**), 5.17-5.13 (m, 3H, O-C**H**(CH_2CH_2N)-C=O and Ph-C**H**$_2$-O), 4.93, 4.75 (s, 2H, N**H**), 4.36 (t, 1H, SiO-C**H**(CH_2CH_2N)-C=O), 3.24 (m, 4H, C**H**$_2$N), 2.10-2.04, 1.95 (m, 4H, C**H**$_2$$CH_2N$),1.42 (s, 18H, O-C(C**H**$_3$)$_3$), 0.91 (s, 9H, (C**H**$_3$)$_3$C-Si), 0.09 (dd, 6H, $(CH_3)_3$C-Si(C**H**$_3$)$_2$-O) ppm; Yield: 12.3g, 90%

N-Boc-AHBA$_4$-tz. Colorless viscous oil; ; ^{1}H NMR (400MHz, $CDCl_3$): δ 7.40-7.32 (m, 5H, Ph-**H**), 5.4-4.80 (m, 9H, O-C**H**(CH_2CH_2N)-C=O, N**H** and Ph-C**H**$_2$-O), 4.41 (t, 1H, SiO-C**H**(CH_2CH_2N)-C=O), 3.4-3.1 (m, 8H, C**H**$_2$N), 2.19-1.96 (m, 8H, C**H**$_2$$CH_2N$), 1.43 (s, 36H, O-C(C**H**$_3$)$_3$), 0.91 (s, 9H, (C**H**$_3$)$_3$C-Si), 0.09 (dd, 6H, $(CH_3)_3$C-Si(C**H**$_3$)$_2$-O) ppm; Yield: 5.3g, 73%

Synthesis of discrete oligo(L-malic acid). *Bz*-MAn-t and *Bz*-MAn-a were dissolved in dry DCM under argon and cooled to 0 °C in ice bath. To the solution, 4-(dimethylamino)pyridinium 4-toluenesulfonate (DPTS, 0.2 eq.) and 1-(3-dimethylaminopropyl)-3-ethylcarbodiimide hydrochloride (EDC•HCl, 1.5 eq.) were added. The reaction mixture was stirred overnight at room temperature. After completion, the reaction mixture was washed with water and brine. The organic layer was dried with $MgSO_4$, filtered, and concentrated under reduced pressure. The crude product was purified by automated column chromatography using

hexane/ethyl acetate as eluent. (*Bz*-MAn-t and *Bz*-MAn-a were prepared by the deallylation and desilylation of according to the described general procedure)

Bz-MA$_2$-ta. Colorless oil; ; ^{1}H NMR (400MHz, $CDCl_3$): δ 7.38-7.29 (m, 5H), 5.83 (m, 1H), 5.56 (t, 1H), 5.32-5.20 (s, 2H), 5.13 (m, 4H), 4.74 (q, 1H), 4.59 (d, 2H), 2.99-2.72 (m, 4H), 0.91 (s, 9H), 0.09 (d, 6H) ppm; Yield: 2.3 g, 88%

Bz-MA$_4$-ta. Colorless viscous oil; ; ^{1}H NMR (400MHz, $CDCl_3$): δ 7.38-7.29 (m, 5H), 5.83 (m, 1H), 5.60-5.49 (m, 3H), 5.32-5.06 (m, 12), 4.71f (q, 1H), 4.57 (d, 2H), 3.06-2.69 (m, 8H), 0.91 (s, 9H), 0.09 (d, 6H) ppm; Yield: 1.32 g, 79%

General procedure for the Hetero-convergent synthesis of AHBAn-b-LAm N-Boc-AHBAn-t and LAm-z were dissolved in dry DCM, and the reaction mixture was cooled to 0 ºC in ice bath. To the solution, 4-(dimethylamino)pyridinium 4-toluenesulfonate (DPTS, 0.3 eq.) and 1-(3-dimethylaminopropyl)-3-ethylcarbodiimide hydrochloride (EDC•HCl, 2 eq.) were added, and the reaction mixture was stirred for 12h at room temperature. After completion, the reaction mixture was washed with water and brine. The organic layer was dried with MgSO4, filtered, and concentrated under reduced pressure. The pure product was isolated via preparative size-exclusion chromatography (prep-SEC). N-Boc-AHBAn-t were prepared by the debenzylation of N-Boc-AHBAn-tz and LAm-z were prepared according to the previously published paper.

N-Boc-AHBA$_4$-LA$_8$-tz. Viscous white solid; ; ^{1}H NMR (400MHz, $CDCl_3$): δ 7.37-7.31 (m, 5H), 5.11-5.30 (m, 11H, O-C**H**(CH3)-C=O, O-C**H**(CH_2CH_2N)-C=O and Ph-C**H**$_2$-O), 3.11-3.46 (m, 8H) 1.96-2.26 (m, 8H), 1.48-1.6 (m, 24H), 1.43 (s, 36H),

0.91 (s, 9H), 0.09 (d, 6H) ppm; MS (MALDI-TOF): m/z calcd for [M+Na]+: 1624.71; found 1625.01. Yield: 850 mg , 81%

N-Boc-AHBA$_4$-LA$_{16}$-tz. White solid; ; ^{1}H NMR (400MHz, $CDCl_3$): δ 7.37-7.31 (m, 5H), 5.11-5.30 (m, 21H, O-C**H**(CH3)-C=O, O-C**H**(CH_2CH_2N)-C=O and Ph-C**H**$_2$-O), 3.11-3.46 (m, 8H) 1.96-2.26 (m, 8H), 1.48-1.6 (m, 48H), 1.43 (s, 36H), 0.91 (s, 9H), 0.09 (d, 6H) ppm; MS (MALDI-TOF): m/z calcd for [M+Na]+: 2200.88; found 2201.32. Yield: 482 mg, 78%

General procedure for the Hetero-convergent synthesis of MAn-b-LAm t-Bu-MAn-t and LAm-z were dissolved in dry DCM, and the reaction mixture was cooled to 0 oC in ice bath. To the solution, 4-(dimethylamino)pyridinium 4-toluenesulfonate (DPTS, 0.2 eq.) and 1-(3-dimethylaminopropyl)-3-ethylcarbodiimide hydrochloride (EDC•HCl, 1.5 eq.) were added, and the reaction mixture was stirred for 12h at room temperature. After completion, the reaction mixture was washed with water and brine. The organic layer was dried with MgSO4, filtered, and concentrated under reduced pressure. The pure product was isolated via preparative size-exclusion chromatography (prep-SEC). t-Bu-MAn-t were prepared by the deallylation of t-Bu-MAn-tz and LAm-z were prepared according to the previously published paper.

Bz-MA$_4$-LA$_8$-ta. Viscous white solid; ; ^{1}H NMR (400MHz, $CDCl_3$): δ 7.37-7.28 (m, 5H), 5.86-5.39 (m, 1H), 5.52-5.61 (m, 3H), 5.07-5.36 (m, 19H) 4.69-4.74 (m, 1H), 4.62 (d, 2H), 2.70-3.05 (m, 8H), 1.45-1.6 (m, 24H), 0.91 (s, 9H), 0.09 (d, 6H) ppm; MS (MALDI-TOF): m/z calcd for [M+Na]+: 1812.53; found 1813.08.Yield: 428 mg , 83%

Bz-MA$_4$-LA$_{16}$-ta. White solid; ; ^{1}H NMR (400MHz, $CDCl_3$): δ 7.37-7.28 (m, 5H), 5.86-5.39 (m, 1H), 5.52-5.61 (m, 3H), 5.07-5.36 (m, 27H) 4.69-4.74 (m, 1H), 4.62 (d, 2H), 2.70-3.05 (m, 8H), 1.45-1.6 (m, 48H), 0.91 (s, 9H), 0.09 (d, 6H) ppm; MS (MALDI-TOF): m/z calcd for [M+Na]+: 2170.70; found 2171.28.Yield: 378 mg , 81%

4.4 Results & Discussions

Scheme 4-1. Syntheses of orthogonally protected hydrophilic monomers

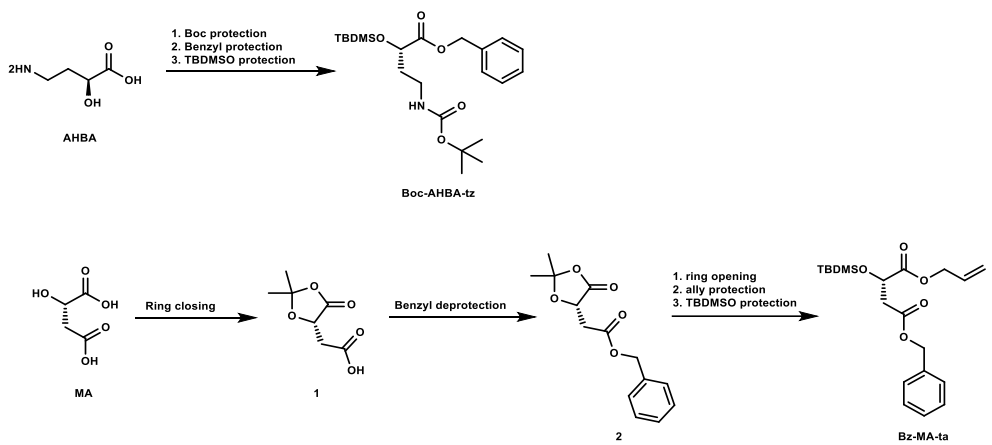

4.4.1 Synthesis of hydrophilic functional α-hydroxy acids. In this work, we introduced new monomers with hydrophilic functional groups into the cross-convergent synthetic methods. α-hydroxy acids based (s)-4-amino-2-hydroxybutyric acid (**AHBA**) and L-malic acid (**MA**) which have additional functional groups (amine or carboxylic acid) bearing on α-carbon were adopted as

hydrophilic functional monomers.[24] Discrete poly(α-hydroxy acids) having functional groups can be synthesized by iterative convergent method with other α-hydroxy acids such as lactide and phenyl lactide. Unlike previously reported monomers, there were three naked functional groups on **AHBA** and **MA**. This synthetic approach necessarily requires orthogonal protection of the functional monomers. We began our work to choose protecting groups for each reactive moieties in the functional monomers. We first synthesized orthogonally protected catanionic monomer N-Boc-**AHBA**-tz ((S)-4-((tert-butoxycarbonyl)amino)-2-((tert-butyldimethylsilyl)oxy)butanoate) composed of *tert*-butylcarbamate (Boc), benzyl ester and *tert*-butyldimethylsilyl (TBDMS) ether protecting groups for each functional moieties.[25] A portion of N-Boc-**AHBA**-tz is converted to N-Boc-**AHBA**-t using hydrogenation with Pd/C. The other portion is subjected to desilylation with tetra-n-butylammonium fluoride (TBAF) and AcOH (TBAF/AcOH = 3/2), which afforded N-Boc-**AHBA**-z in a good manner. Compare to the last work, TBAF and AcOH was used instead of boron trifluoride etherate (BF_3·Et2O) because BF_3·Et2O can also mediate the deprotection of N-Boc groups. But, TBAF can also attack the ester backbone of the dimer or tetramer. Therefore, addition of AcOH was necessary to lower the reactivity of TBAF (Table 4-1). After the successful deprotection of deprotected partners, an equal amount of deprotected building blocks were allowed to react with each other using EDC and DPTS with high yield and produced **AHBA** dimer (N-Boc-**AHBA$_2$**-tz).

Table 4-1. TBDMS deprotection of NBoc-AHBA$_2$-tz

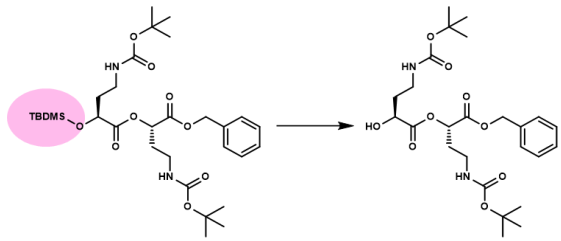

Entry	TBAF	AcOH	conc. (M)	temp. (˚C)	Time (h)	product	Byproduct[a]	SM
1	1	0	0.05	RT	3	-	70%	-
2	3	1	0.05	RT	3	45%	30%	-
3	3	2	0.05	RT	3	86%	10%	-
4	3	2	0.05	0	3	74%	10%	-
5	3	3	0.025	RT	6	60%	-	20%
6	2	8	0.1	RT	overnight	60%	10%	30%

[a] Byproduct contains NBoc-AHBA and NBoc-AHBA-z through the hydrolysis of ester backbone by TBAF.

In the case of MA, two carboxylic acid groups coexist in the monomer unit. Selective lactonization could prevent the α-carbon attached carboxylic acid from unwanted coupling and enabled the desired benzyl protection of naked β-carboxylic acid. Subsequent ring-opening made hydroxy and carboxylic acid groups reactive.[26,27] TBDMS ether and allyl protection resulted in the orthogonally protected 1-allyl 4-benzyl (S)-2-((tert-butyldimethylsilyl)oxy)succinate (Bz-**MA**-ta) as an anionic monomer. TBDMS ether group was successfully deprotected with $BF_3 \cdot Et2O$ without byproducts thanks to the inertness of the benzyl group (Bz-**MA**-a). Cleavage of the allyl ester was processed with tetrakis(triphenylphosphine)-palladium(0) and morpholine condition and generated Bz-**MA**-t in high yield

(>95%). The stoichiometric mixture of both coupling partners yielded dimeric MA as a product (Bz-**MA$_2$**-tz).

4.3.2 Discrete ionic amphiphilic block copolymer using iterative convergent method. Synthesized hydrophilic monomers could serve as hydrophilic units for the construction of discrete functional poly(α-hydroxy acids) by the cross-convergent synthetic method.[22,23] This method allows the rapid synthesis of precisely determined polymers composed of α-hydroxy acid monomer units including previously reported lactic acid and phenyl lactic acid.

For the discrete amphiphilic block copolymers, we began to synthesize hydrophilic blocks through the iteration of deprotection and coupling steps of hydrophilic functional monomers. (s)-4-amino-2-hydroxybutyric acid dimer (NBoc-**AHBA**$_2$-tz) was divided into two species. Each part was converted to the coupling precursor for the synthesis of **AHBA** tetramer through selective deprotection. Debenzylated NBoc-**AHBA**$_2$-t and desilylated dimer NBoc-**AHBA**$_2$-z were directly delivered to the EDC coupling to afford the tetramer NBoc-**AHBA**$_4$-tz. After the column chromatography to remove the excess reagents, we could get the cationic tetramer with fine yield. After the hydrogenation of the benzyl ester group, NBoc-**AHBA**$_4$-t was used as hydrophilic blocks for the cationic amphiphilic block copolymer. For the hydrophobic blocks, c) **LA**$_8$-tz, and **LA**$_{16}$-tz were prepared according to previous work. After the hydrogenation of dPLAs with $BF_3 \cdot Et2O$, hydrophilic block NBoc-**AHBA**$_4$-t and hydrophobic blocks (**LA**$_8$-z, and **LA**$_{16}$-z) were coupled with EDC and DPTS. Generated NBoc-**AHBA**$_4$-*b*-**LA**$_8$-tz

and NBoc-**AHBA**$_4$-*b*-**LA**$_{16}$-tz could be purified with column chromatography. But, during this process, several steps of purification was unavoidable due to low resolution between the product and reagents. Fast and convenient purification was possible by using preparative size exclusion chromatography (prep-SEC) (Fig 4-3). This purification method allowed us to split product and other reagents dependent on their hydrodynamic volume. After the purification, block copolymer NBoc-**AHBA**$_4$-*b*-**LA**$_8$-tz and NBoc-**AHBA**$_4$-*b*-**LA**$_{16}$-tz were characterized unambiguously by ^{1}H NMR and MALDI-TOF mass spectrometry. The anionic amphiphilic block copolymer was also synthesized via the similar iterative convergent method. Orthogonally protected Bz-**MA$_2$**-ta was split into two portions and the following deprotection and coupling steps have proceeded in the same way as the dimeric **MA** compound. Direct deprotection of allyl ester using $Pd(PPh_3)_4$ and morpholine of the produced tetramer Bz-**MA**$_4$-ta made the anionic hydrophilic block Bz-**MA**$_4$-t (Fig 4-2b).[27] discrete polylactides (dPLAs) were also used as hydrophobic coupling partners. But we have to substitute the benzyl ester group of the dPLAs with allyl ester groups. To prevent the interference between the benzyl group at the MA units and the benzyl ester at the dPLAs (**LA**$_8$-tz, and **LA**$_{16}$-tz to **LA**$_8$-ta, and **LA**$_{16}$-ta). After the exchange of terminal benzyl ester group to the allyl ester moiety, deprotection of allyl ester and EDC coupling reaction with Bz-**MA**$_4$-t successfully led to the generation of anionic amphiphilic block copolymers (Bz-**MA**$_4$-*b*-**LA**$_8$-ta and Bz-**MA**$_4$-*b*-**LA**$_{16}$-ta). After the purification with prep-SEC, ^{1}H NMR and MALDI-TOF mass spectrometry analysis indicates the right synthesis of the products.

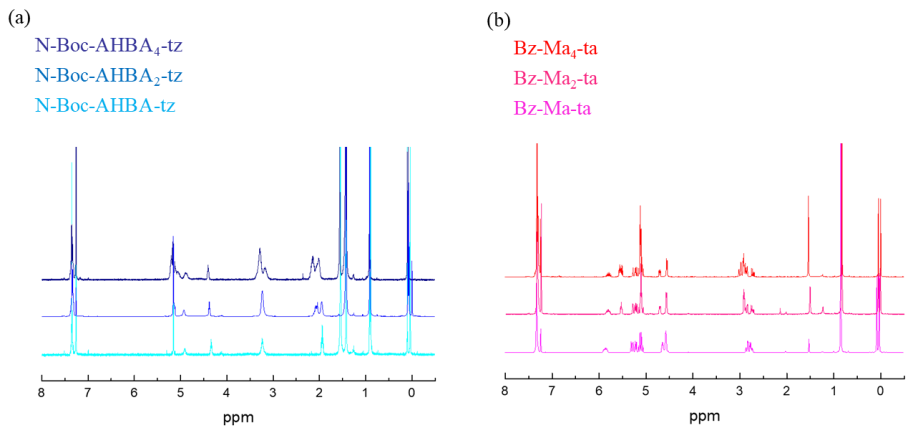

Figure 4-2. (a) ^{1}H NMR spectra of N-Boc-AHBA$_n$-tz (n = 1, 2, 4). (b) ^{1}H NMR spectra of Bz-Ma$_n$-ta (n = 1, 2, 4).

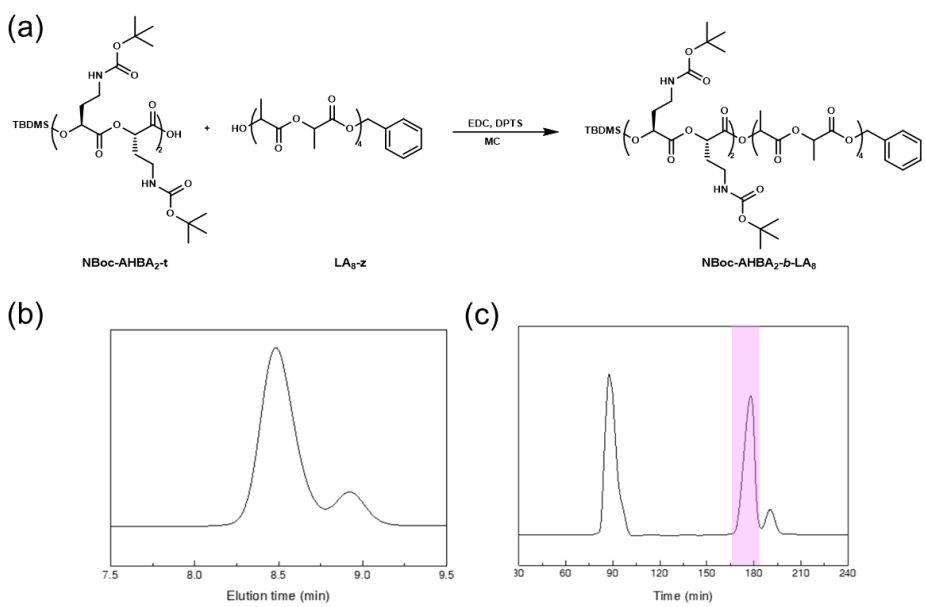

Figure 4-3. (a) Scheme of EDC coupling of N-Boc-AHBA$_4$-tz and LA$_8$-z. (b) NGPCMR spectra of Bz-Ma$_n$-ta (n = 1, 2, 4).

Activation of dormant ionic functional groups was proceeded with the deprotection of each cationic and anionic block copolymers. Carbamate groups from NBoc-**AHBA**$_4$-*b*-**LA**$_8$-tz and NBoc-**AHBA**$_4$-*b*-**LA**$_{16}$-tz were cleaved with 30% TFA in the MC for 1h.[28,29] If reaction time exceeds 3h, The TBDMS ether group was also transformed into the naked alcohol functional group. The existence of the TBDMS ether group affected the colloidal stability of the self-assembled structure. So, reaction times should be observed. Ionic diblock copolymers with naked amines were precipitated with cold hexane. The disappearance of the *tert*-butyl group at ^{1}H NMR and the shift from the MALDI-TOF data showed the clear deprotection of Boc groups without any byproducts (**AHBA**$_4$-*b*-**LA**$_8$-tz and **AHBA**$_4$-*b*-**LA**$_{16}$-tz) (Fig 4-4). Bz ester of the Bz-**MA**$_4$-*b*-**LA**$_8$-ta and Bz-**MA**$_4$-*b*-**LA**$_{16}$-ta were converted to carboxylic acid groups by hydrogenation with Pd/C. Unfortunately, the terminal allyl ester group turned to propyl ester through the hydrogenation process (Bz-**MA**$_4$-*b*-**LA**$_n$-ta to **MA**$_4$-*b*-**LA**$_n$-tp) (Fig 4-5). Since our experimental goal is to see a self-assembled structure, deformation of the terminal group was not a big problem.

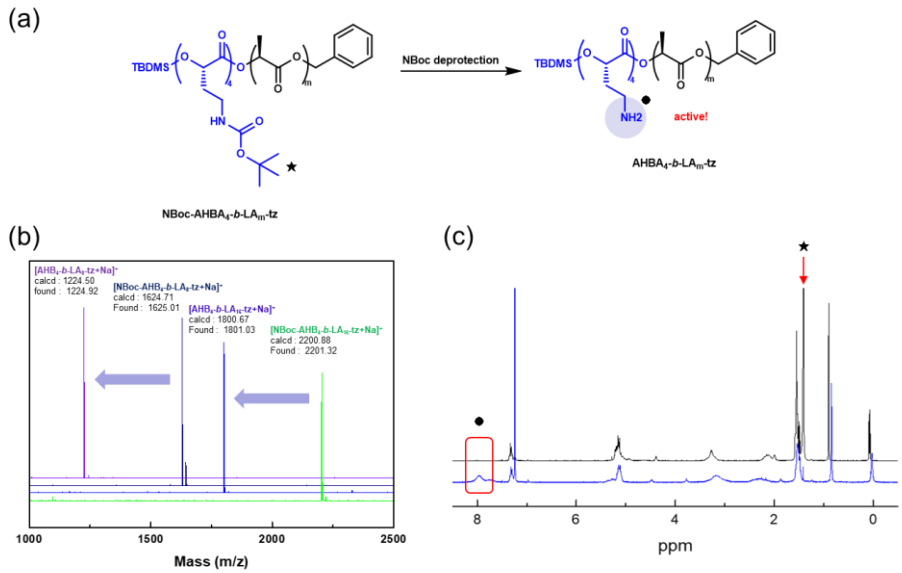

Figure 4-4. (a) Scheme of NBoc deprotection of NBoc-AHBA$_4$-*b*-LA$_n$-tz (b) MALDI-TOF mass spectra of cationic discrete block copolymers before and after the deprotection of ionic functional groups. (c) ^{1}H NMR spectra of NBoc-AHBA$_4$-*b*-LA$_8$-tz (black) and AHBA$_4$-*b*-LA$_8$-tz (blue).

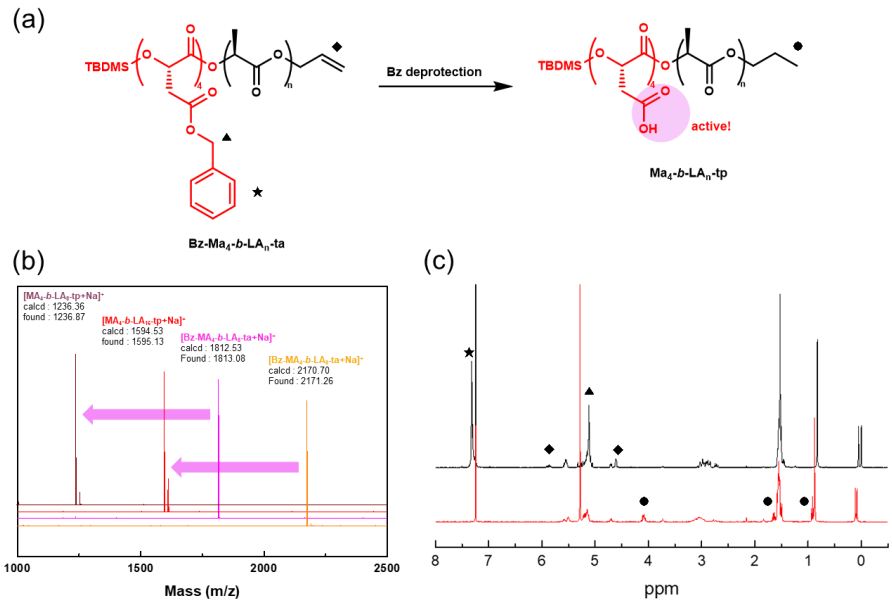

Figure 4-5. (a) Scheme of NBoc deprotection of NBoc-AHBA$_4$-*b*-LA$_n$-tz (b) MALDI-TOF mass spectra of cationic discrete block copolymers before and after the deprotection of ionic functional groups. (c) ^{1}H NMR spectra of NBoc-AHBA$_4$-*b*-LA$_8$-tz (black) and AHBA$_4$-*b*-LA$_8$-tz (blue).

4.3.3 Self-assembly of Ionic block copolymers Synthesized amphiphilic block polymers with exact molecular weight and repeating units were self-assembled with the solvent-switch method.[11] polymers were first dissolved in good solvent THF (8 mM, 400 μl) and stirred for 1 hour for the formation of charge complexes. Addition of water into the polymer blend solution induced the self-assembly of the polymers. We varied the solution ratio from 5 to 20% (v/v) THF/H_2O by changing the amount of water for the self-assembly. The mixture was stirred for additional 12 hours for the electrostatic stabilization of the structures. After vigorous stirring, we removed the organic solvent by slow evaporation (~24 h). The self-assembled

structures were characterized by Cryo-TEM and DLS. Hydrophobic units with 16-mer were first self-assembled. 3.6 ml of water was added to 400 μl of THF containing cationic **AHBA**$_4$-*b*-**LA**$_{16}$-tz to make 10% (v/v) THF/H_2O and slow evaporation led to the self-assembly of small colloidal particles with ~400 nm mean radius. And with the same procedure, anionic **MA**$_4$-*b*-**LA**$_{16}$-ta showed spherical vesicles. Yet, the catanionic mixture showed different structures from positively or negatively charged samples. We couldn't find spherical vesicles from **MA**$_4$-*b*-**LA**$_{16}$-ta. Instead, colloidal particles with crumpled surface membranes were observed. Similar structures were also observed with solvent quality with 5% and 20% (v/v) THF/H_2O. Complexation of the ionic hydrophilic groups reduced the net charge of the polymers. The polymer tried to avoid the hydrophobic sixteen hydrophobic lactic acid units led the formation of colloidal particles. Electrostatic interaction makes surface membrane solid. To avoid the charge and strain accumulation, the colloidal particle showed crumpled surfaces rather than smooth spherical colloidal particles.

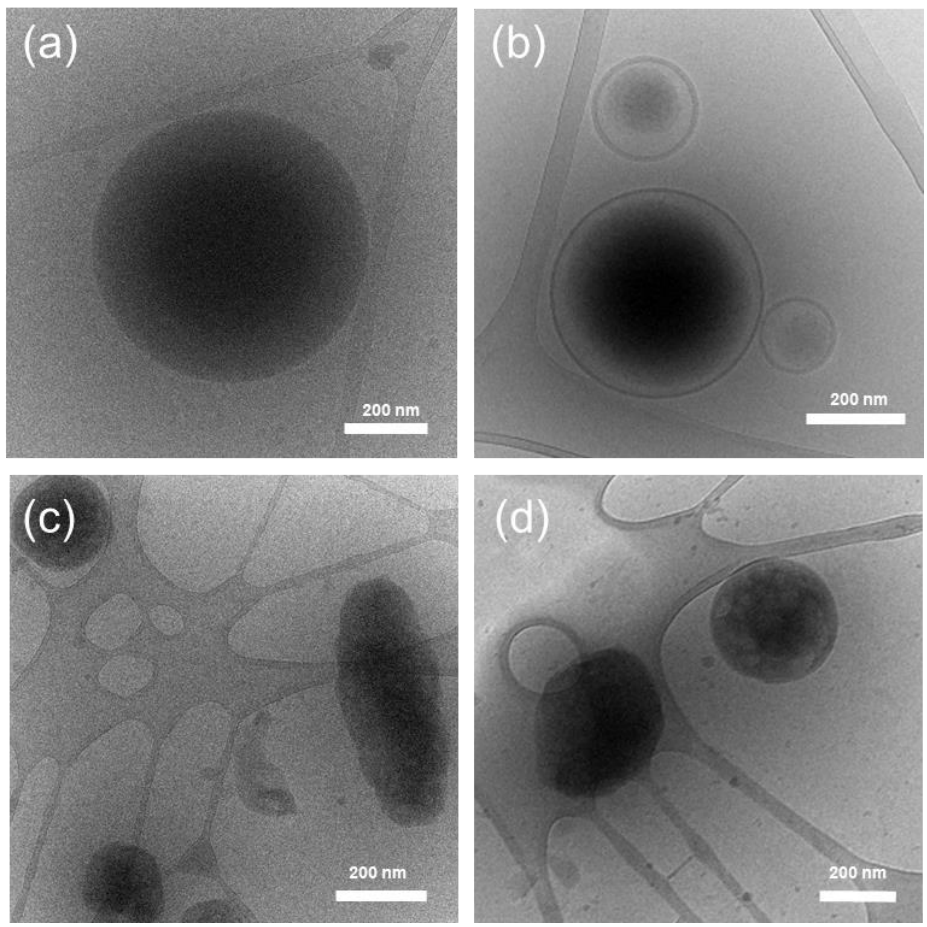

Figure 4-6. Cryo-TEM images after the self-assembly of (A) **AHBA**$_4$-*b*-**LA**$_{16}$-tz (B) **MA**$_4$-*b*-**LA**$_{16}$-tp, (C, D) 1:1 Mixture of **AHBA**$_4$-*b*-**LA**$_{16}$-tz, **MA**$_4$-*b*-**LA**$_{16}$-tp

We tried to alleviate the hydrophobicity of the polymer. With the iterative exponential growth technique, we could exactly target the desired number of repeating units. With reduced hydrophobic repeating units compared to the

previous polymers, cationic **AHBA**$_4$-*b*-**LA**$_8$-tz and anionic **MA**$_4$-*b*-**LA**$_8$-tp were newly synthesized. This time, similar self-assembled structures were observed regardless of the hydrophilic ionic head groups. Both anionic and cationic polymers showed micellar structures (~ 100 nm) on the condition of 5, 10, and 20% (v/v) THF/H_2O. Next, we blended two ionic block copolymers to watch the self-assembly behavior after the ionic complexation. The equimolar ratio of **AHBA**$_4$-*b*-**LA**$_8$-tz and **MA**$_4$-*b*-**LA**$_8$-tp were premixed in the 400 μl THF and stirred for 1 h. Subsequent addition of water induced self-assembly of the polymers. But, the self-assembled solutions of the catanionic mixture showed different turbidity dependent on the solvent ratio indicating the different self-assembly behavior. In the 10% (v/v) THF/H_2O solution, we could get the vesicles with faceted surface membranes. The electrostatic interactions among charged hydrophilic groups affected the elasticity of the polymersome membrane. Strong lateral correlations of the ionic groups can be considered as a solid membrane. When the surface membrane has a certain curvature, the internal strain applied to the membrane increases due to the intermolecular interactions. This stretching energy can be partially alleviated by buckling the solid membrane.[7,8] These faceted polymersomes showed more than 10 times larger particle sizes compare to the structures from single ionic polymers. Evidently, the DLS analysis performed on the polymer solution doubly confirms the particle size of the self-assembled structures (Fig S3-1). Structures generated from the catanionic mixture 20% (v/v) THF/H_2O solution also showed faceted vesicles. However excess THF hampered the buckling of the vesicle membrane. And the self-assembled structures were kinetically trapped during the evaporation process before the buckling was completed. In the case of the 5% (v/v) THF/H_2O solution, we couldn't find the self-assembled structures. Instead, only aggregated

polymer samples were observed. The self-assembly process of the cationic mixture of **AHBA**$_4$-*b*-**LA**$_8$-tz and **MA**$_4$-*b*-**LA**$_8$-tp were strongly influenced by the solvent quality.

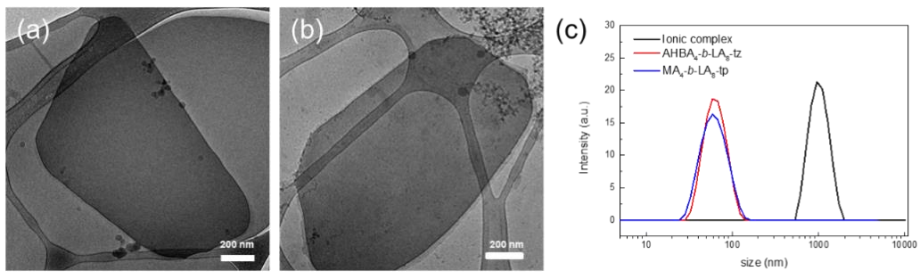

Figure 4-7. (A, B) Cryo-TEM images after the self-assembly structure of 1:1 Mixture of **AHBA**$_4$-*b*-**LA**$_8$-tz, **MA**$_4$-*b*-**LA**$_8$-tp (10% (v/v) THF/H_2O) (c) DLS of self-assembly structure of **AHBA**$_4$-*b*-**LA**$_8$-tz (red), **MA**$_4$-*b*-**LA**$_8$ (blue), and their 1:1 ionic complex (black).

4.5 Conclusion

In summary, due to the synthetic complexities and ill-defined structures, the ionic complex of the polymers was hard to achieve. Using the iterative exponential growth method, we could synthesize a series of amphiphilic block copolymers (**AHBA**$_4$-*b*-**LA**$_n$-tz and **MA**$_4$-*b*-**LA**$_n$-tp) with precisely defined chemical structures. The hydrophilic part of each polymer can participate in the ionic complexation between amine and carboxylic acid. Absolutely defined structure minimizes the generation of the byproducts and uncertainty of the self-assembly processes. Self-

assembly of discrete polymer mixture led to the electrostatically connected solid membrane due to the intermolecular ionic interactions. To reduce the applied strain, the solid membrane buckled to make faceted polymersomes. We demonstrated the buckling of structure membrane with a mixture of **AHBA**$_4$-*b*-**LA**$_8$-tz and **MA**$_4$-*b*-**LA**$_8$-tp and self-assembled structures were characterized with Cryo-TEM and DLS. We anticipate polymers with precisely defined chemical structures will provide new opportunities to get in touch with highly ordered structures. And our strategy can be a powerful tool for the preparation of faceted polymersomes which can serve as hollow faceted inorganic nanoparticles or building blocks for superlattices or drug delivery vehicles.

4.6 References

1. Kim, K. T.; Zhu Z.; Meeuwissen, S. A.; Cornelissen, J. J. L. M.; Pochan, D. J.; Nolte, R. J. M.; van Hest, J. C. M. *J. Am. Chem. Soc.* **2010** *132* (*36*), 12522-12524
2. Wilson, D.; Nolte, R.; van Hest, J. *Nat. Chem*. **2012**, *4*, 268–274
3. La, Y.; Park, C.; Shin, T. J.; Joo, S. J.; Kang, S.; Kim, K. T. *Nat. Chem.* **2014**, *6*, 534–541.
4. Park, C.; La, Y.; An, Jeong, H. Y.; Kang, S.; Joo, S. H.; Ahn, H.; Shin, T. J.; Kim, K. T. *Nat. Commun.* **2015**, *6,* 6392

5. Christian, D. A.; Tian, A.; Ellenbroek, W. G.; Levental, I.; Rajagopal, K.; Janmey, P. A.; Liu, A. J.; Baumgart, T.; Discher, D. E. *Nat. Mater*. **2009**, *8*, 843−849

6. Xie, H.; She, Z.-G.; Wang, S.; Sharma, G.; Smith, J. W. *Langmuir* **2012** *28* (*9*), 4459-4463

7. Dubois, M.; Deme, B.; Gulik-Krzywicki, T.; Dedieu, J. C.; Vautrin, C.; Desert, S.; Perez, E.; Zemb, T. *Nature* **2001**, *411*, 672–675.

8. Greenfield, M. A.; Palmer, L. C.; Vernizzi, G.; Olvera de la Cruz, M.; Stupp, S. I. *J. Am. Chem. Soc.* **2009**, *131*, 12030–12031.

9. Solis, F. J.; Stupp, S. I.; Olvera de la Cruz, M. J. *Chem. Phys*. **2005**, *122*, 054905.

10. Leung, C.-Y.; Palmer, L. C.; Qiao, B. F.; Kewalramani, S.; Sknepnek, R.; Newcomb, C. J.; Greenfield, M. A.; Vernizzi, G.; Stupp, S. I.; Bedzyk, M. J.; de la Cruz M. O. *ACS Nano* **2012** *6* (*12*), 10901-10909

11. Wong, C. K.; Martin, A. D.; Floetenmeyer, M.; Parton, R.G.; Stenzel, M. H.; Thordarson, P. *Chem. Sci*. **2019**, *10* , 2725 —2731

12. Vernizzi, G.; de la Cruz, M. O. *PNAS* **2007**, *104*, 18382–18386

13. Solis, F. J.; Stupp, S. I.; Olvera de la Cruz, M. J. *J. Chem. Phys.* **2005**, *122*, 054905

14. Merrifield, R. B. *J. Am. Chem. Soc.* **1963**, *85*, 2149.

15. Malenfant, P. R. L. Frechet, J. M. J. *Chem. Commun.* **1998**, 2657-2658.

16. Pfeifer, S.; Zarafshani, Z.; Badi, N.; Lutz, J.-F. *J. Am. Chem. Soc.* **2009**, *131*, 9195.

17. Espeel, P.; Carrette, L. L. G.; Capenberghs, K. Bury, S.; Martins, J. C.; Du prez F. E.; Madder, A. *Angew. Chem. Int. Ed.* **2013**, *52*, 13261-13264.

18. Trinh, T.; T. Laure C.; Lutz, J. F. *Macromol. Chem. Phys.* **2015**, *216*, 1498-1506.

19. Lawrence, J.; Lee, S.-H.; Abdilla, A.; Nothling, M. D.; Ren, J. M.; Knight, A. S.; Fleischmann, C.; Li, Y.; Abrams, A. S.; Schmidt, B. V. K. J.; Hawker, M. C.; Connal, L. A.; McGrath, A. J.; Clark, P. G.; Gutekunst, W. R.; Hawker, C. J. *J. Am Chem. Soc*. **2016**, *138*, 6306-6310

20. Jiang, Y.; Golder, M. R.; Nguyen, H. V. T.; Wang, Y.; Zhong, M.; Barnes, J. C.; Ehrlich, D. J. C.; Johnson, J. A. *J. Am. Chem. Soc.* **2016**, *138*, 9369.

21. Barnes, J. C.; Ehrlich, D. J. C.; Gao, A.; X. Leibfarth, F. A.; Jiang, Y.; Zhou, E.; Jamison, T. F.; Johnson, J. A. *Nat. Chem.* **2015**, *7*, 810–815

22. Lee, J. M.; Koo, M. B.; Lee, S. W.; Lee, H.; Kwon, J.; Shim, Y. H.; Kim, S. Y.; Kim, K. T. *Nat. Commun*. **2020**, *11*, 56.

23. Koo, M. B.;Lee, S. W.; Lee, J. M.; Kim, K. T. *J. Am. Chem. Soc*. **2020**, *142*, 14028-14032

24. Yu, Y.; Zou, J.; Cheng, C. *Polym. Chem.* **2014**, *5*, 5854

25. Farkas, M. E.; Li, B. C.; Dose, C.; Dervan, P. B. *Bioorganic Med. Chem. Lett.* **2009**, *19*, 3919–3923

26. Pounder, R. J.; Dove, A. P. *Biomacromolecules* **2010**, *11*, 1930–1939

27. Franz, N.; Menin, L.; Klok, H.-A. Eur. J. Org. Chem. **2009**, 2009, 5390–5405.

28. Takizawa, K.; Tang, C.; Hawker, C. J. *J. Am. Chem. Soc.* **2008**, *130*, 1718-1726

29. Maron, E.; Swisher, J. H.; Haven. J. J.; Meyer, T. Y.; Junkers, J.; Bcrner, H. G *Angew. Chem. Int. Ed*. **2019**, *58*, 10747 –10751

ABSTRACT (Korean)

뚜렷한 특징을 지니는 분자로 설계된 블록 공중합체의 용액상에서의 자기조립거동과 그 응용

김 준 영

화학부 유기화학 전공

서울대학교 대학원

자기조립을 이용한 잘 정의된 나노구조의 합성은 현대 연구에서 매우 중요한 연구 주제이다. 자기조립으로 만들어지는 형태의 종류가 매우 다양하기 때문에 분자 수준에서 나노구조를 정확하게 예측하는 것 또한 중요한 숙제이다. 작용기 또는 뚜렷한 특성을 가진 폴리머는 용액에 첨가되는 물질 또는 내부 및 외부의 환경에 민감하게 반응하여 용액상에서 자기 조립 거동에 크게 영향을 미치게 된다.

본 연구에서는 블록 공중합체의 잘 정의된 자기 조립 구조에 대한 다양한 제조 방법을 다룬다. 잘 정의된 복잡한 구조의 나노 구조를 관찰하기 위해 독특한 작용기 또는 특성을 지닌 단량체를 이용해 블록 공중합체의 합성이 선행되었다. 이를 이용해 다양한 나노 구조체의 합성 사례를 보고한다.

2 장에서는 폴리(에틸렌 글리콜) 폴리(아크릴벤질보레이트) 블록 공중합체 (PEG-*b*-PABB)를 준비하여 PEG-*b*-PS 와의 혼합을 통해 산화 반응성 폴리머좀을 합성하였다. 산화반응을 통해 PABB 를 친수성 PAA (폴리아크릴산)로 전환하여 선택적 용해를 통해 폴리머좀 막에 포어를 생성하게 된다. 자극 반응성 블록 공중합체의 조성을 제어함으로써, 크기 선택적 투과도를 지니는 폴리머좀을 합성할 수 있음을 보고한다.

3 장에서는 무정형의 폴리에틸헥실싸이오펜을 KCTP 를 통해 결정형의 폴리헥실싸이오펜에 연결하여 용해도 및 결정성의 변화가 자기 조립 거동에 미치는 영향을 조사하였다. 이를 토대로 폴리싸이오펜 블록공중합체를 이용해 길이 조절이 가능한 나노섬유의 제조가 가능함을 보이며 또한, 트리블록공중합체가 나노섬유의 연결을 도와 나노네트워크를 이루는 것을 이용해 나노섬유 기반의 유기젤의 합성이 가능함을 보인다.

4 장에서는 수렴 방법을 통해 합성된 카르복실산 또는 아민을 친수성 기능 블록으로, 올리고(락트산)를 소수성 블록으로 갖는 정밀하게 정의된 이온성 블록 공올리고머를 이용하여 용액상에서의 자기조립 거동을 조사하였다. 이를 통해 결정성의 각진 구조를 지니는 고분자 주머니를 관찰하였음을 보고한다.

핵심어: 블록 공중합체, 자극 반응성 고분자주머니, 용액상 자기조립, 결정화 구동 자기조립, 단일 분자량 고분자

학번: 2016-29404